

Nucleon Electromagnetic Form Factors in perturbative QCD



Dissertation
zur Erlangung des Doktorgrades
der Naturwissenschaften (Dr. rer. nat.)

Fakultät für Physik
–Institut für theoretische Physik–
Universität Regensburg

vorgelegt von

Michael Knödlseher

aus Ruhstorf a.d. Rott

Mai 2015

Promotionsgesuch eingereicht am: 18.06.2014

Die Arbeit wurde angeleitet von: Prof. Dr. V. Braun

Prüfungsausschuss:

Vorsitzender: Prof. Dr. D. Bougeard

1. Gutachter: Prof. Dr. V. Braun

2. Gutachter: Prof. Dr. G. Bali

weiterer Prüfer: Prof. Dr. J. Fabian

Termin Promotionskolloquium: 14.07.2015

Abstract

In this thesis we calculate α_S -corrections – in perturbative quantumchromodynamics (pQCD) – to the hard scattering kernel of nucleon form factors within the collinear factorization approach. Due to the fact of dealing with a huge number of Feynman diagrams it is necessary to solve this problem computer-assisted. Therefore we make use of the computational software program Mathematica [1] and the packages FeynCalc, FeynArts [2] and the multidimensional numerical integration Cuba. We present three highly nontrivial and independent checks for the consistency of our results.

Contents

| | |
|---|-----------|
| 1. Introduction | 5 |
| 2. Theoretical Framework | 9 |
| 2.1. Quantumchromodynamics | 9 |
| 2.1.1. Gauge theories | 9 |
| 2.1.2. Regularization and renormalization procedure | 14 |
| 2.1.3. Renormalization group equation | 18 |
| 2.2. Nucleon form factors | 19 |
| 2.2.1. History of nucleon form factors | 19 |
| 2.2.2. From scattering amplitudes to matrix elements | 22 |
| 2.2.3. Experimental point of view | 28 |
| 2.3. Factorization and the concept of distribution amplitudes | 34 |
| 2.3.1. Collinear factorization | 35 |
| 2.3.2. Nucleon wave function and distribution amplitudes | 36 |
| 2.4. FeynArts | 39 |
| 2.5. Reduction algorithm | 42 |
| 3. Calculations | 47 |
| 3.1. Leading order | 48 |
| 3.1.1. Dirac algebra | 49 |
| 3.1.2. Color algebra | 51 |
| 3.1.3. Results obtained by Chernyak et al. | 53 |
| 3.1.4. Results obtained by automated procedure | 58 |
| 3.2. Next-to-leading order | 69 |
| 3.2.1. Generating the possible diagrams for the NLO case | 69 |
| 3.2.2. Color | 75 |
| 3.2.3. Tracing | 79 |

| | |
|--|------------|
| 3.2.4. Integration | 81 |
| 4. Results and checks | 83 |
| 5. Conclusion and outlook | 87 |
| A. Color | 89 |
| B. Feynman Rules | 91 |
| C. Dimensional regularization | 95 |
| D. Mandelstam variables | 97 |
| E. Experimental results for G_E and G_M | 99 |
| E.1. Rosenbluth separation method | 100 |
| E.2. Polarization transfer | 102 |
| F. Light-cone kinematics | 105 |
| G. Decomposition of the three quark matrix element | 107 |
| H. Dirac algebra | 111 |
| Bibliography | 115 |

1. Introduction

Since the advent of modern physics scientists have tried to understand the most fundamental processes of a given problem. For this reason the structure of the nucleons which are the heartstone of matter is not only a subject of hadronic physics. The first hint on the fact that the proton was not a pointlike spin-1/2 particle was the ≈ 2.8 time bigger magnetic moment measured by Stern in 1933. From the first evidence that the proton is not a pointlike particle to the first measurement giving hints on it's internal structure by Hofstadter et al. [3] nearly 20 years elapsed. Hofstadter combined the Mott cross section with an internal charge density to describe the experimental deviation from a pointlike target. The charge and magnetization distributions of the nucleons are encoded in the form factors which can be measured in scattering experiments. They reveal the nature and dynamics of the constituents of which proton and neutron are made of [4–8].

The main tools for accessing the internal structure of protons and neutrons are elastic electron scattering experiments. Experiments for investigating the internal structures have been started right after the first works on the topic done by the group around Hofstadter [3] in various countries. At the beginning of the 1970s the operating state of numerous accelerators was reached. So for example: The Cambridge Electron Accelerator[9, 10], the Electron-Synchrotron at Bonn [11] and Deutsches Elektronen-Synchrotron (DESY) in Hamburg [12] and later in the early 90s the Stanford Linear Accelerator Center (SLAC) [13, 14]. These facilities produced various values for the electromagnetic proton and neutron form factors in elastic electron-proton and electron-deuteron scattering. A compilation of measurements, i.e. world-data plots, can be found in the work of Gao [4]. The latest values for the ratio G_E/G_M measured at the Jefferson Lab [15, 16] were the first to show the deviation of the dipole behavior of the form factors obtained by the Rosenbluth cross section separation method due to the polarization transfer technique. These discrepancy emerged at very high Q^2 .

There have been quite a few models trying to describe the interactions within the nucleons theoretically. So for example the vector dominance model, the constituent quark model

or the chiral effective field theory of QCD. At very large momentum transfer perturbative QCD can be applied and the form factors can be written in factorized form [17, 18]. In this approach it is possible to calculate a hard kernel and convolute this perturbatively accessible quantity with a distribution amplitude, which incorporates the soft scale dynamics. These non perturbative functions can be calculated via sum rules and lattice QCD. The first complete leading order calculations of the hard scattering kernel in collinear factorization were done by Lepage et al. [19] and Chernyak et al. [20]. We will recalculate these results and present a completely automated way to reproduce the results of Chernyak. Afterwards we will apply the same procedure to the next-to-leading order case.

This thesis is organized as follows: First we will give a short review of the basic concepts of QCD. Starting from the Lagrange density we will recap the procedure of regularization and renormalization. We state the renormalization constants for all parameters of the Lagrangian which will partially be needed during this work to renormalize our results. Furthermore we will provide the reader with a short historical overview of the progress of elastic scattering in the last century up to the state of the art access to form factors via collinear factorization and the concept of distribution amplitudes. This chapter will be concluded by introducing the reader to the Mathematica [1] package FeynArts invented by Hagen Eck [21], Sepp Küblbeck et al. [22] and Thomas Hahn [2]. This library enables us to generate not only all possible diagrams but also the corresponding physical amplitudes which can be further processed with the FeynCalc package. In addition we present an algorithm for calculating massless one-loop N -point Feynman integrals in dimensional regularization approach which was formulated by Duplanić and Nižić [23]. The tensor reduction used in the algorithm was derived by Davydychev [24]. This algorithm is based on the integration by parts method and is recursive which makes it ideal for implementation into a computer code. This was done by Nils Offen who wrote a complete Mathematica based code for the reduction of N -point tensor integrals.

In chapter 3 we will first recalculate the leading order result obtained by Chernyak et al. [20], which will lead to a factor 2 discrepancy which can be ruled out by a redefinition of the normalization constant of the corresponding distribution amplitude. Afterwards we will present a detailed guide for calculating the leading order result in a completely automated way with aid of the FeynArts and FeynCalc package. The code used there will then be applied identically to the next-to-leading order case up to the point of the integration of the loop momenta via the reduction algorithm. The final step is to integrate over the momentum fractions which pose the biggest problems and could not be solved up to now.

The fourth chapter is dedicated to giving three non trivial checks for the results obtained. First the aforementioned consistency with the leading order result of Chernyak. Second the cancellation of double poles in the sum of all diagrams. And finally the cancellation of all ultraviolet singularities when combining the results to the physical amplitude, including only renormalized parameters.

We finish with a brief conclusion and will state some possible applications of our routine to other processes.

2. Theoretical Framework

In this chapter we will provide a short overview of all tools needed to understand and reproduce our calculations. At the beginning we will give a short introduction to quantum field theory. Illustrating the basic concepts on the example of the $U(1)$ gauge theory QED and later generalize it to the non Abelian $SU(3)$ gauge group. For this Yang-Mills theory we will perform the renormalization procedure associated with it. Followed by a history lessons about the developments of the nucleon picture throughout the 20th century. After this we will dedicate ourselves to the experimental physics approach to nucleon form factors. I.e. we will scratch the basics of the two fundamental techniques used in the last 60 years to achieve insight into the inner structure of the building blocks of matter. Afterwards we will present the definitions of the form factors in the context of scattering theory and theoretical accessible matrix elements. For this purpose we introduce the concepts of distribution amplitudes and collinear factorization. The last part of this chapter will cover the tools and methods we use for accomplishing our goals. More concretely we will introduce the reader to the FeynArts and FeynCalc Mathematica packages and present a reduction algorithm for the appearing seven point tensor integrals.

In this chapter we will use natural units $\hbar = c = 1$ and Einstein sum convention, i.e. a summation over indices that appear twice is assumed. Greek letters will denote Lorentz indices, small Latin letters Dirac indices and capital Latin letters are color indices. We will work within Feynman gauge.

2.1. Quantumchromodynamics

2.1.1. Gauge theories

In this section we will give a brief introduction to the non-Abelian $SU(3)$ gauge theory, the so called Yang-Mills theory. For a more detailed review of strong interaction in the quantum field theory approach we refer the reader to the standard textbooks[25–27]. In

the following we will mainly use the work of [26].

In order to present the basic concepts of gauge theories we will limit ourselves to the case of QED, which describes the motion of charged fermionic elementary particles and is the quantization of classical electrodynamics which incorporates spin-1/2 particles.

Starting from the Maxwell equations of classical electrodynamics,

$$\begin{aligned}\vec{\nabla} \times \vec{E} + \frac{\partial \vec{H}}{\partial t} &= 0, & \vec{\nabla} \cdot \vec{H} &= 0, \\ \vec{\nabla} \times \vec{H} + \frac{\partial \vec{E}}{\partial t} &= Q\vec{j}, & \vec{\nabla} \cdot \vec{E} &= Q\rho,\end{aligned}\quad (2.1)$$

which describe the motion of charged particles in electromagnetic fields

$$\vec{E} = -\vec{\nabla}\Phi - \frac{\partial \vec{A}}{\partial t} \quad \vec{H} = \vec{\nabla} \times \vec{A}. \quad (2.2)$$

Here A is the vector and Φ is a scalar potential, respectively. One can formulate the covariant versions of these equations of motion:

$$\partial^\mu F_{\mu\nu} = Qj_\nu, \quad (2.3)$$

where F is the electromagnetic field strength tensor,

$$F^{\mu\nu} = \partial^\mu A^\nu - \partial^\nu A^\mu, \quad (2.4)$$

and j^μ is the electromagnetic current,

$$j^\mu = (\rho, \vec{j}). \quad (2.5)$$

In order to describe relativistic charged particles in an electric field we need the Dirac equation:

$$\left[i\gamma^\mu \left(\partial_\mu + iQA_\mu \right) - m \right] \Psi = 0, \quad (2.6)$$

where Ψ is the Dirac field for charged fermions. The Lagrangian of a certain physical system contains all information needed to derive equations of motion or conserved quantities. The Lagrange density for QED is given by:

$$\mathcal{L}_{\text{QED}} = -\frac{1}{4}F_{\mu\nu}F^{\mu\nu} + \bar{\Psi}[i\gamma^\mu D_\mu - m]\Psi. \quad (2.7)$$

Here $D_\mu = (\partial_\mu + iQA_\mu)$ is the so called covariant derivative. One can show the invariance of the QED Lagrangian (2.7) under the global gauge transformation:

$$\Psi \rightarrow e^{-iQ\Theta} \Psi . \quad (2.8)$$

All transformations (2.8) with Θ being a real constant and Q being a commutative (Abelian) number form the unitary group $U(1)$. In order to guarantee the invariance under Abelian local transformations, which means to allow a dependence on x for the parameter $\Theta \rightarrow \Theta(x)$, one has to modify the gauge field A^μ in the following way:

$$A^\mu \rightarrow A^\mu + \frac{1}{Q} \partial^\mu \Theta . \quad (2.9)$$

In order to describe the strong interaction of quarks and gluons one has to allow for a more general group structure, the non-Abelian or Yang-Mills gauge theories. In the case of QCD we have to deal with the special unitary group in $N = 3$ dimensions, the Lie group $SU(3)$ also denoted as color group. So the transformation of the quark fields $\Psi_i(x)$, $i = 1, 2, 3$ which transform under the 3-dimensional fundamental representation of the gauge group $SU(3)$ takes the form:

$$\Psi_i(x)' = U_{AB} \Psi_B(x) \quad (2.10)$$

with the matrix U being

$$U = e^{-iQT^A\Theta^A} , \quad (2.11)$$

where T^A , $A = 1, \dots, 8$ are the corresponding Lie algebra's generators which fulfill the following commutation relation:

$$[T^A, T^B] = if^{ABC} T^C . \quad (2.12)$$

Here f^{ABC} are the structure constants which characterize the group algebra and is described in more detail in Appendix A. Likewise to the QED case, we have to modify the gauge field in order to secure gauge invariance also for local transformations $\Theta(x)$:

$$T^A A_\mu^A = U \left(T^A A_\mu^A - \frac{i}{g} U^{-1} \partial_\mu U \right) U^{-1} . \quad (2.13)$$

Now we are able to formulate the Lagrangian for the interaction of quarks which transform under the fundamental representation via gluons which transform under the adjoint representation of the color gauge group $SU(3)$:

$$\mathcal{L} = -\frac{1}{4} F_{\mu\nu}^A F^{A\ \mu\nu} + \bar{\Psi}(x)(i\gamma^\mu D_\mu - m)\Psi(x) . \quad (2.14)$$

Here D_μ denotes the covariant derivative and reads as:

$$D_\mu = \partial_\mu - igT^A A_\mu^A . \quad (2.15)$$

In order to quantize the theory the usual canonical approach fails [26]. On the one hand unphysical degrees of freedom occur, which can be cured by introducing an additional field, the Faddeev-Popov ghosts. But on the other hand one has to eliminate the freedom of the gauge transformation for the gauge field A^μ :

$$A_\mu^A \rightarrow A_\mu^A + f^{ABC} \Theta^B A_\mu^C - \frac{1}{g} \partial_\mu \Theta^A . \quad (2.16)$$

This can be achieved by constraining or fixing the field transformation in a certain way the so called gauge fixing condition:

$$\begin{aligned} \partial^\mu A_\mu &= 0 && \text{Lorenz gauge} \\ \partial_i A_i &= 0 && \text{Coulomb gauge} \\ A_0 &= 0 && \text{temporal gauge} \\ A_3 &= 0 && \text{axial gauge} \\ n \cdot A &= 0 && \text{light-cone gauge} . \end{aligned} \quad (2.17)$$

Here n denotes a light-like vector and defined in Appendix F. Another way to impose constraints on a dynamic system is the method of Lagrange multipliers. According to this approach one has to add a term

$$\lambda(\partial_\mu A^{\mu A})^2 \quad (2.18)$$

containing the Lagrange multiplier

$$\lambda = -\frac{1}{2a} , \quad (2.19)$$

which incorporates the gauge fixing parameter a . Because this gauge fixing parameter does not have any influence on the physical quantities one can chose it to be set to certain values, for example

$$a = 1 , \quad (2.20)$$

the so called Feynman gauge which is used in this work.

In non-Abelian gauge theories we have to cope with the problem of breaking the Ward identity:

$$k^\mu \Pi_{\mu\nu}^{AB}(k) = 0 . \quad (2.21)$$

Here $\Pi_{\mu\nu}^{AB}(k)$ denotes the gluonic part of the one-loop corrections for the gauge field propagator. The problem can be solved with the path-integral trick introducing artificial fields, the Faddeev-Popov ghost fields. These anti-commutating scalar fields cancel unphysical polarization of the gluon fields in physical amplitudes when added to every gauge field loop.

Finally the QCD Lagrangian density, which includes the interaction of spin-1/2 fermions – the quarks – due to spin-1 vector bosons – gluons – can be split up into a fermion-, gauge-gauge fixing- and Faddeev-Popov ghosts term:

$$\mathcal{L} = \mathcal{L}_F + \mathcal{L}_G + \mathcal{L}_{GF} + \mathcal{L}_{FP} . \quad (2.22)$$

The fermion term of our Lagrange density is

$$\mathcal{L}_F = \sum_f \bar{\Psi}_f^A(x) (i\gamma^\mu D_\mu^{AB} - m_f \delta^{AB}) \Psi_f^B(x) , \quad (2.23)$$

where f labels quark flavors (up u , down d , strange s , charm c , bottom b and top t), $\Psi_f^B(x)$ being a fermion field of flavor f and color B . The part carrying the information about the gauge fields reads as

$$\mathcal{L}_G = -\frac{1}{4} F_{\mu\nu}^A F^{A\ \mu\nu} , \quad (2.24)$$

with $F_{\mu\nu}^A = \partial_\mu A_\nu^A - \partial_\nu A_\mu^A + gf^{ABC} A_\mu^B A_\nu^C$ being the field strength tensor, which contains the gauge fields A_μ^A and the structure constant f^{ABC} of the algebra and fulfills the relation $F_{\mu\nu} = -ig[D_\mu, D_\nu]$. The gauge fixing, necessary for quantization is

$$\mathcal{L}_{GF} = -\frac{1}{2a} (\partial^\mu A_\mu^A) , \quad (2.25)$$

where a is the gauge parameter. In order to avoid unphysical polarization we include a ghost field χ part into the Lagrangian:

$$\mathcal{L}_{FP} = (\partial^\mu \chi^{*A}) D_\mu^{AB} \chi^B . \quad (2.26)$$

From this Lagrange density we can derive Feynman rules with which we can translate Feynman diagrams into calculable amplitudes in an easy and straightforward way. The corresponding rules are assembled in Appendix B.

2.1.2. Regularization and renormalization procedure

One way to calculate physical quantities in the limit of weakly coupled QCD is the use of perturbative QCD (pQCD). In general one starts from the the free theory and gradually takes into account more and more interactions. So for example the full QCD quark propagator $S(p)$ takes the form

$$S(p) = S_0(p) + S_0(p)\Sigma(p)S_0(p) + S_0(p)\Sigma(p)S_0(p)\Sigma(p)S_0(p) + \dots , \quad (2.27)$$

where

$$S_0(p) = \frac{1}{(m - \not{p})} . \quad (2.28)$$

and the quark self-energy $\Sigma(p)$ which contribute to the full propagator

$$S(p) = \frac{1}{S_0^{-1} - \Sigma(p)} . \quad (2.29)$$

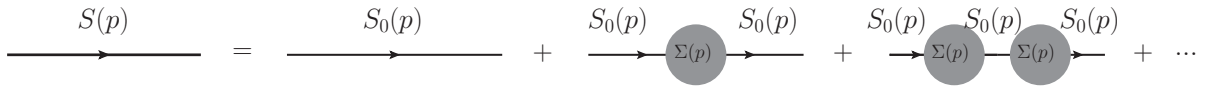


Figure 2.1.: Expansion of the quark propagator $S(p)$

When calculating the quark self energy one discovers the appearance of divergences at large momenta (ultraviolet divergences) due to the loop integration. For this reason we have to modify the calculation to ensure the convergence of the loop integrals. This can be achieved by regularizing the divergent integrals. Here we state the most common regularization methods and their properties.

- Cut-off regularization: One modifies the integration boundaries by allowing the momentum only to go up to some scale M ,

$$\int^{\infty} dq \rightarrow \int^M dq , \quad (2.30)$$

which breaks Lorentz invariance and is therefore not suitable

- Pauli-Villars regularization: Here one modifies the propagator

$$\frac{1}{m^2 - q^2 - i\epsilon} \rightarrow \frac{1}{m^2 - q^2 - i\epsilon} - \frac{1}{M^2 - q^2 - i\epsilon} \quad (2.31)$$

by introducing some artificial mass term, which unfortunately breaks gauge invariance.

- Dimensional regularization: In this scheme all loop integrations are performed in $D = 4 \pm 2\epsilon$ dimension.

A more detailed review and suitable references on the dimensional regularization approach is given in Appendix C. Now we are able to calculate loop corrections of all physical quantities in a straightforward way and represent all divergences by a series in ϵ . But a theory which gives only infinite quantities seems not to be the way to do it.

Therefore we will replace the QCD Lagrangian which is built of divergent or bare quantities like the masses, the coupling or the fields themselves by a renormalized Lagrange density in which all the infinite parameters are replaced by renormalized, i.e. finite quantities. The relation between the bare X_0 and renormalized X quantities is given by:

$$\Psi_0 = Z_\Psi^{1/2} \Psi \quad \text{quark field renormalization} \quad (2.32)$$

$$A_0 = Z_A^{1/2} A \quad \text{gauge field renormalization} \quad (2.33)$$

$$\chi_0 = Z_\chi^{1/2} \chi \quad \text{ghost field renormalization} \quad (2.34)$$

$$a_0 = Z_a^{1/2} a \quad \text{gauge fixing parameter renormalization} \quad (2.35)$$

$$g_0 = Z_g^{1/2} g \quad \text{coupling constant renormalization} \quad (2.36)$$

$$m_0 = Z_m^{1/2} m \quad \text{mass renormalization} . \quad (2.37)$$

The way to obtain the renormalization constants Z for each order of perturbation theory is to calculate the corresponding loop diagrams. For showcasing the renormalization procedure for the quark propagator we need all one particle irreducible loop corrections at a given order. To one loop order there is only one relevant Feynman diagram, which is shown in Fig. 2.2:

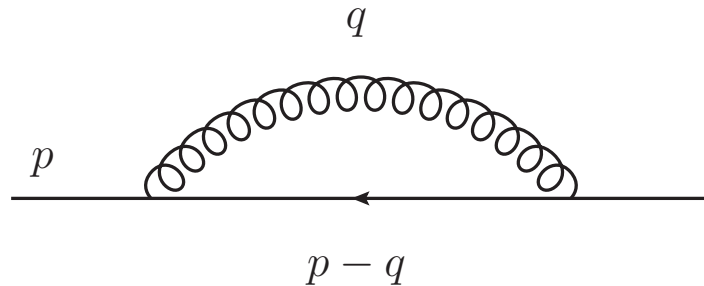


Figure 2.2.: Quark self energy $\Sigma(p)$ Feynman diagram

Using the Feynman rules from Appendix B for massless quarks we obtain:

$$\Sigma(p) = g^2 C_F \int \frac{d^D q}{(2\pi)^{D_i}} \frac{1}{(q-p)^2 q^2} \left(\gamma^\mu (\not{q} - \not{p}) \gamma_\mu - (1-a) \frac{\not{q}(\not{q} - \not{p})\not{q}}{q^2} \right). \quad (2.38)$$

And taking the color algebra from Appendix A into account:

$$C_F = T^A T^A = \frac{4}{3} \quad \text{for} \quad N = 3. \quad (2.39)$$

After using Feynman parametrization

$$\frac{1}{D_1 D_2} = \int_0^1 d\lambda \frac{1}{\lambda D_1 + (1-\lambda) D_2} \quad (2.40)$$

and applying Wick rotation we end up with

$$\Sigma(p) = a\alpha_S^2 C_F \not{p} \left(\frac{1}{\epsilon} - \gamma_E + 1 - \ln \frac{-p^2}{4\pi\mu^2} \right) + \mathcal{O}(\epsilon). \quad (2.41)$$

Here $\alpha_S = g^2/(4\pi)$ and γ_E is the Euler constant. Now we will illustrate the renormalization procedure for the case of the massless quark propagator. Inserting (2.41) into (2.29) the full propagator reads as

$$S(p) = -\frac{1}{\not{p}} \frac{1}{1 + \sigma(p^2)} \quad (2.42)$$

with

$$\sigma(p^2) = a\alpha_S^2 C_F \left(\frac{1}{\epsilon} - \gamma_E + 1 - \ln \frac{-p^2}{4\pi\mu^2} \right) + \mathcal{O}(\epsilon). \quad (2.43)$$

The easiest way to get rid off the divergences in (2.43) is to subtract them in the denominator:

$$S^R(p) = -\frac{1}{\not{p}} \frac{1}{1 + \sigma(p^2) - z_{\text{scheme}}}. \quad (2.44)$$

The constant z_{scheme} can be seen as the second term in a power series expansion in g^2 :

$$Z_\Psi = 1 - z_{\text{scheme}} \mathcal{O}(g^2) + \mathcal{O}(g^4). \quad (2.45)$$

Disregarding the terms proportional to ϵ we renormalize the quark propagator multiplicatively by the quark field renormalization constant Z_Ψ and obtain a finite – renormalized – quark field propagator $S^R(p)$:

$$S^R(p) = Z_\Psi^{-1} S(p). \quad (2.46)$$

The index “scheme” of z_{scheme} indicates that there are actually different ways of renormalizing a physical quantity, which are called renormalization schemes and differ by the subtraction prescription z_{scheme} :

$$z_{\text{OnS}} = \sigma(0) \quad \text{On-shell subtraction} \quad (2.47)$$

$$z_{\text{OffS}} = \sigma(p^2 = -\lambda^2 < 0) \quad \text{Off-shell subtraction} \quad (2.48)$$

$$z_{\text{MS}} = a\alpha_S^2 C_F \frac{1}{\epsilon} \quad \text{minimal subtraction} \quad (2.49)$$

$$z_{\overline{\text{MS}}} = a\alpha_S^2 C_F \left(\frac{1}{\epsilon} - \gamma_E + \ln(4\pi) \right) \quad \text{modified minimal subtraction} . \quad (2.50)$$

In principle this procedure can be applied to all parameters in the QCD Lagrangian, but we will only give the final results for the renormalization constants in the \overline{MS} scheme:

$$Z_\Psi = 1 - \frac{g_R^2}{(4\pi)^2} C_F \frac{1}{\epsilon} a_R + \mathcal{O}(g_R^4) \quad (2.51)$$

$$Z_A = 1 - \frac{g_R^2}{(4\pi)^2} \frac{1}{\epsilon} \left[\frac{4}{3} T_f n_f - \frac{1}{2} C_A \left(\frac{13}{3} - a_R \right) \right] + \mathcal{O}(g_R^4) \quad (2.52)$$

$$Z_\chi = 1 + \frac{g_R^2}{(4\pi)^2} C_A \frac{1}{\epsilon} \frac{(3 - a_R)}{4} + \mathcal{O}(g_R^4) \quad (2.53)$$

$$Z_m = 1 - \frac{g_R^2}{(4\pi)^2} C_F \frac{1}{\epsilon} (3 - a_R) + \frac{g_R^2}{(4\pi)^2} C_F \frac{1}{\epsilon} a_R + \mathcal{O}(g_R^4) \quad (2.54)$$

$$Z_g = 1 + \frac{g_R^2}{(4\pi)^2} \frac{1}{\epsilon} \left(\frac{1}{3} n_f - \frac{11}{2} \right) + \mathcal{O}(g_R^4) . \quad (2.55)$$

Note that Z_a , the renormalization constant of the gauge fixing parameter, is chosen to be the same as for the gauge field A_μ . The constant T_F is defined via:

$$\text{Tr}[T^A T^B] = T_F \delta^{AB} . \quad (2.56)$$

The renormalization scheme can be transformed into \overline{MS} scheme by simply replacing

$$\frac{1}{\epsilon} \rightarrow \frac{1}{\hat{\epsilon}} = \frac{1}{\epsilon} + \ln(4\pi) - \gamma_E . \quad (2.57)$$

With the constants in Eq. (2.51),..., (2.55) it is possible to reformulate the QCD Lagrangian to be free of divergences up to order $\mathcal{O}(g_S^2)$. So one could in principle redefine the corresponding Feynman rules and calculate finite quantities with those modified rules. But there is also the possibility to use the “old” Feynman rules containing only the bare parameters and subtract the divergences afterwards. This can be done by multiplying all external lines with the suitable renormalization constant. In this way it is possible to calculate the

renormalization constant for the coupling without calculating the actual diagrams. So for example the renormalization factor Z_Γ for the quark-gluon vertex depicted in Fig. 2.3

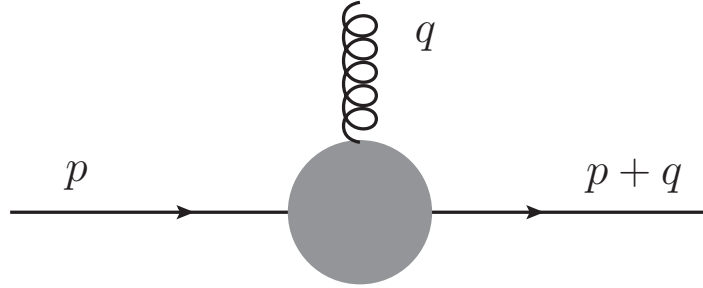


Figure 2.3.: Quark-gluon vertex Γ

can be calculated via:

$$Z_\Gamma = \frac{1}{Z_\Psi} \frac{1}{\sqrt{Z_{\alpha_S}} \sqrt{Z_A}} . \quad (2.58)$$

Here Z_{α_S} is the coupling renormalization constant which can be identified with Z_g via $\alpha_S = g^2/4\pi$.

2.1.3. Renormalization group equation

At the beginning of this section we stated that if we would assume a weakly coupled system we can expand quantities or amplitudes in a power series in the coupling g or α_S , respectively. In the following we show why we are allowed to do so. Here we use the \overline{MS} -scheme.

One can show that the renormalization constant Z_{α_S} to one loop accuracy reads as

$$Z_{\alpha_S} = 1 - \left(\frac{11}{3} C_A - \frac{4}{3} T_F n_f \right) \frac{\alpha_S}{4\pi\epsilon} . \quad (2.59)$$

Here n_f is the number of flavors. The bare coupling g is related to the renormalized via

$$g = Z_{\alpha_S}^{1/2} g_R . \quad (2.60)$$

The running coupling can be written as

$$\frac{\alpha_S(\mu)}{4\pi} = \mu^{-2\epsilon} \frac{g_R^2}{(4\pi)^{D/2}} e^{\gamma_E} \quad (2.61)$$

and with Eq. (2.60) we end up with:

$$\frac{g^2}{(4\pi)^{D/2}} = \mu^{-2\epsilon} \frac{\alpha_S(\mu)}{4\pi} Z_{\alpha_S}(\mu) e^{\gamma_E} . \quad (2.62)$$

The renormalization group equation reads as:

$$\frac{d \log \alpha_S(\mu)}{d \log(\mu)} = -2\beta\alpha_S(\mu) . \quad (2.63)$$

The QCD β -function to one-loop accuracy gives:

$$\beta(\alpha_S) = \beta_0 \frac{\alpha_S}{4\pi} + \dots . \quad (2.64)$$

Here the first coefficient of the series reads as:

$$\beta_0 = \frac{11}{3} C_A - \frac{4}{3} T_F n_f . \quad (2.65)$$

The theory becomes asymptotically free as long as $\beta_0 > 0$, so for $n_f < 33/2$. The solution of the Eq. (2.63) leads to:

$$\alpha_S(\mu) = \frac{2\pi}{\beta_0 \log \frac{\mu}{\Lambda_{QCD}}} . \quad (2.66)$$

Here Λ_{QCD} is the scale of QCD. In the limit $\mu \gg \Lambda_{QCD}$ perturbation theory can be applied.

2.2. Nucleon form factors

Form factors encode the information of a strongly coupled many body system in a huge variety of scattering processes. With the help of form factors one can parametrize cross sections for diverse elastic and inelastic processes. Since we are interested in the distribution of charge and magnetization inside the nucleons we scatter high energy electrons elastically on the protons and neutrons. There are two different experimental approaches, the Rosenbluth separation method and polarization transfer technique, which we will discuss in this chapter.

2.2.1. History of nucleon form factors

In order to give a brief historical overview of the developments in the last decades we will follow the review of Perdrisat et al. [7]. We will illustrate the progression in the field of

nucleon form factors from first theoretical efforts in the wide field of elastic scatterings up to state of the art experimental approaches and results. At the beginning of the 20th century Ernest Rutherford was the first to show the internal structure of atoms via elastic scattering of atomic particles. Due to elastic scattering of α -particles on different targets he could identify the structure of helium nuclei. In the following years the experiments yield to the discovery of the proton. Rutherford was also the first who proposed the neutron which was discovered in 1932 by James Chadwick. All these enormous efforts in the field of subatomic physics are consequences of the Rutherford cross section formula

$$\left(\frac{d\sigma}{d\Omega}\right)_{\text{Ruth}} = \frac{Z_1 Z_2 \alpha}{4E_{\text{kin}}} \frac{1}{\sin^4(\theta/2)} \quad (2.67)$$

which describes the scattering of two pointlike particles. Here Z_i are the atomic numbers of target and projectile, $\alpha = e^2/(4\pi)$ is the fine-structure constant, θ is the scattering angle, $\beta = v$ and E_{kin} the kinetic energy of the projectile. Mott modified the Rutherford formula

$$\left(\frac{d\sigma}{d\Omega}\right)_{\text{Mott}} = \left(\frac{d\sigma}{d\Omega}\right)_{\text{Ruth}} \cdot (1 - \beta^2 \sin^2(\theta/2)) \quad (2.68)$$

in order to describe the scattering two pointlike particles where one of them has spin-1/2. Although the discovery of the internal structure of atoms was a huge effort of experimental physics, it was already in 1933 when Stern measured the magnetic moment of the proton and showed that it was 2.8-times bigger than expected for a pointlike spin-1/2 particle. But it took almost 20 years before in 1950 Rosenbluth [28] gave a formula for the scattering of high energy electrons and protons, which leads to modification of the proton charge and anomalous magnetic moment.

$$\sigma = \left(\frac{e'e''}{2E}\right)^2 \cot\left(\frac{\theta}{2}\right) \csc^2\left(\frac{\theta}{2}\right) \frac{1 + 2\gamma \sin^2(\frac{\theta}{2}) + \gamma^2 \sin^2(\frac{\theta}{2}) [2(1 + \kappa')^2 \tan^2(\frac{\theta}{2}) + \kappa'^2]}{[1 + 2\gamma]^2 \sin^2(\frac{\theta}{2})}. \quad (2.69)$$

Here e'' and e' are the effective charges of the electron and the proton. κ' is the effective anomalous moment of the proton and $\gamma = E/M$ being the energy of the incident electron E divided by the rest mass of the proton M . In this paper Rosenbluth, proposed that at high enough energy 50 MeV and appropriate angles the structure of the meson cloud associated with the proton should be experimentally accessible.

At the beginning of the 1950s the Stanford linear accelerator (SLAC) program was started to resolve the inner structure within the nuclei. In 1953 the group around Hofstadter

[3] could detect – via elastic scattering of electrons on a gold foil – a deviation from the scattering behavior of the pointlike target.

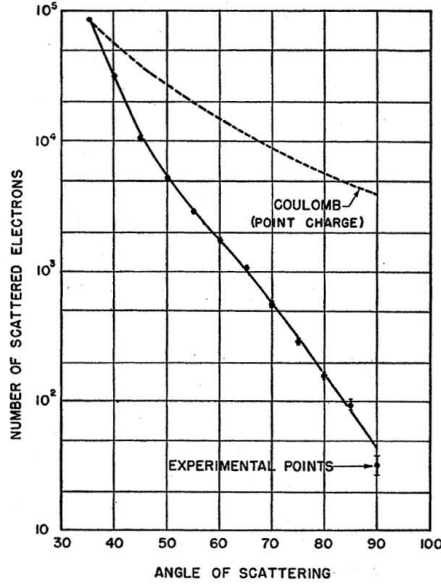


Figure 2.4.: Typical angular distribution obtained at 116 MeV with a 0.000051 m gold foil. The gold foil was oriented at 45 degrees with respect to the incident beam for all angular settings of the spectrometer magnet. Picture taken from [3]

The first who introduced the concept of form factors as the internal charge density distribution in context of the elastic scattering of electrons on a proton (hydrogen target) were Hofstadter and McAllister in the year 1955 [29]. One year later Hofstadter gave the first systematic work about electron scattering and nuclear structure [30] in which he defines the form factor or structure function for the first time.

$$\sigma(\theta) = \sigma_{\text{Mott}} \left| \int \rho(\vec{r}) e^{i\vec{q} \cdot \vec{r}} d^3\vec{r} \right|^2 = \sigma_{\text{Mott}} |F(q)|^2. \quad (2.70)$$

Here θ is the scattering angle, \vec{q} the momentum transfer, $q = |\vec{q}|$ and $\rho(\vec{r})$ the charge density. The first work on probing the internal structure of the nuclei with different models for the charge density was done by McAllister et al. [31]. In fact there have been a huge

variety of charge distributions tried in order to match the experimental results. So for example the connection between spherical-symmetrical charge densities with radius a and the form factor in Born approximation [32]:

| | Form factor $F(q^2)$ | charge density | |
|----------|----------------------|--------------------------------------|-------------|
| constant | 1 | $\delta(r)/(4\pi)$ | point |
| dipole | $(1 + q^2/a^2)^{-2}$ | $(a^3/(8\pi)) \exp(-ar)$ | exponential |
| Gaussian | $\exp(-q^2/2a^2)$ | $(a^2/(2\pi))^{3/2} \exp(-a^2r^2/2)$ | Gaussian |

2.2.2. From scattering amplitudes to matrix elements

As mentioned in the section before Hofstadter et al. were the first who generalized the concept of effective charge and magnetic moment by connecting the first to the deviation from a point like charged particle and the second with the difference to a point like anomalous magnetic moment. These two deviations are associated with the Dirac form factor F_1 and the Pauli form factor F_2 . In lowest order the scattering of an electron and a proton in the single photon exchange picture corresponds to the Feynman diagram in Fig. 2.5.

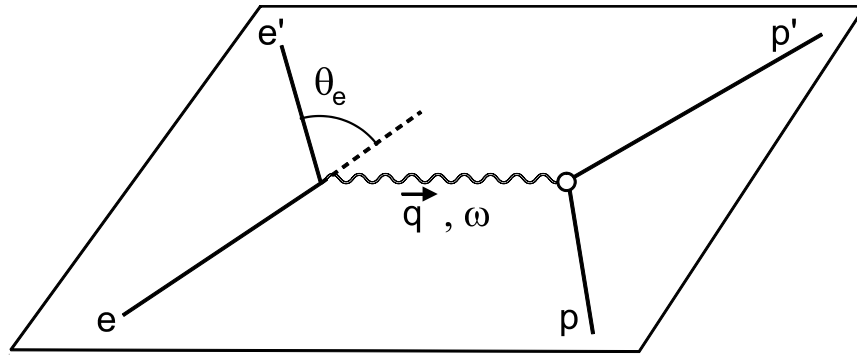


Figure 2.5.: Feynman diagram for elastic electron-proton scattering in leading order. Picture taken from [7].

The invariant mass q^2 of the virtual photon can be defined in the t -channel as:

$$\begin{aligned}
 q^2 = t &= (p_e - p_{e'})^2 = 2m_e^2 + 2|\vec{p}_e||\vec{p}_{e'}| \cos(\theta) - E_e E_{e'} \\
 &\approx -2(1 - \cos(\theta))E_e E_{e'} \\
 &= -4 \sin^2(\theta/2)E_e E_{e'}.
 \end{aligned} \tag{2.71}$$

Here $p_e = (E_e, \vec{p}_e)$ and $p_{e'} = (E_{e'}, \vec{p}_{e'})$ are the four-momenta of the initial (beam) electron and the final (scattered) electron and t is one of the Mandelstam variables, which can be found in Appendix D. In the last two steps we neglect the electron mass m_e and use the identity $1 - \cos(x) = 2 \sin^2(x/2)$. Since E_e , $E_{e'}$ and $\sin(\theta/2)^2$ are always positive the virtuality of the photon in the t channel scattering is always negative. It is convenient to define a positive momentum transfer:

$$Q^2 = -q^2 . \quad (2.72)$$

The s channel scattering leads to a positive momentum transfer $q^2 > 0$. Form factors associated with $q^2 < 0$ are called space-like form factors and for positive momentum transfer the form factors are called time-like. The major difference between the two channels lies in the decay width. The t channel decay width is much larger than the decay width of the s channel due to the fact that the probability for the decay $\gamma \rightarrow p + \bar{p}$ is very small. Using the definition of transition matrix elements (i and f are denoting the final and initial state and \mathcal{H}_{int} the interaction Hamiltonian)

$$\mathcal{M}_{\text{fi}} = \langle \psi_f | \mathcal{H}_{\text{int}} | \psi_i \rangle = \int \Psi_f^* \mathcal{H}_{\text{int}} \Psi_i dV . \quad (2.73)$$

In order to connect the amplitude \mathcal{M}_{fi} in (2.73) with an experimental accessible quantity like the differential cross section $d\sigma$ we will briefly recap a few basic correlations which can be found in all textbooks about particle physics, for example [33] or [32], which we follow. Scattering processes provide informations about the interaction potential and the coupling constant. Necessary input parameters are the reaction rate, angular distribution and energy distribution of the participating particles. A crucial quantity for describing the dynamics of the aforementioned processes is the so called cross section which is a measure for the probability of an interaction between the projectile and the target. Now we will introduce the quantities needed to define the cross section.

N_a = number of beam particles

N_b = number of targets

n_a = projectile density

n_b = target density

Φ_a = flux

σ_b = scattering area of one target

A = area cross-section of the beam

\dot{N} = number of interactions per time .

The flux Φ_a is defined as

$$\Phi_a = \frac{\dot{N}_a}{A} = v_a \cdot n_a . \quad (2.74)$$

Here v_a is the velocity of the beam particles. The geometric cross section for a beam which is homogeneous and constant over time is defined as:

$$\sigma_b = \frac{\dot{N}}{\Phi_a \times N_b} = \frac{\text{number of reactions per time}}{\text{number of beam-particles per time and area} \times \text{number of targets}} . \quad (2.75)$$

Although the geometric cross section is a good approximation it became obvious that the geometry of the particles is not sufficient to describe the experimental data. The geometric cross section is a good approximation for high energetic proton-proton scattering since the geometric size of the proton is comparable to the range of interaction. But for a lot of other processes, for example electron-proton scattering, the geometric cross section does not give exact results. So for collider experiments a slightly modified cross section, which takes non homogeneous beams and a constant area density of targets into account, is needed: the total cross section σ_{tot} :

$$\sigma_{\text{tot}} = \frac{\text{number of reactions per time unit}}{\text{number of beam particles per time} \times \text{number of targets per area unit}} . \quad (2.76)$$

In practice not all of the reactions of a given process are measured but only the scattering under certain angles θ is detected. Therefore we introduce the differential cross section

$$\frac{d\sigma(E, \theta)}{d\Omega} = \frac{\dot{N}(E, \theta, \Delta\Omega)}{\Delta\Omega} \frac{1}{\mathcal{L}} \quad (2.77)$$

which depends on the energy E and is differentiated by the solid angle element $d\Omega$. Here $\mathcal{L} = \Phi_a N_b$ is the luminosity and $\Delta\Omega = A_D/r^2$ solid angle element. If one integrates over all solid angles and up to the maximal allowed energy one reproduces the total cross section.

$$\sigma_{\text{tot}}(E) = \int_0^{E'_{\text{max}}} dE' \int_{4\pi} d\Omega \frac{d^2\sigma(E, E', \theta)}{d\Omega dE'} . \quad (2.78)$$

If we assume the spin of the particles does not change during the process the number of possible final states $n(E')$ gives for the density of final states:

$$\rho(E') = \frac{dn(E')}{dE'} = \frac{V 4\pi E'}{(2\pi)^3} . \quad (2.79)$$

The factor of $(2\pi)^3$ is due to the volume a particle needs in the six-dimensional phase-space. Using Fermi's golden rule we can connect the reaction rate W per target particle to the amplitude \mathcal{M}_{fi} via:

$$W = 2\pi \cdot |\mathcal{M}_{fi}| \cdot \rho(E') . \quad (2.80)$$

Remembering (2.76) we can also associate the reaction rate with the total cross section

$$W = \frac{dN/dt}{N_a \cdot N_b} = \frac{\sigma \cdot v_a}{V} \quad (2.81)$$

and we end up with

$$\sigma = \frac{2\pi}{v_a} |\mathcal{M}_{fi}|^2 \cdot \frac{dn(E')}{dE'} \cdot V . \quad (2.82)$$

The Feynman diagram in Fig. 2.5 can be translated, using Feynman gauge, into the following expression:

$$-i\mathcal{M}_{\text{tot}} = \frac{i}{q^2} l_\mu \mathcal{J}^\mu = \frac{-ig_{\mu\nu}}{q^2} [ie\bar{u}(p_e)\gamma^\nu u(p_{e'})] [-ie\bar{N}(p')\Gamma^\mu(p', p)N(p)] . \quad (2.83)$$

The amplitude \mathcal{M}_{tot} is a product of a four dimensional leptonic l_μ and hadronic \mathcal{J}_μ current. Here u and N are the electron and proton spinors, respectively, p and p' are the momenta of the incident and scattered proton and Γ_μ contains informations about the structure of the nucleon. The most generic parameterization for the hadronic part of Eq. (2.83) is illustrated in Fig. 2.6

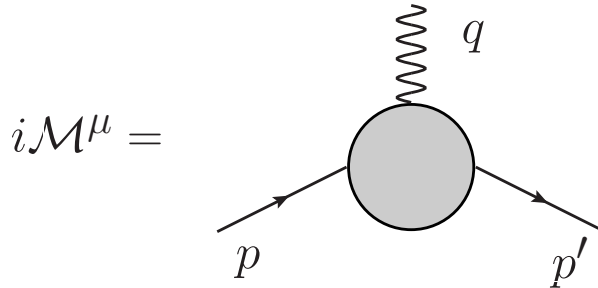


Figure 2.6.: Feynman diagram for the one photon exchange for arbitrary loop order

and can be decomposed, including all possible Lorentz vectors, as:

$$i\mathcal{M}^\mu = \bar{N}(p')(\mathcal{F}_1 \gamma^\mu + \mathcal{F}_2 q^\mu + \mathcal{F}_3 p^\mu + \mathcal{F}_4 p'^\mu)N(p) . \quad (2.84)$$

Here the coefficient functions \mathcal{F}_i are unknown functions which depend only on contracted momenta:

$$p \cdot q, p' \cdot q, p \cdot p', q \cdot q, \not{p} \text{ or } \not{q} . \quad (2.85)$$

Not all of the \mathcal{F}_i 's are independent. Using four momentum conservation $q = p' - p$ we can immediately get rid of the q^μ term and therefore set \mathcal{F}_2 to zero. Since we have on shell external spinors we can remove all terms in the \mathcal{F}_i which are proportional to \not{p} or \not{p}' due to the Dirac equation:

$$\not{p}N(p) = mN(p) \quad \bar{N}(p')\not{p}' = m\bar{N}(p') . \quad (2.86)$$

The real functions \mathcal{F}_i can only depend on

$$q^2 = 2m^2 - 2p \cdot p' \quad \text{and} \quad m^2 \quad (2.87)$$

and therefore are functions of q^2/m^2 . Using the Ward identity

$$q^\mu \mathcal{M}_\mu(q, p, p') = 0 \quad (2.88)$$

our remaining expression reads:

$$q^\mu \bar{N}(p') (\mathcal{F}_1 \gamma_\mu + \mathcal{F}_3 p_\mu + \mathcal{F}_4 p'_\mu) N(p) = 0 . \quad (2.89)$$

Once again the Dirac equation comes in handy to get rid of \mathcal{F}_1 due to:

$$\mathcal{F}_1 \bar{N}(p') \not{q} N(p) = \mathcal{F}_1 \bar{N}(p') (\not{p}' - \not{p}) N(p) = 0 . \quad (2.90)$$

Now we are left with only two Lorentz scalars \mathcal{F}_3 and \mathcal{F}_4 . Using $q = p' - p$

$$\begin{aligned} p \cdot q &= p \cdot p' - m^2 \\ p' \cdot q &= m^2 - p \cdot p' \end{aligned} \quad (2.91)$$

which leads to

$$q \cdot p = -q \cdot p' \quad (2.92)$$

and therefore

$$\mathcal{F}_3 q \cdot p + \mathcal{F}_4 q \cdot p' = 0 \rightarrow \mathcal{F}_3 = \mathcal{F}_4 . \quad (2.93)$$

Using the Gordon identity for on shell spinors

$$\bar{N}(p') \gamma^\mu N(p) = \bar{N}(p') \left[\frac{(p' + p)^\mu}{2m} + \frac{i\sigma^{\mu\nu} (p' - p)_\nu}{2m} \right] N(p) \quad (2.94)$$

and applying the restriction of the \mathcal{F}_i from above to Eq. (2.84) we obtain:

$$\mathcal{J}^\mu = \bar{N}(p') \left[\gamma^\mu F_1(Q^2) + \frac{i\sigma^{\mu\nu} q_\nu}{2M} F_2(Q^2) \right] N(p) . \quad (2.95)$$

This is the most generic form of the hadronic current respecting relativistic invariance and current conservation for scattering an electron on a proton with internal structure. Combining Eq. (2.82), Eq. (2.83) and Eq. (2.95) we can formulate the expression for the lab cross section:

$$\frac{d\sigma}{d\Omega} = \frac{|\mathcal{M}_{\text{tot}}|^2}{64\pi^2} \left(\frac{E_2}{E_1} \right)^2 \frac{1}{M} \quad \text{with} \quad |\mathcal{M}_{\text{tot}}|^2 = \frac{1}{Q^4} |l \cdot \mathcal{J}|^2, \quad (2.96)$$

The standard form of the laboratory frame differential cross section for the elastic electron nucleon scattering takes the form:

$$\frac{d\sigma}{d\Omega} = \left(\frac{d\sigma}{d\Omega} \right)_{\text{Mott}} \frac{E_{e'}}{E_e} \left\{ F_1^2(Q^2) + \tau \left[F_2^2(Q^2) + 2(F_1(Q^2) + F_2(Q^2))^2 \tan^2 \frac{\theta}{2} \right] \right\} . \quad (2.97)$$

With $\tau = \frac{Q^2}{4M^2}$. The functions F_1 and F_2 are the aforementioned Dirac and Pauli form factors which only depend on the momentum transfer and are real functions for the case of single photon exchange processes .

In the forward limit with zero momentum transfer the Dirac and Pauli form factors are:

$$\begin{aligned} F_{1p}(0) &= 1, & F_{2p}(0) &= \kappa_p = \mu_p - 1 = 1.7928, \\ F_{1n}(0) &= 0, & F_{2n}(0) &= \kappa_n = \mu_n = -1.9130. \end{aligned}$$

Here n denotes the neutron form factor and p the proton case. The anomalous magnetic moments κ are given in units of the nuclear magneton $\mu_N = \frac{e\hbar}{2m_N}$. The magnetic moment for a current distribution \vec{j} is defined via:

$$\vec{\mu} = \frac{1}{2} \int d^3r \vec{r} \times \vec{j}(\vec{r}) . \quad (2.98)$$

For a particle with intrinsic angular momentum \vec{L} and spin \vec{S} one can also define a magnetic moment as:

$$\vec{\mu} = (g_L \vec{L} + g_S \vec{S}) \mu_N . \quad (2.99)$$

Here $\mu_N = \frac{e}{2M}$ is the magneton of the nucleon. For the total angular momentum $\vec{I} = \vec{L} + \vec{S}$ the magnetic moment reads as:

$$\vec{\mu}_I = \mu_K g_I \vec{I} . \quad (2.100)$$

The anomalous magnetic moment is the difference between only taking the born approximation into account and also considering corrections due to quantum field theory effects. Note that in principle one can define several g factors or magnetic moments depending on which angular momentum one takes into account (e.g. spin angular momentum, orbital angular momentum or the total angular momentum also called the Landé g -factor). The Dirac equation predicts a spin angular momentum g factor for the electron of $g = 2$. Through experiments and QED calculations we know, that this value does not hold, which is due to loop corrections. The most precise value of the g -factor of the electron is [34]:

$$\frac{g - 2}{2} = (1159.65218076 \pm 0.00000027) \cdot 10^{-6} . \quad (2.101)$$

In the next section we will dedicate ourselves to experimental techniques to solve the inner structure of the nucleons. For this it is necessary to introduce a new set of electromagnetic form factors which make it possible to decouple the magnetic and electric information encoded in the form factors from each other. This can be achieved due to the so called Sachs form factors, which can be expressed through the Dirac and Pauli form factors in the following way:

$$G_E = F_1 - \tau F_2 \quad \text{and} \quad G_M = F_1 + F_2 . \quad (2.102)$$

We can now write the differential cross section (2.97) in a simpler form

$$\frac{d\sigma}{d\Omega} = \left(\frac{\alpha}{2E_{e'} \sin(\frac{\theta_e}{2})} \right)^2 \frac{E_e}{E_{e'}} \left(\frac{\cot^2(\frac{\theta_e}{2})}{1 + \tau} [G_E^2 + \tau G_M^2] + 2\tau G_M^2 \right) . \quad (2.103)$$

The big advantage of this parameterization of the scattering matrix element is that we do not have any interference term left. At zero momentum transfer the electric and magnetic Sachs form factors G_E and G_M read:

$$\begin{aligned} G_{Ep}(0) &= 1 , & G_{Mp}(0) &= \mu_p , \\ G_{En}(0) &= 0 , & G_{Mn}(0) &= \mu_n . \end{aligned}$$

2.2.3. Experimental point of view

Now we will give a brief insight on experimental approaches. We mainly will follow the reviews [4, 7]. The first measurements which gave rise to the question of the underlying structure of the nucleons were the experiments of Stern in 1933. He measured the

anomalous magnetic moment of the proton and found that it was bigger than expected for the proton viewed at this time. In the 1950s Hofstadter et al. made the first elastic electron scattering experiments at the Stanford linear accelerator. At the beginning they use solid targets like gold, beryllium and carbon [3] to obtain curves for different angles and energies of the incident electron. Later they used gaseous probes like hydrogen [29] and helium probes [30] as scattering targets. In the 1970s a lot of accelerator projects were finished and a huge amount of data was collected. The scattering of electron on protons and neutrons were interpreted with the Rosenbluth approach. In the early 90s huge efforts using polarization transfer experiments to probe the inner structure of the nucleons were made.

In the following section we will present a short introduction in the techniques used in the last decades to obtain values for the electric and magnetic form factors of the nucleons. First we will describe the concepts of Rosenbluth separation method and afterwards give a brief insight on polarization transfer methods. Note that we will mainly focus on the proton, because of the much more complicated structure of deuteron and Helium targets, which are mainly used to obtain experimental results for the neutron form factors.

Rosenbluth cross section separation method

In the 1970 the construction of whole a bunch of accelerators was completed and they started to collect data by measuring $G_{Ep,n}$ and $G_{Mp,n}$ via elastic electron-proton and electron-deuteron scattering processes. The method they used is called the Rosenbluth cross section separation method [28]. This technique allowed the measurement of separate values of G_E and G_M and not only their ratio. The cross section for elastic electron-nucleon scattering can be written as:

$$\frac{d\sigma}{d\Omega} = \left(\frac{d\sigma}{d\Omega} \right)_{\text{Mott}} \left[\frac{G_E^2(Q^2) + \tau G_M^2(Q^2)}{1 + \tau} + 2\tau G_M^2(Q^2) \tan^2(\theta/2) \right]. \quad (2.104)$$

This can be re-written as

$$\frac{d\sigma}{d\Omega} = \left(\frac{d\sigma}{d\Omega} \right)_{\text{Mott}} \frac{\tau}{\epsilon(1 + \tau)} \left[G_M^2 + \frac{\epsilon}{\tau} G_M^2 \right], \quad (2.105)$$

where $\epsilon = 1/(1 + 2(1 + \tau) \tan^2(\theta_e/2))$ is the polarization of the exchanged virtual photon, $\tau = \frac{Q^2}{4M^2}$ and $\left(\frac{d\sigma}{d\Omega} \right)_{\text{Mott}}$ the differential Mott cross section. For $M \rightarrow \infty$ which means neglecting the recoil of the target the cross section can be formulated as:

$$\sigma_{\text{Mott}} = \frac{e^4 \cos^2(\theta/2)}{4E^2 \sin^4(\theta/2)}. \quad (2.106)$$

Note that the cross section for a scattering with recoil would take the form

$$\sigma_{\text{Mott}} = \frac{e^4 E' \cos^2(\theta/2)}{4E^3 \sin^4(\theta/2)}. \quad (2.107)$$

The modern form of the Rosenbluth formula only depends linearly on the parameter ϵ :

$$\left(\frac{d\sigma}{d\Omega}\right)_{\text{reduced}} = \frac{\epsilon(1+\tau)}{\tau} \left(\frac{d\sigma}{d\Omega}\right)_{\text{measured}} \bigg/ \left(\frac{d\sigma}{d\Omega}\right)_{\text{Mott}} = G_M^2 + \frac{\epsilon}{\tau} G_E^2. \quad (2.108)$$

Now the measurement is taken at a fixed value of Q^2 while varying the beam energy and the scattering angle over a reasonable range of values. A linear fit of $\left(\frac{d\sigma}{d\Omega}\right)_{\text{reduced}}$ gives separate values for $\frac{1}{\tau}G_E^2$ as the slope and G_M^2 as the intercept. Now one can repeat this procedure for a feasible range of Q^2 values for all form factors. By scaling them in the appropriate way it is possible to fit all of them, except for the electric neutron form factor, by a dipole fit [32]. The electric neutron form factor is small compared to the other three form factors. In this context the dipole form factor is defined as:

$$G_D = \frac{1}{(1 + Q^2/(0.71 \text{ GeV}^2))^2} \quad \text{with} \quad G_{Ep} = G_D, \quad G_{Mp} = \mu_p G_D, \quad \text{and} \quad G_{Mn} = \mu_n G_D. \quad (2.109)$$

Here $\mu_p = 2.79\mu_N$ and $\mu_n = -1.91\mu_N$. Most of the results obtained via the Rosenbluth separation method are normalised to this dipole form factor.

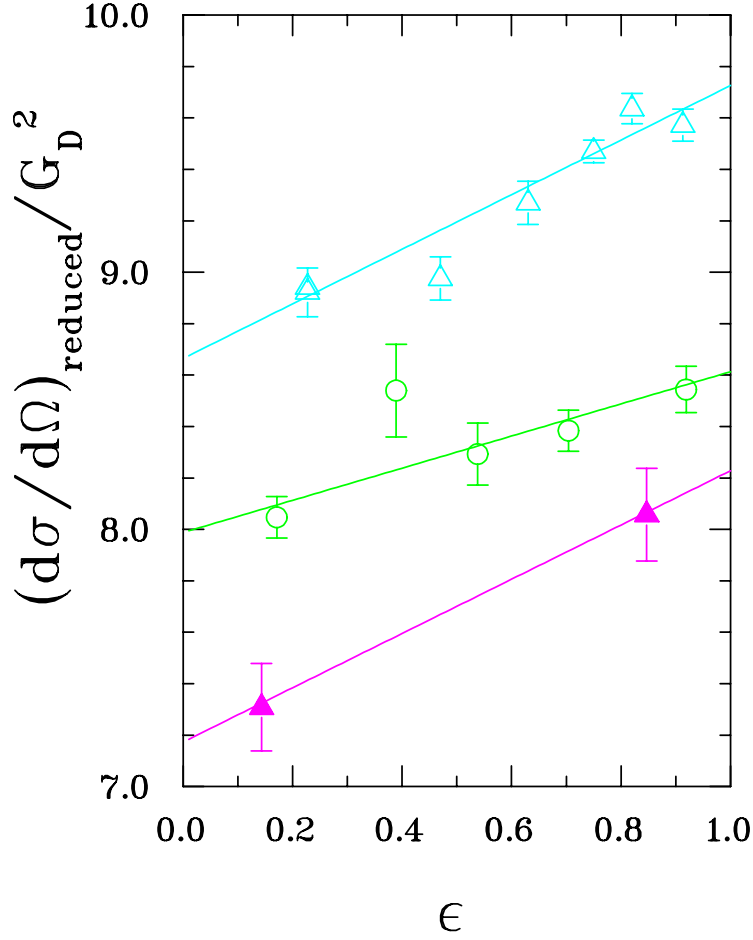


Figure 2.7.: Example for the Rosenbluth separation method for $Q^2 = 2.5, 5.0, 7.0 \text{ GeV}^2$ (open triangle, circle and filled triangle) of the proton. Values for $1/\tau \cdot G_{Ep}^2$ and G_{Mp}^2 can be extracted from the slope and the intercept, respectively. The data is provided by [14]. Picture taken from [7]

The main disadvantages of this technique are:

- For large Q^2 the part proportional to τG_M^p in Eq. (2.108) becomes dominant and it is impossible to obtain any information on G_E^p .
- And even for small Q^2 the electric form factor is suppressed by a factor of μ_p^2 .

Note that the neutron form factors are much more complicated to measure. Due to the fact that they had to be measured mainly by electron-deuteron scattering one needs three form factors: The charge, quadrupole and magnetic distribution. The most complicated form factor to obtain experimentally is the electric neutron form factor, because it is non zero only at high Q^2 .

Polarization transfer technique

Up to the early 90s the Rosenbluth separation method was the only available technique to obtain independent values for the electric and magnetic form factors of the nucleon. Experiments like the Continuous Electron Beam Accelerator Facility (CEBAF) at the Jefferson national laboratory (JLab) and Bates Linear Accelerator in Middleton, with their polarized electron beams, paved the way to prove the ideas of polarization transfer measurement in experiments. For the upcoming overview we will follow the work of Dombey [35], Swartz [36], Arnold et al. [37] and Perdrisat [7]. Note that the fundamental paper which is usually associated with polarization transfer is the work of Alkhiezer et al. [38]. The polarization $\vec{\mathcal{P}}$ of an ensemble of particles can be written in the following way:

$$\vec{\mathcal{P}} = f(\hat{s})\hat{s} . \quad (2.110)$$

Here \hat{s} is the particles spin in the rest frame and the function f is defined as:

$$f(\hat{n}) = \frac{N(\text{spins parallel to } \hat{n}) - N(\text{spins anti-parallel to } \hat{n})}{N(\text{spins parallel to } \hat{n}) + N(\text{spins anti-parallel to } \hat{n})} . \quad (2.111)$$

A fermion with spin vector \hat{s} being collinear to the direction of travel is called longitudinally polarized and if \hat{s} is orthogonal to the direction of travel it is transversely polarized. If the spin vector \hat{s} is oriented parallel or anti-parallel to the momentum direction the particle is in a right handed or left handed helicity eigenstate, respectively. The process we are interested in is the elastic scattering of electrons on nucleons with corresponding polarizations τ and λ and momenta k and p :

$$e(k, \tau) + N(p, \lambda) \rightarrow e(k', \tau') + N(p', \lambda') . \quad (2.112)$$

The appropriate matrix element for the scattering of a polarized electron and a polarized proton can be written as

$$\mathcal{M}_{\text{tot}} = \frac{ie^2}{Q^2} \langle k', \tau' | j^\mu | k, \tau \rangle \langle P', \lambda' | \mathcal{J}_\mu | P, \lambda \rangle . \quad (2.113)$$

The squared matrix element in the one-photon exchange limit reads:

$$|\mathcal{M}_{\text{tot}}|^2 = \frac{e^2}{q^2} L^{\mu\nu} T_{\mu\nu} . \quad (2.114)$$

The leptonic part of Eq. (2.114)

$$L_{\mu\nu} = \frac{e^2}{2q^2} \sum_{\tau\tau'} \langle k', \tau' | j_\mu | k, \tau \rangle^* \langle k', \tau' | j_\nu | k, \tau \rangle \quad (2.115)$$

and the hadronic part of (2.114)

$$T_{\mu\nu} = \frac{1}{2} \sum_{\tau\tau'} \langle P', \lambda' | \mathcal{J}_\mu | P, \lambda \rangle^* \langle P', \lambda' | \mathcal{J}_\nu | P, \lambda \rangle \quad (2.116)$$

are understood as averaged over initial und summed over final state's spins. The leptonic tensor in Eq. (2.115) for a polarized electron in the initial state takes the form:

$$L^{\mu\nu} = \frac{1}{k^2} (k'^\mu k^\nu + k^\mu k'^\nu - k \cdot k' q^{\mu\nu} + ia\epsilon^{\mu\nu\rho\sigma} k_\rho k_\sigma) . \quad (2.117)$$

Here a is the polarization of the incident electron which we have assumed to be massless. Note that the polarization ϵ of the photon, when assumed to be real, is defined via:

$$\frac{1 + \epsilon}{1 - \epsilon} = L_{11} = \frac{1}{2} \left(1 + \frac{q^2}{|\vec{q}|^2} \cot(\theta/2) \right) . \quad (2.118)$$

For a virtual photon with $q = k - k' = P' - P$ where $q_0 = 0$ and $\vec{q} = \vec{P}$ we can define:

$$\frac{1 + \epsilon}{1 - \epsilon} = \csc(\theta_B/2) . \quad (2.119)$$

Here θ_B is the scattering angle in the Breit frame and can be associated with the scattering angle in the laboratory frame θ via $\tau = Q^2/(4M^2)$:

$$\frac{\cot(\theta/2)^2}{1 + \tau} = \cot(\theta_B/2)^2 . \quad (2.120)$$

The hadronic tensor can be written as sum over unpolarized protons, initial proton is polarized, final proton is polarized and both protons are polarized part:

$$T_{\mu\nu} = T_{\mu\nu}^{\text{NP}} + T_{\mu\nu}(\mathbf{P}_\lambda) + T_{\mu\nu}(\mathbf{P}'_\lambda) + T_{\mu\nu}(\mathbf{P}_\lambda, \mathbf{P}'_\lambda) . \quad (2.121)$$

Here $\mathbf{P}_\lambda, \mathbf{P}'_\lambda$ denote the polarization of the initial and final proton state. The components for a unpolarized proton in the initial state reads as [35]:

$$T_{11} = T_{22} = q^2 G_M^2, \quad T_{00} = -4M^2 G_E^2, \quad (2.122)$$

$$T_{33} = 0, \quad T_{\mu\nu} = 0 \text{ for } \mu \neq \nu . \quad (2.123)$$

Now we have different options for our starting conditions, i.e. which of the participating particles is considered to be polarized. Assuming \vec{q} is along the z -axis we obtain for the scattering of a longitudinally polarized electron (positive helicity) off an unpolarized proton the following expression:

$$L^{\mu\nu}T_{\mu\nu} = \frac{1}{2}(q^2G_M^2(2 + \cot(\theta_B/2)^2) + 4M^2G_E^2 \cot(\theta_B/2)^2) . \quad (2.124)$$

The polarization of the recoiled proton, which has only two allowed components, a transverse P_x and a longitudinal P_z , can be measured by a second scattering process. Transforming Eq. (2.124) from the center of mass into the laboratory frame we can write down the components of the polarization vector, \mathbf{P}'_λ of the recoiled proton [37]:

$$I_0P'_{\lambda x} \sim -G_E(Q^2)G_M(Q^2) \tan \frac{\theta_e}{2} \quad (2.125)$$

$$I_0P'_{\lambda z} \sim G_M(Q^2)^2 \tan^2 \frac{\theta_e}{2} \quad (2.126)$$

with

$$I_0 = G_E^2(Q^2) + \frac{\tau}{\epsilon}G_M^2(Q^2) .$$

Combining Eq. (2.125) and (2.126) one can directly determine the ratio of G_E/G_M by only measuring the polarization of the recoil proton:

$$\frac{G_E}{G_M} = -\frac{P_x}{P_z} \frac{(E_{\text{beam}} + E_e)}{2M} \tan \left(\frac{\theta_e}{2} \right). \quad (2.127)$$

In Appendix E a compilation of experimental result will be presented.

2.3. Factorization and the concept of distribution amplitudes

In this section we will give a short introduction into the field of factorization. Since QCD is an asymptotically free gauge theory, which means that the coupling $\alpha_S(Q^2)$ becomes very small at short distances or large momentum Q^2 , we can apply perturbation theory. This statement is true for ideal cases which only involve one hard scale. But in reality physical processes depend on multiple scales, i.e. long range interactions, and therefore it is not possible to describe the whole process within the perturbative approach.

For our brief overview about the wide field of factorization we will restrict our discussion

to the system of pion form factors. Therefore we follow the work of Efremov et al. [17]. They state that the main task for any process is the factorization of the corresponding full cross section $d\sigma_{\text{full}}$. This amplitude can be written as a convolution of a hard part with a function $\phi(\mu^2, k^2)$ incorporating all the informations about the long distance effects. In addition one has a regular term $r(Q^2, k^2)$ which does not factorize but is suppressed by powers of the hard scale:

$$d\sigma_{\text{full}}(Q^2, k^2) = d\sigma_{\text{hard}}(Q^2, \mu^2) \otimes f_{\text{soft}}(\mu^2, k^2) + r(Q^2, k^2) . \quad (2.128)$$

Here k^2 is the soft scale, Q^2 the hard scale and μ the parameter which “divides” short and long distance effects. The hard part in Eq. (2.128) can be calculated via perturbation theory. Informations about the soft part has to be obtained in a different way. They can be gained via experiments or through non perturbative theories which are applicable at low momentum transfer such as lattice QCD and QCD sum rules.

2.3.1. Collinear factorization

We will mainly follow the work of Braun et al. [39]. The basic idea of collinear factorization is to handle the partons in the nucleon as a bunch of collinear moving particles. This picture is only valid at very high momentum transfer Q^2 . On the one hand a nucleon consists of only three valence quarks q but on the other hand we can have an arbitrary amount of quark anti quark $q\bar{q}$ pairs and gluons g in the Fock state:

$$\begin{aligned} |\text{meson}\rangle &= |q\bar{q}\rangle + |q\bar{q}g\rangle + |q\bar{q}q\bar{q}\rangle + \dots \\ |\text{baryon}\rangle &= |qqq\rangle + |qqqg\rangle + |qqqq\bar{q}\rangle + \dots \end{aligned} \quad (2.129)$$

Therefore the nucleon consists of a beam of N sea and valence quarks which exchange intermediate gluons. In the hard gluon-exchange-picture the incoming nucleon is struck by a hard photon. More precisely one of the quarks in the proton or neutron absorbs all the momentum. In order to stay intact, the large momentum has to be split up between all partons. The nucleon can be pictured as N collinear moving valence quarks. Each of the partons carries a certain momentum fraction $x_i \cdot P$ of the nucleon momentum P . In order to ensure momentum conservation:

$$\sum_{i=1}^3 x_i = 1 . \quad (2.130)$$

The initial transverse momentum, which also can be interpreted as transverse-momentum fluctuations, of the quarks $k_{\perp i}$ can be neglected compared to the transverse momentum transfer q_{\perp} . This is exactly the reason for applicability of perturbation theory for the calculation of the hard scattering kernel T_H . One can show that in the large- Q^2 limit, form factors can be written as a convolution of distribution amplitudes with perturbative coefficient functions. So for the Dirac form factor F_1 this decomposition reads:

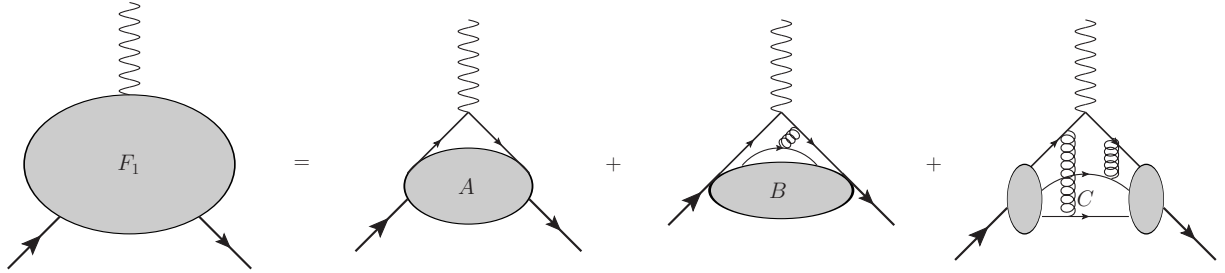


Figure 2.8.: Graphic illustration of the decomposition of the nucleon form factor F_1

$$F_1(Q^2) \sim A(Q^2) + \frac{\alpha_S(Q^2) B(Q^2)}{\pi Q^2} + \left(\frac{\alpha_S(Q^2)}{\pi} \right)^2 \frac{C}{Q^4} + \dots$$

The function C is a constant determined by distribution amplitudes which we will discuss in detail in the next section. Here $A(Q^2)$ and $B(Q^2)$ are two low energy (i.e. low virtuality) functions which can not be calculated in any form in a perturbative manner. These soft form factor like functions are estimated to behave like [39]

$$A(Q^2) \lesssim \frac{1}{Q^6}, \quad B(Q^2) \lesssim \frac{1}{Q^4}. \quad (2.131)$$

The biggest problem is the dominance of A and B at moderate Q^2 . This is because of having an additional suppression of the term proportional to C by a factor of 10 due to $\alpha_S/\pi \sim 0.1$. This can be overcome at very high Q^2 were the suppression of the non perturbative part proportional to A and B compensates the factor 10.

2.3.2. Nucleon wave function and distribution amplitudes

In this section we will now investigate the properties and the shape of the nucleon wave functions and introduce the concept of distribution amplitudes in order to take the long distance effects associated with the internal structure of the nucleon into account. For this

2.3. FACTORIZATION AND THE CONCEPT OF DISTRIBUTION AMPLITUDES

short introduction we will follow the works of [19, 20, 40]. One of the first works associating the interaction of bound states with the all order calculations of scattering processes was done by Bethe and Salpeter [41]. The shape of the so called Bethe Salpeter wave function ψ_{BS} and its properties have been discussed in a multitude of works. One of them for example is the work by Wick [42].

Salpeter et al. have given (using a bound state system of two Dirac fermions) different integral representation for the wave function. This concept was further improved by Chernyak et al. [20] and Lepage et al. [40]. These are the works which we will follow to introduce the basic framework. Later in this section we will follow the works of Braun et al. [43] and use their expressions for the distribution amplitudes to calculate the form factors.

As we have seen in the previous section the form factor can be written as convolution of two amplitudes $\phi(z_i, Q)$ and a hard scattering kernel:

$$F(Q^2) = \int_0^1 d\bar{x}_i \int_0^1 d\bar{y}_i \phi^*(x_i, Q^2) T_H(x_i, y_i) \phi(y_i, Q^2) , \quad (2.132)$$

with $d\bar{z}_i = \delta(1 - z_1 - z_2 - z_3) dz_1 dz_2 dz_3$ and $Q^2 = -q^2$ being the momentum transfer. In this framework the concept of distribution amplitudes which are non-perturbative functions describing the momentum distribution within hadrons was introduced.

The distribution amplitude $\phi(z_i, Q)$ can be associated with the probability to find a quark with distinct momentum fraction inside the nucleon or in other words the amplitude to transform a proton into three valence quarks with specific momentum fractions. Using light cone variables introduced in Appendix F $x_i = \frac{k_i^+}{p^+} = \frac{k_i^0 + k_i^1}{p^0 + p^1}$ and light cone gauge $n \cdot A = 0$ we can associate the hadronic wave function $\Psi(x_i, k_i)$ with the distribution amplitude $\phi(x_i, Q)$ via:

$$\phi(x_i, Q) \propto \int_0^Q \prod_{j=1}^3 d^2 k_{j\perp} \delta^2(\vec{k}_{1\perp} + \vec{k}_{2\perp} + \vec{k}_{3\perp}) \Psi(x_i, k_i) . \quad (2.133)$$

The distribution amplitude's Q^2 -dependence, which can be calculated in light-cone gauge via a one gluon exchange kernel, up to first order is given by the following evolution equation:

$$Q^2 \frac{\partial}{\partial Q^2} \phi(x_i, Q^2) = \frac{\alpha_S(Q^2)}{4\pi} \int_0^1 [dz] V(x_i, z_i) \phi(z_i, Q^2) . \quad (2.134)$$

With $[dz] \equiv dz_1 dz_2 dz_3 \delta(1 - z_1 + z_2 + z_3)$ and V being a function which we will introduce shortly. The distribution amplitudes $\phi(x_i, Q^2)$, which can be identified as the probability amplitude to find the valence quarks near the light-cone,

$$\phi(x_i, Q^2) = x_1 x_2 x_3 \sum_{n=0}^{\infty} a_n \left(\ln \frac{Q^2}{\Lambda_{QCD}^2} \right)^{-\gamma_n} \tilde{\phi}_n \quad (2.135)$$

solve the evolution equation in Eq. (2.134). The eigensolutions $\tilde{\phi}_n$ and eigenvalues γ_n of Eq. (2.134) together with the coefficients a_n characterize the DA which are the starting point for the discussion of distribution amplitudes in a special approach. From now on we will follow the work of Braun et al. [43]. As we have mentioned above distribution amplitudes can be seen as the amplitude to transform the hadron into a bunch of collinear moving particles. To be more precise in the context of the definition of nucleon or hadron distribution amplitudes one speaks of hadron-to-vacuum matrix elements of nonlocal operators consisting of quark and gluon fields separated by light-like distance. The gauge invariant object defining the DA takes the form:

$$\langle 0 | \epsilon^{ijk} u_\alpha^l(a_1 z) [a_1 z, a_0 z]_{li} u_\beta^m(a_2 z) [a_2 z, a_0 z]_{mj} d_\gamma^n(a_3 z) [a_3 z, a_0 z]_{nk} | P(P, \lambda) \rangle \quad (2.136)$$

Here the Greek letters are Dirac indices, Latin letters refer to color, a_i are real numbers, z is an arbitrary light-like vector, and

$$[a, b] = \text{P exp} \left[ig \int_0^1 dx (a - b)_\mu A^\mu(xa + (1-x)b) \right]. \quad (2.137)$$

is the Wilson gauge link ensuring gauge invariance [44]. $|P(P, \lambda)\rangle$ denotes a proton state with momentum P and helicity λ .

If one takes Lorentz covariance, spin and parity of the nucleon into account the matrix element (2.136) can be decomposed into 24 different functions $\mathcal{F} = \mathcal{A}_i, \mathcal{S}_i, \mathcal{T}_i, \mathcal{V}_i$, which is done in detail in Appendix G. Since we deal with massless nucleons and quarks all terms proportional to the nucleon mass vanish and only the following invariant functions contribute:

$$\begin{aligned} 4 \langle 0 | \epsilon^{ijk} u_\alpha^i(a_1 z) u_\beta^j(a_2 z) d_\gamma^k(a_3 z) | P(P, \lambda) \rangle = \\ = \mathcal{V}_1 (\not{P} C)_{\alpha\beta} (\gamma_5 N)_\gamma + \mathcal{A}_1 (\not{P} \gamma_5 C)_{\alpha\beta} N_\gamma + \mathcal{T}_1 (P^\nu i \sigma_{\mu\nu} C)_{\alpha\beta} (\gamma^\mu \gamma_5 N)_\gamma. \end{aligned} \quad (2.138)$$

Where N_γ is a nucleon spinor, $\sigma_{\mu\nu} = \frac{i}{2} [\gamma_\mu, \gamma_\nu]$ and C is the charge conjugation matrix. Note that the reader should remember the expression in Eq. (2.138) since it is crucial for

our further computations. Since we are only interested in the leading twist case there is no difference between the invariant functions A_1 , V_1 , T_1 and \mathcal{A}_1 , \mathcal{V}_1 , \mathcal{T}_1 , i.e. see Appendix G. The axial A_1 , vector V_1 , and tensor T_1 distribution amplitudes possess certain symmetry properties:

$$\begin{aligned} A_1(x_1, x_2, x_3) &= -A_1(x_2, x_1, x_3) \\ V_1(x_1, x_2, x_3) &= V_1(x_2, x_1, x_3) \\ T_1(x_1, x_2, x_3) &= T_1(x_2, x_1, x_3) . \end{aligned} \tag{2.139}$$

Using Fiertz transformations it follows:

$$2T_1(x_1, x_2, x_3) = (V_1 - A_1)(x_1, x_3, x_2) + (V_1 - A_1)(x_2, x_3, x_1) . \tag{2.140}$$

Now one can identify Eq. (2.140) with the only remaining independent distribution amplitude, which is comparable to $\Phi_N(x_1, x_2, x_3)$ defined in [20]:

$$\phi_3(x_1, x_2, x_3) = (V_1 - A_1)(x_1, x_2, x_3) . \tag{2.141}$$

This leading twist distribution amplitude ϕ_3 can be associated with the pion decay constant f_π , and determines the nucleon wave function at the origin [45]:

$$f_N = \int [dx] \phi_3(x_1, x_2, x_3) . \tag{2.142}$$

In the asymptotic limit, where $\mu^2 \sim Q^2 \rightarrow \infty$, the distribution amplitudes take a very simple form:

$$V_1(x, Q^2 \rightarrow \infty) = T_1(x, Q^2 \rightarrow \infty) = \phi_{\text{asy}} , \quad A_1(x, Q^2 \rightarrow \infty) = 0 . \tag{2.143}$$

Here $\phi_{\text{asy}} = 120x_1x_2x_3$ is the asymptotic wave function. Later we will need the decomposition of the matrix element in Eq. (2.138) in order to simplify our calculations.

2.4. FeynArts

The calculation of the electromagnetic form factor in next-to-leading order gives rise to the problem of a tremendous amount of graphs which have to be taken into account. In order to ensure the completeness of our calculation we used, in addition to counting by hand, the Mathematica package FeynArts (FA) to generate the corresponding diagrams. This

To get the fully analytical output one has to perform the following steps:

1. The first step is to generate the corresponding topologies. For FA topologies are a set of lines (propagators) and points (vertices) which are all connected. The command reads:

```
tops = CreateTopologies[ l, i -> o, "options" ],
```

where `l` is the loop order (up to three for the latest version), `i` and `o` are the number of incoming and outgoing particles. Also several options can be implemented at this stage of computation. Since the program offers a big variety of options, only the ones used in our calculations are presented.

| option | default value | affects |
|---------------------|---------------|-----------------------------|
| Adjacencies | 3,4 | order of vertices |
| CTOrder | 0 | counter-term order |
| ExcludeTopologies | | filtering topologies |
| Starting Topologies | All | list of starting topologies |

Here order of vertices can be used for example to exclude all diagrams which contain a four gluon vertices by simply setting

```
Adjacencies->{3}.
```

The counter term order would automatically generate also the counter term topologies for divergent diagrams. For the option `ExcludeTopologies` the following restriction are available:

| option | excludes[] | of adjacencies |
|----------------------|---------------------------------|-------------------|
| Loops[<i>patt</i>] | loops | <i>patt</i> |
| CTs[<i>patt</i>] | counter-terms | <i>patt</i> |
| Tadpoles | loops | 1 |
| SelfEnergies | loops | 2 |
| Triangles | loops | 3 |
| WFCorrections | self-energy or tadpole loops | on external lines |
| Internal | one-particle reducible topology | |

Since we work in dimensional regularization all tadpole diagrams can be neglected

due to the fact that they would produce scaleless integrals which can be set to zero. In addition we neglect all one particle reducible diagrams which correspond to the renormalization of the external quark lines. This will be done in a more elaborate way in Chapter 4.

2. After the topologies has been generated we have to insert the fields into the topologies.

```
infi = InsertFields[ tops, {i1, i2, ...} -> {o1, o2, ...}].
```

Here $i1, i2, \dots$ are the incoming and $o1, o2, \dots$ outgoing fields. There are three different level of fields in the FA framework: *Generic, Classes and Particles*. The *Generic* fields are: F (fermion), S (scalar), V (vector), U (ghost), T (tensor) and SV (scalar-vector mixing). The next level, the class level, specifies a generic field. E.g. $F[2]$ for the class of leptons. With the particle level one can pick certain particles. The electron for example $F[2,1]$. Antiparticles are represented by putting a minus in front of the the fields.

3. In order to cross check with our counting we have drawn all the Feynman graphs:

```
painfi = Paint[ infi ].
```

4. The last step is to create the Feynman amplitudes.

```
amps = CreateFeynAmp[ infi ].
```

The generated amplitudes will now be further processed with the FeynCalc package.

2.5. Reduction algorithm

In this section we will summarize the basic ideas of the reduction algorithm for calculating one-loop N -point massless Feynman integrals in dimensional regularization. The most complex integral which we have to solve for our problem:

$$I_7^{\mu\nu\rho\sigma} = \int \frac{d^D q}{(2\pi)^D} \frac{q^\mu q^\nu q^\rho q^\sigma}{(q - p_1)^2 \dots (q - p_7)^2}. \quad (2.144)$$

In order to solve these integral we use the reduction algorithm proposed by Duplanić and Nizić [23]. With this method it is possible to reduce one-loop N -point massless integrals to a limited number of basic integrals. Older algorithms were not able to solve the problem when more than two collinear momenta appeared, which is the case for our problem.

We will now state the basic concepts of the method and will provide the reader with all tools necessary to understand the implemented code. In the following section we will use the notation and formulas of Duplanić and Nizić [23].

The fundamental object is the following integral, which will arise in every loop calculation in massless gauge theories:

$$I_{\mu_1 \dots \mu_P}^N(D; \{p_i\}) \equiv (\mu^2)^{2-D/2} \int \frac{d^D q}{(2\pi)^D} \frac{q_{\mu_1} \dots q_{\mu_P}}{A_1 A_2 \dots A_N}. \quad (2.145)$$

Here q is the loop momentum, D is the space-time dimension, p_i are the external momenta and μ is the dimensional regularization scale. The massless propagators A_i are defined as:

$$A_i \equiv (q + r_i)^2 + i\epsilon, \quad i = 1, \dots, N, \epsilon > 0. \quad (2.146)$$

With $r_i = p_i + r_{i-1}$, $i = 1, \dots, N$ and $r_0 = r_N$. The scalar integrals take the form:

$$I_0^N(D; \{p_i\}) \equiv (\mu^2)^{2-D/2} \int \frac{d^D q}{(2\pi)^D} \frac{1}{A_1 A_2 \dots A_N}. \quad (2.147)$$

After using Feynman parametrization [27]

$$\frac{1}{A_1^{\nu_1} \dots A_N^{\nu_N}} = \frac{\Gamma(\nu_1 + \dots + \nu_N)}{\Gamma(\nu_1) + \dots + \Gamma(\nu_N)} \int_0^1 dy_1 \dots \int_0^1 dy_N \frac{\delta(\sum_{i=1}^N y_i - 1) y_1^{\nu_1-1} \dots y_N^{\nu_N-1}}{(y_1 A_1 + \dots + y_N A_N)^{\sum_{i=1}^N \nu_i}} \quad (2.148)$$

and the standard integral [27]

$$\int \frac{d^D q}{(2\pi)^D} \frac{1}{(q^2 - x)^n} = \frac{(-1)^n i \Gamma(n - D/2)}{(4\pi)^{D/2} \Gamma(n)} \left(\frac{1}{x}\right)^{n-D/2} \quad (2.149)$$

the integral in Eq. (2.147) can be rewritten as:

$$I_0^N(D; \{\nu_i\}) = \frac{i}{(4\pi)^2} (4\pi\mu^2)^{2-D/2} \frac{\Gamma\left(\sum_{i=1}^N \nu_i - D/2\right)}{\prod_{i=1}^N \Gamma(\nu_i)} (-1)^{\sum_{i=1}^N \nu_i} \times \int_0^1 \left(\prod_{i=1}^N dy_i y_i^{\nu_i-1} \right) \delta\left(\sum_{i=1}^N y_i - 1\right) \left[-\sum_{\substack{i,j=1 \\ i < j}}^N y_i y_j (r_i - r_j)^2 - i\epsilon \right]^{D/2 - \sum_{i=1}^N \nu_i}. \quad (2.150)$$

The use of the Passerino Veltman decomposition for the tensor structure enables us to rewrite the integral in Eq. (2.145) in a similar way:

$$I_{\mu_1 \dots \mu_P}^N(D; \{\nu_i\}) = \frac{i}{(4\pi)^2} (4\pi\mu^2)^{2-D/2} \sum_{\substack{k, j_1, \dots, j_N \geq 0 \\ 2k + \sum_{i=1}^N j_i = P}} \{[g]^k [r_1]^{j_1} \dots [r_N]^{j_N}\}_{\mu_1 \dots \mu_P} \times \frac{\Gamma(\sum_i \nu_i - D/2 - k)}{2^k \prod_i \Gamma(\nu_i)} (-1)^{\sum_i \nu_i + P - k} \int_0^1 \left(\prod_i dy_i y_i^{\nu_i + j_i - 1} \right) \times \delta\left(\sum_{i=1}^N y_i - 1\right) \left[-\sum_{\substack{i,j=1 \\ i < j}}^N y_i y_j (r_i - r_j)^2 - i\epsilon \right]^{k + D/2 - \sum_{i=1}^N \nu_i}. \quad (2.151)$$

The structure

$$\{[g]^k[r_1]^{j_1} \cdots [r_N]^{j_N}\}_{\mu_1 \cdots \mu_P} \quad (2.152)$$

in Eq. (2.151) represents a totally symmetric expression for the Lorentz structure. A showcase for one possible Lorentz pattern is the following expression:

$$\{gr_1\}_{\mu_1 \mu_2 \mu_3} = g_{\mu_1 \mu_2} r_{1 \mu_3} + g_{\mu_1 \mu_3} r_{1 \mu_2} + g_{\mu_2 \mu_3} r_{1 \mu_1} . \quad (2.153)$$

After comparing Eq. (2.151) and (2.150) one can identify:

$$\begin{aligned} I_{\mu_1 \cdots \mu_P}^N(D; \{\nu_i\}) &= \sum_{\substack{k, j_1, \dots, j_N \geq 0 \\ 2k + \sum j_i = P}} \{[g]^k[r_1]^{j_1} \cdots [r_N]^{j_N}\}_{\mu_1 \cdots \mu_P} \\ &\times \frac{(4\pi\mu^2)^{P-k}}{(-2)^k} \left[\prod_{i=1}^N \frac{\Gamma(\nu_i + j_i)}{\Gamma(\nu_i)} \right] I_0^N(D + 2(P - k); \{\nu_i + j_i\}) . \end{aligned} \quad (2.154)$$

Many recursion relations found in the literature are based on the integration by parts approach. It can be shown that the translational invariance of the dimensionally regularized integrals for $z_0 = \sum_i^N z_i$ fulfills the identity

$$0 \equiv \int \frac{d^D q}{(2\pi)^D} \frac{\partial}{\partial q^\mu} \left(\frac{z_0 q^\mu + \sum_{i=1}^N z_i r_i^\mu}{A_1^{\nu_1} \cdots A_N^{\nu_N}} \right) . \quad (2.155)$$

Here z_i ($i = 0 \dots N$) are arbitrary constants. Using the definition of the scalar N -point integral (2.147), Eq. (2.155) can be transformed into the relation

$$\begin{aligned} \sum_{j=1}^N \left(\sum_{i=1}^N [(r_j - r_i)^2 + 2i\epsilon] z_i \right) \nu_j I_0^N(D; \{\nu_k + \delta_{kj}\}) &= \\ = \sum_{i,j=1}^N z_i \nu_j I_0^N(D; \{\nu_k + \delta_{kj} - \delta_{ki}\}) - \left(D - \sum_{j=1}^N \nu_j \right) z_0 I_0^N(D; \{\nu_k\}) , \end{aligned} \quad (2.156)$$

where δ_{ij} is the Kronecker delta. Eq. (2.156), due to the identity

$$I_0^N(D; \nu_1, \dots, \nu_{l-1}, 0, \nu_{l+1}, \dots, \nu_N) \equiv I_0^{N-1}(D; \nu_1, \dots, \nu_{l-1}, \nu_{l+1}, \dots, \nu_N) , \quad (2.157)$$

constitutes the starting point of the recursion relation for scalar integrals. The arbitrary constants z_i define a linear equation system

$$\sum_{i=1}^N (r_i - r_j)^2 z_i = C, \quad j = 1, \dots, N, \quad (2.158)$$

with C being an arbitrary constant. Using the relation [24]

$$-\sum_{j=1}^N \nu_j I_0^N(D; \{\nu_k + \delta_{kj}\}) = (4\pi\mu^2)^{-1} I_0^N(D-2; \{\nu_k\}), \quad (2.159)$$

and Eq. (2.158), Eq. (2.157) can be transformed into the final recursion relation:

$$C I_0^N(D-2; \{\nu_k\}) = \sum_{i=1}^N z_i I_0^N(D-2; \{\nu_k - \delta_{ki}\}) + 4\pi\mu^2 \left(D-1 - \sum_{j=1}^N \nu_j \right) z_0 I_0^N(D; \{\nu_k\}). \quad (2.160)$$

Now we will introduce two matrices S and R which only depend on the external momenta and the arbitrary constants z_i and C . The matrix S is defined via the linear equations in Eq. (2.158)

$$\underbrace{\begin{pmatrix} 0 & r_{12} & \cdots & r_{1N} \\ r_{12} & 0 & \cdots & r_{2N} \\ \vdots & \vdots & \ddots & \vdots \\ r_{1N} & r_{2N} & \cdots & 0 \end{pmatrix}}_S \begin{pmatrix} z_1 \\ z_2 \\ \vdots \\ z_N \end{pmatrix} = \begin{pmatrix} C \\ C \\ \vdots \\ C \end{pmatrix}, \quad (2.161)$$

with $r_{nm} = (r_n - r_m)^2$, and the matrix R via slightly modified system of equations

$$\underbrace{\begin{pmatrix} 0 & 1 & 1 & \cdots & 1 \\ 1 & 0 & r_{12} & \cdots & r_{1N} \\ 1 & r_{12} & 0 & \cdots & r_{2N} \\ \vdots & \vdots & \vdots & \ddots & \vdots \\ 1 & r_{1N} & r_{2N} & \cdots & 0 \end{pmatrix}}_R \begin{pmatrix} -C \\ z_1 \\ z_2 \\ \vdots \\ z_N \end{pmatrix} = \begin{pmatrix} z_0 \\ 0 \\ 0 \\ \vdots \\ 0 \end{pmatrix}. \quad (2.162)$$

Remembering $z_0 = \sum_i z_i$ the two systems in (2.161) and (2.162) allow for always solving the system in Eq. (2.160). In the following we will distinguish 4 cases for the kinematic determinants $\det(S)$ and $\det(R)$ to obtain the applicable recursion relation. The cases and the corresponding recursion relations are [46]:

Cases 1: $\det(S) \neq 0$, $\det(R) \neq 0$; ($C \neq 0$ and $z_0 \neq 0$)

$$\sum_{j=1}^N (r_k - r_j)^2 \nu_j I_0^N(D; \{\nu_i + \delta_{ij}\}) = (4\pi\mu^2)^{-1} \left[\sum_{j=1}^N (z_j - \delta_{jk}) I_0^N(D-2; \{\nu_i - \delta_{ij}\}) - C I_0^N(D-2; \{\nu_i\}) \right], \quad k = 1, \dots, N \quad (2.163)$$

Cases 2: $\det(S) \neq 0, \det(R) = 0; (C = 0 \text{ and } z_0 = 1)$

$$I_0^N(D; \{\nu_k\}) = \frac{1}{4\pi\mu^2(D-1-\sum_{j=1}^N \nu_j)} \left[-\sum_{i=1}^N z_i I_0^N(D-2; \{\nu_k - \delta_{ki}\}) \right] \quad (2.164)$$

Cases 3: $\det(S) = 0, \det(R) \neq 0; (C \neq 1 \text{ and } z_0 = 0)$

$$I_0^N(D; \{\nu_k\}) = \sum_{i=1}^N z_i I_0^N(D; \{\nu_k - \delta_{ki}\}) \quad (2.165)$$

Cases 4: There are two recursion relations for $\det(S) = 0, \det(R) = 0$ and $z_0 = 0$:

$$I_0^N(D; \{\nu_k\}) = \sum_{i=1}^N z_i I_0^N(D; \{\nu_k - \delta_{ki}\}), \text{ for } C \neq 0 \quad (2.166)$$

and

$$z_1 I_0^N(D; \{\nu_k\}) = -\sum_{i=2}^N z_i I_0^N(D; \{\nu_k + \delta_{k1} - \delta_{ki}\}) \text{ for } C = 0 \quad (2.167)$$

This reduction algorithm for N-point tensor integrals was implemented into a Mathematica environment and is capable of reducing 6-point integrals of rank 2 in a reasonable time. The code allows for switching between different schemes, namely the MS - and \overline{MS} - scheme.

3. Calculations

Now we are finally prepared to start the real calculation. In the first section of this chapter we will discuss the well known result for the leading order calculation of the form factors. The second section will concern the next-to-leading order calculation of the Dirac form factor F_1 . The general setting is the same in both cases. We will use collinear factorization to separate the non perturbative and perturbative part. Then we will use the decomposition of the distribution amplitudes to construct projectors in order to contract all open Lorentz indices except for one which forms the characteristic structure for the nucleon Dirac form factor F_1 , namely $\bar{N}\gamma^\mu N$. For the leading order case we will first reproduce the results by Chernyak et al. [20, 47] and afterwards present our method for the calculation. With this new approach we will generate all possible diagrams via Mathematica [1] FeynArts package [2, 21, 22] and produce the analytic expression for each of the generated Feynman diagrams. After this we will switch to FeynCalc and edit the amplitudes. Therefore we will apply projectors to the hard scattering kernel to reduce our problem to only one open Lorentz index. Up to this point all steps are exactly the same for the leading order and next-to-leading order case. Let us point out this crucial fact: We will show that our fully automated method reproduces the result for the leading order contribution obtained by several other groups. With the same code we will then perform the next-to-leading order calculations.

Since at leading order there is no free momentum there are no integrals to be solved and therefore calculations for the leading order and next-to-leading order deviate after this stage of computation. Now the big challenge is to handle huge amounts of data. In leading order only 48 diagrams are generated. In next-to-leading order there are already 1890 Feynman diagrams generated. As mentioned before not only the huge amount of diagrams pose problems but next-to-leading order (NLO) requires the solution of seven point integrals with up to four open Lorentz indices. We will now show in several steps how we have solved the different tasks which we had to face in computing next-to-leading order corrections to the hard scattering kernel of the electromagnetic nucleon form factors.

3.1. Leading order

In this section we will demonstrate the consistence of the result obtained by our fully automated procedure with the calculations for the leading order contribution given by Chernyak and Zhitnitsky (1983) and Chernyak [20], Avdeenko and Korenblit (1980) [47]. Therefore we will follow the notation used in the paper from 1983.

The starting point is the formula for the Dirac and Pauli form factors derived in Section 2.2.2:

$$\langle P' | J_\mu(0) | P \rangle = \bar{N}(P') \left[\gamma_\mu F_1(q^2) - \frac{\sigma_{\mu\nu} q^\nu}{2M_N} F_2(q^2) \right] N(P) . \quad (3.1)$$

Here $|P\rangle$ and $|P'\rangle$ are the initial and final proton states, $N(P)$ are the corresponding nucleon spinors. J_μ is the electromagnetic current and M_N is the nucleon mass. F_1 and F_2 are the Dirac and Pauli form factors.

In Section 2.3.1 the decomposition of the physical matrix element (3.1) was described. It was shown that the matrix element can be written as a convolution of two distribution amplitudes and a hard scattering kernel:

$$\langle P' | J^\mu(0) | P \rangle \rightarrow \int_0^1 dx \int_0^1 dy \phi_N(x, \mu) T_H^\mu(x, y, q, \mu) \phi_N(y, \mu) . \quad (3.2)$$

Here $dx = \delta(1 - x_1 - x_2 - x_3) dx_1 dx_2 dx_3$ and $x = (x_1, x_2, x_3)$. The same holds for y . In Section 2.3.2 we have shown the tensor decomposition of the distribution amplitudes. For leading twist the distribution amplitudes can be written as:

$$\begin{aligned} \epsilon^{ijk} \langle 0 | u_\alpha^i(a_1 z) u_\beta^j(a_2 z) d_\gamma^k(a_3 z) | P \rangle = & \frac{1}{4} (V_1 (\not{P} C)_{\alpha\beta} (\gamma_5 N(P))_{\gamma+} \\ & A_1 (\not{P} \gamma_5 C)_{\alpha\beta} (N(P))_{\gamma-} \\ & T_1 (\sigma_{\mu\nu} P^\nu C)_{\alpha\beta} (\gamma_\mu \gamma_5 N(P))_{\gamma}) . \end{aligned} \quad (3.3)$$

Here i, j, k denote color indices and α, β, γ are Dirac indices. In order to get the full amplitude we have to construct the non local matrix element for the final state. This can be achieved by complex conjugating the element defined in (3.3).

In the next two sections we will exactly demonstrate how we relate the expression for the distribution amplitudes and the hard scattering kernel to the physical amplitude \mathcal{M} . Note that we will omit numerical prefactors in the discussion of the Dirac structure and will discuss them in the section about color algebra.

3.1.1. Dirac algebra

Omitting the color indices and the electromagnetic coupling the matrix element can be written as:

$$\langle P'|J|P\rangle \approx \langle P'|\bar{u}_\mu\bar{u}_\nu\bar{d}_\rho|0\rangle\langle 0|T_H^{\mu\nu\rho\alpha\beta\gamma}|0\rangle\langle 0|u_\alpha u_\beta d_\gamma|P\rangle. \quad (3.4)$$

Note that on the right hand side only the formally dominant part in $1/Q^2$ is taken into account. This corresponds to the diagram shown in Figure 3.1.

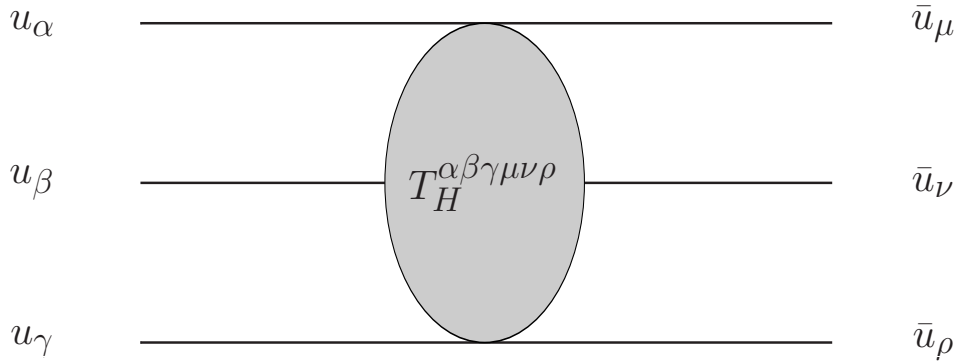


Figure 3.1.: Basic graph

Here the $T_H^{\mu\nu\rho\alpha\beta\gamma} = \Gamma_1^{\alpha\mu}\Gamma_2^{\beta\nu}\Gamma_3^{\gamma\rho}$ and the Γ_i denote the Lorentz structure of the corresponding fermion line. We will see in a moment how this exactly affects our calculations. The corresponding notation and convention we used for the next considerations are summarized in Appendix H. and lower Lorentz indices in cases for γ_0 and γ_5 since they do not change in sign. First we will construct the complex conjugated matrix element for the axial part of the distribution amplitude decomposition in (3.3):

$$\langle 0|u_\alpha u_\beta d_\gamma|P\rangle^* = \langle P|d_\gamma^\dagger u_\beta^\dagger u_\alpha^\dagger|0\rangle = \langle P|\bar{d}_i\bar{u}_j\bar{u}_k|0\rangle(\gamma_0)_{\rho\gamma}(\gamma_0)_{\sigma\beta}(\gamma_0)_{\kappa\alpha}. \quad (3.5)$$

In the last step we use the identity $\bar{q} = q^\dagger\gamma_0$.

Complex conjugating the axial part of distribution amplitude decomposition (3.3) we obtain:

$$\begin{aligned}
 \langle P | \bar{d}_i \bar{u}_j \bar{u}_k | 0 \rangle_A &= [A_1 (\not{P} \gamma_5 C)_{\alpha\beta} (N(P))_\gamma]^* (\gamma_0)_{\gamma i} (\gamma_0)_{\beta j} (\gamma_0)_{\alpha k} \\
 &= A_1^* (\not{P} \gamma_5 C)_{\alpha\beta}^* (N(P))_\gamma^* (\gamma_0)_{\gamma i} (\gamma_0)_{\beta j} (\gamma_0)_{\alpha k} \\
 &= A_1^* ((\not{P} \gamma_5 C)^\dagger)_{\beta\alpha} \bar{N}(P)_i (\gamma_0)_{\beta j} (\gamma_0)_{\alpha k} \\
 &= A_1^* (\gamma_0^T C^T \gamma_5^T \not{P}^\dagger \gamma_0)_{jk} \bar{N}(P)_i \\
 &= A_1^* (\gamma_0 C \gamma_0 \gamma_0 \gamma_5 \gamma_0 \gamma_0 \not{P}^\dagger \gamma_0)_{jk} \bar{N}(P)_i \\
 &= A_1^* (C \gamma_5 \not{P})_{jk} \bar{N}(P)_i .
 \end{aligned} \tag{3.6}$$

The last step is to reorder the quarks to restore the right ordering of quark flavors in the distribution amplitude.

$$\langle P | \bar{u}_\gamma \bar{u}_\beta \bar{d}_\alpha | 0 \rangle_A = A_1^* (C \gamma_5 \not{P})_{\gamma\beta} \bar{N}(P)_\alpha . \tag{3.7}$$

For the complex conjugated vector and tensor distribution amplitudes the same procedure has to be done. The final result for the vector case can be written in the following way:

$$\langle P | \bar{u}_\gamma \bar{u}_\beta \bar{d}_\alpha | 0 \rangle_V = -V_1^* (C \not{P})_{\gamma\beta} (\bar{N}(P) \gamma_5)_\alpha . \tag{3.8}$$

And similar for the tensor distribution amplitude:

$$\langle P | \bar{u}_\gamma \bar{u}_\beta \bar{d}_\alpha | 0 \rangle_T = -T_1^* (C P_\nu \sigma^{\mu\nu})_{\gamma\beta} (\bar{N}(P) \gamma_5 \gamma_\mu)_\alpha . \tag{3.9}$$

The last step is to convolute the distribution amplitudes for the final and the initial nucleon with the hard scattering kernel T_H . We will demonstrate the calculation for the case of two axial projectors:

$$\begin{aligned}
 \langle P' | J | P \rangle_A &= \langle P' | \bar{u}_\mu \bar{u}_\nu \bar{d}_\rho | 0 \rangle_A \langle 0 | T_H | 0 \rangle \langle 0 | u_\alpha u_\beta d_\gamma | P \rangle_A \\
 &= A_1^* (C \gamma_5 \not{P}')_{\mu\nu} (\bar{N}(P'))_\rho (\Gamma_1)_{\mu\alpha} (\Gamma_2)_{\nu\beta} (\Gamma_3)_{\rho\gamma} A_1 (\not{P} \gamma_5 C)_{\alpha\beta} N(P)_\gamma \\
 &= |A_1|^2 \cdot \bar{N}(P') \Gamma_3 N(P) [- (\Gamma_1)_{\mu\alpha} (\not{P} \gamma_5 C)_{\alpha\beta} (\Gamma_2^T)_{\beta\nu} (C \gamma_5 \not{P}')_{\nu\mu}] \\
 &= -|A_1|^2 \cdot \bar{N}(P') \Gamma_3 N(P) \text{Tr} [\Gamma_1 \not{P} \gamma_5 C \Gamma_2^T C \gamma_5 \not{P}'] \\
 &= (-1)^{1+2 \cdot n_2} |A_1|^2 \cdot \bar{N}(P') \Gamma_3 N(P) \text{Tr} [\Gamma_1 \not{P} \overleftrightarrow{\Gamma}_2 \not{P}'] .
 \end{aligned} \tag{3.10}$$

Here and from now on n_i denotes the number of gamma matrices in the i -th fermion line. $\overleftrightarrow{\Gamma}_2$ is the second fermion line with reversed ordering of the Dirac matrices. So for example:

$$\Gamma_2 = \gamma_\alpha \gamma_\beta \gamma_\gamma \rightarrow \overleftrightarrow{\Gamma}_2 = \gamma_\gamma \gamma_\beta \gamma_\alpha . \tag{3.11}$$

Note that the number of gamma matrices in one fermion line is always odd and therefore the last line in Eq.(3.10) is reduced to:

$$\mathcal{AA} = -|A_1|^2 \cdot \bar{N}(P')\Gamma_3 N(P) \text{Tr} [\Gamma_1 \not{P} \overleftrightarrow{\Gamma}_2 \not{P}'] . \quad (3.12)$$

The same routine can be done for the other three cases:

The vector-vector projection gives:

$$\mathcal{VV} = (-1)^{1+n_2+n_3} |V_1|^2 \cdot \bar{N}(P')\Gamma_3 N(P) \text{Tr} [\Gamma_1 \not{P} \overleftrightarrow{\Gamma}_2 \not{P}'] . \quad (3.13)$$

Which gives for the same reason as above (n_i are odd numbers):

$$\mathcal{VV} = -|V_1|^2 \cdot \bar{N}(P')\Gamma_3 N(P) \text{Tr} [\Gamma_1 \not{P} \overleftrightarrow{\Gamma}_2 \not{P}'] . \quad (3.14)$$

For the mixed cases we obtain:

$$\mathcal{VA} = -(V_1 A_1^* + A_1 V_1^*) \cdot \bar{N}(P')\Gamma_3 \gamma_5 N(P) \text{Tr} [\Gamma_1 \not{P} \gamma_5 \overleftrightarrow{\Gamma}_2 \not{P}'] . \quad (3.15)$$

Using Fiertz transformations one can eliminate the γ_5 dependence. This enables us to take the traces in D dimensions. The improved version is given by:

$$\mathcal{VA}_{\text{improved}} = (V_1 A_1^* + A_1 V_1^*) \cdot P^\lambda P'^\kappa \bar{N}(P') \gamma^\eta \Gamma_1 \gamma^\delta N(P) \text{Tr} [\Gamma_3 \sigma_{\delta\lambda} \overleftrightarrow{\Gamma}_2 \sigma_{\eta\kappa}] . \quad (3.16)$$

Last but not least the tensor-tensor amplitude reads as:

$$\mathcal{TT} = |T_1|^2 \cdot P^\lambda P'^\kappa \bar{N}(P') \gamma^\eta \Gamma_3 \gamma^\delta N(P) \text{Tr} [\Gamma_1 \sigma_{\delta\lambda} \overleftrightarrow{\Gamma}_2 \sigma_{\eta\kappa}] . \quad (3.17)$$

3.1.2. Color algebra

In this section we will investigate the color structure of our problem. Similar to the previous section we will now omit the Dirac structure and therefore have a slightly modified basic graph 3.2, which corresponds to the amplitude

$$\mathcal{M} = \langle P' | \bar{u}_l \bar{u}_m \bar{d}_n | 0 \rangle \langle 0 | T_H^{lmn,ijk} | 0 \rangle \langle 0 | u_i u_j d_k | P \rangle . \quad (3.18)$$

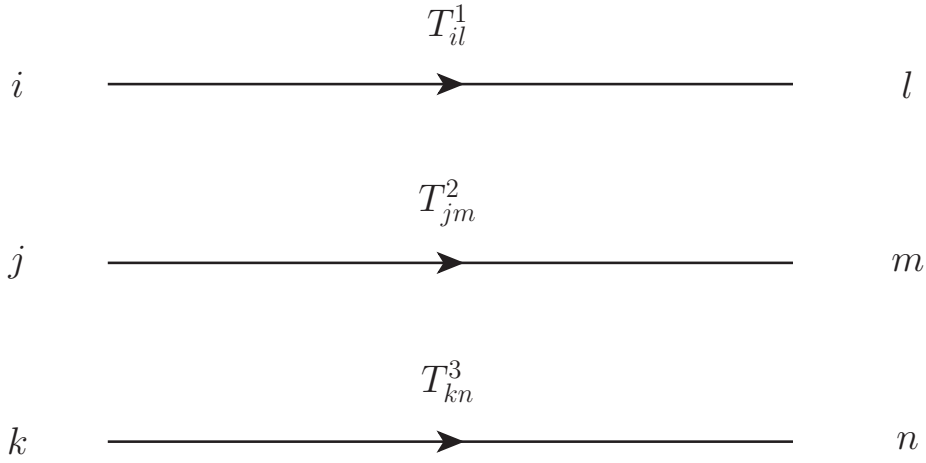


Figure 3.2.: Basic diagram for the illustration of the color structure

The T_{xy} in Fig. 3.2 denote the color matrices in the corresponding fermion line. Replacing the forward matrix element with those of Eq. (3.3), and its complex conjugated, Eq. (3.18) takes the form:

$$\mathcal{M} = \left(\frac{1}{6}\right)^2 \left(\frac{1}{4}\right)^2 |f_N|^2 \epsilon_{ijk} \epsilon_{lmn} \langle 0 | T_H^{ijk,lmn} | 0 \rangle . \quad (3.19)$$

Note that the factor $1/4$ is due to the definition of the distribution amplitude decomposition 2.3.2 and the factor $1/6$ arises due to

$$\epsilon^{ijk} \epsilon^{ijk} = 6 . \quad (3.20)$$

With

$$\epsilon^{ijk} \epsilon^{lmn} = \det \begin{pmatrix} \delta^{il} & \delta^{im} & \delta^{in} \\ \delta^{jl} & \delta^{jm} & \delta^{jn} \\ \delta^{kl} & \delta^{km} & \delta^{kn} \end{pmatrix} \quad (3.21)$$

and the combination of color matrices in the corresponding fermion-lines T_{il}^1 , T_{jm}^2 and T_{kn}^3 we obtain the following expression for the color structure CS:

$$\begin{aligned} \text{CS} &= \epsilon^{ijk} \epsilon^{lmn} T_{il}^1 T_{jm}^2 T_{kn}^3 = \text{Tr}(T^1) \text{Tr}(T^2) \text{Tr}(T^3) + \text{Tr}(T^1 T^2 T^3) \\ &\quad + \text{Tr}(T^1 T^3 T^2) - \text{Tr}(T^2) \text{Tr}(T^1 T^3) \\ &\quad - \text{Tr}(T^1) \text{Tr}(T^2 T^3) - \text{Tr}(T^1 T^2) \text{Tr}(T^3) . \end{aligned} \quad (3.22)$$

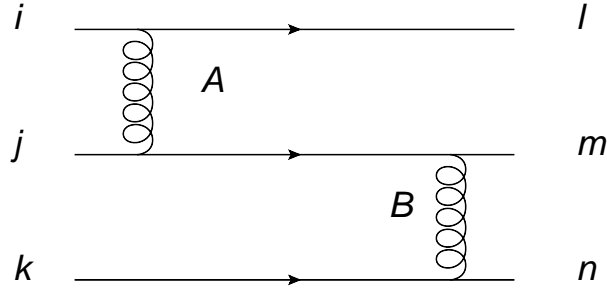


Figure 3.3.: Tree level contribution to the hard scattering kernel

The color structure for one of six basic diagrams with anti-symmetric final states takes the following form:

$$\text{CSLO} = \epsilon^{ijk} \epsilon^{lmn} (T^A)_{il} (T^A T^B)_{jm} (T^B)_{kn} . \quad (3.23)$$

Taking the relations in Appendix A into account we can show that the color structure associated with Fig. 3.3 is the only occurring color structure in the leading order case. This is because of the fact that all diagrams containing a three gluon vertex are zero. For the leading order diagrams the color structure CSLO obtained via Mathematica FeynCalc package reads as:

$$\text{CSLO} = \frac{1}{4} (1 - C_A) (2 - C_A) (C_A + 1)^2 (C_A - 2C_F) . \quad (3.24)$$

Which also can be expressed via

$$\text{CSLO} = \frac{1}{4} (1 - N) (2 - N) (N + 1)^2 \left(N - \frac{N^2 - 1}{N} \right) = \frac{8}{3} . \quad (3.25)$$

3.1.3. Results obtained by Chernyak et al.

In this section we will recap the results obtained by Chernyak et al. [20] and point out some ambiguities of their paper. First we recap some basic definitions.

$$\langle P' | J_\mu(0) | P \rangle = \bar{N}(P') \left[\gamma_\mu F_1(q^2) - \frac{\sigma_{\mu\nu} q^\nu}{2M_N} F_2(q^2) \right] N(P) . \quad (3.26)$$

And the connection between the magnetic Sachs form factor and the Pauli and Dirac form factors reads:

$$G_M(q^2) = F_1(q^2) + F_2(q^2) . \quad (3.27)$$

The power law behavior [20, 48] for the Dirac und Pauli form factors

$$F_1 \sim \frac{1}{q^4} \quad \text{and} \quad F_2 \sim \frac{1}{q^6} \quad (3.28)$$

leaves us, in the asymptotic limit, which Chernyak et al. consider, with

$$G_M(q^2) \approx F_1(q^2) . \quad (3.29)$$

Using the symmetry properties of the distribution amplitudes V_1, A_1 and T_1 the formula for the calculation of the Dirac form factor $F_1(q^2)$ is given in the work of Chernyak et al. via:

$$F_1(q^2) \rightarrow \frac{1}{q^4} \frac{4\pi\bar{\alpha}_S}{54} |f_N|^2 \int_0^1 dx \int_0^1 dy \delta(x)\delta(y) \left[2 \sum_{i=1}^7 e_i T_i(x, y) + \sum_{i=8}^{14} e_i T_i(x, y) \right] . \quad (3.30)$$

From now on we will write for the hard part including the distribution amplitudes:

$$T_H^{\text{incl}}(x, y, e_i) = \int_0^1 dx \int_0^1 dy \delta(x)\delta(y) \left[2 \sum_{i=1}^7 e_i T_i(x, y) + \sum_{i=8}^{14} e_i T_i(x, y) \right] . \quad (3.31)$$

With $\bar{\alpha}_S = \alpha_S^2 \left(\frac{\alpha_S(q^2)}{\alpha_S(\mu^2)} \right)^{\frac{4}{3}\beta_0}$, $\beta_0 = 11 - \frac{2}{3}n_f$, $dx = dx_1 dx_2 dx_3$ and $\delta(x) = \delta(1 - x_1 - x_2 - x_3)$. The constant f_N refers to the wave function at the origin. $T_i(x, y)$ are the contributions to the leading order hard scattering kernel for each diagram shown in Table 3.1 and Table 3.2. The e_i are the corresponding charges for each diagram. So if one wants to calculate the proton form factor one has to insert (denoted by the circle with the X) the up quark charge $e_u = 2/3$ for the first two fermion lines and the down quark charge $e_d = -1/3$ for the lowest line. For the neutron one simply exchanges e_u and e_d . Note that there is a misprint in the amplitude for the diagram 10 in [20]. In Table 3.1 and Table 3.2 the leading twist dimensionless wave functions of the nucleon

$$\phi_N(x, \mu^2) = V_1(x, \mu^2) - A_1(x, \mu^2) \quad \text{and} \quad T_1(x, \mu^2) \quad (3.32)$$

can be reduced to:

$$\phi_N(x) = V_1(x_1, x_2, x_3) - A_1(x_1, x_2, x_3) \quad (3.33)$$

$$T_1(x_1, x_2, x_3) = \frac{1}{2} (\phi_N(x_1, x_3, x_2) + \phi_N(x_2, x_3, x_1)) \quad (3.34)$$

and in the asymptotic limit they reduce to

$$V_1(x, q^2 \rightarrow \infty) = T_1(x, q^2 \rightarrow \infty) = \phi_{\text{AS}}(x) = 120x_1x_2x_3 \quad \text{and} \quad A_1(x, q^2 \rightarrow \infty) \rightarrow 0 . \quad (3.35)$$

The final result for the Dirac form factor of the neutron in the asymptotic limit reads:

$$F_1^n(q^2) \rightarrow \frac{1}{q^4} 4\pi \bar{\alpha}_S |f_N|^2 \frac{100}{3} . \quad (3.36)$$

For the proton $F_1^p = 0$. We have recalculated Eq. (3.31) analytically with Mathematica and numerically with the Cuba library using momentum conservation $x_3 = 1 - x_1 - x_2$ and $y_3 = 1 - y_1 - y_2$ and therefore having only to deal with 4- and not 6- dimensional integrals when integrating over the momentum fractions:

$$\int_0^1 dx_1 \int_0^1 dx_2 \int_0^1 dx_3 \delta(1 - x_1 - x_2 - x_3) F(x_1, x_2, x_3) \rightarrow \int_0^1 dx_1 \int_0^{1-x_1} dx_2 F'(x_1, x_2) \quad (3.37)$$

The result obtained analytically for the hard part $T_H^{\text{incl}}(x, y, e_i)$ using the asymptotic wave function ϕ_{AS} are:

$$T_H^n = 1800 \quad \text{and} \quad T_H^p = 0 . \quad (3.38)$$

Combining the results in Eq. (3.38) with the values in the paper of Chernyak et al. [20] reproduces the result $1/54 \cdot 1800 = 100/3$ for the neutron.

Table 3.1.: Contributing diagrams for the calculation of Chernyak et al. I.

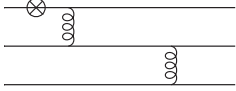
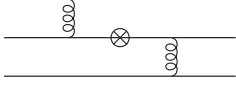
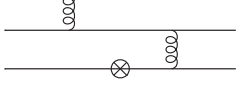
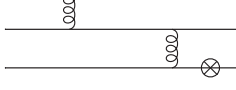
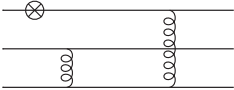
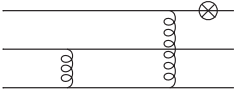
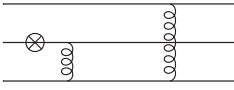
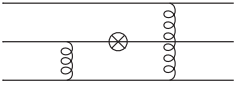
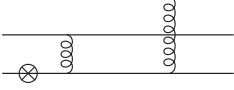
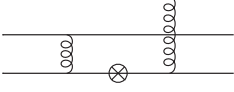
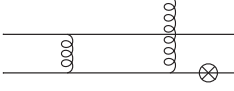
| i | Graph | $T_i(x, y)$ |
|-----|---|--|
| 1 |  | $\frac{\phi_N(x)\phi_N(y) + 4T(x)T(y)}{(1-x_1)^2(1-y_1)^2x_3y_3}$ |
| 2 |  | 0 |
| 3 |  | $\frac{-4T(x)T(y)}{(1-x_2)(1-y_1)x_1x_3y_1y_3}$ |
| 4 |  | $\frac{\phi_N(x)\phi_N(y)}{(1-x_3)(1-y_1)x_1x_3y_1y_3}$ |
| 5 |  | $\frac{-\phi_N(x)\phi_N(y)}{(1-x_3)(1-y_1)x_2x_3y_2y_3}$ |
| 6 |  | 0 |
| 7 |  | $\left(\frac{1}{x_1y_1} + \frac{1}{x_2y_2}\right) \frac{\phi_N(x)\phi_N(y)}{(1-x_3)^2(1-y_3)^2}$ |

Table 3.2.: Contributing diagrams for the calculation of Chernyak et al. II.

| i | Graph | $T_i(x, y)$ |
|-----|---|---|
| 8 |  | 0 |
| 9 |  | $\frac{\phi_N(x)\phi_N(y) + 4T(x)T(y)}{(1-x_1)^2(1-y_1)^2x_2y_2}$ |
| 10 |  | $\frac{\phi_N(x)\phi_N(y) + 4T(x)T(y)}{(1-x_1)^2(1-y_1)^2x_2y_2}$ |
| 11 |  | 0 |
| 12 |  | $\frac{-\phi_N(x)\phi_N(y)}{(1-x_3)(1-y_1)x_1x_2y_1y_2}$ |
| 13 |  | $\frac{4T(x)T(y)}{(1-x_1)(1-y_2)x_1x_2y_1y_2}$ |
| 14 |  | $\frac{-\phi_N(x)\phi_N(y)}{(1-x_1)(1-y_3)x_1x_2y_1y_2}$ |

3.1.4. Results obtained by automated procedure

Chernyak used various symmetry properties of the corresponding amplitudes in order to decrease the number of possible diagrams. In their case only 14 diagrams had to be considered. Since we have computer power we will not make use of any symmetries from the start but allow the program to generate all possible diagrams. This is not exactly true. We use a trick in order to make the program only generate half of the diagrams needed by pretending a nucleon consist of three flavors. This omits crossing diagrams which would occur in the full consideration.

Generating the possible diagrams for the LO case

The first step is to generate all possible diagrams contributing to the order of perturbation theory. In order to apply collinear factorization, which we introduced in Section 2.3.1, we need at least two gluons which connect all three fermion lines. Since we do not rely completely on the machine intelligence we will first try to generate all diagrams via combinatorial analysis. With the restriction mentioned above we can construct 6 basic diagrams.

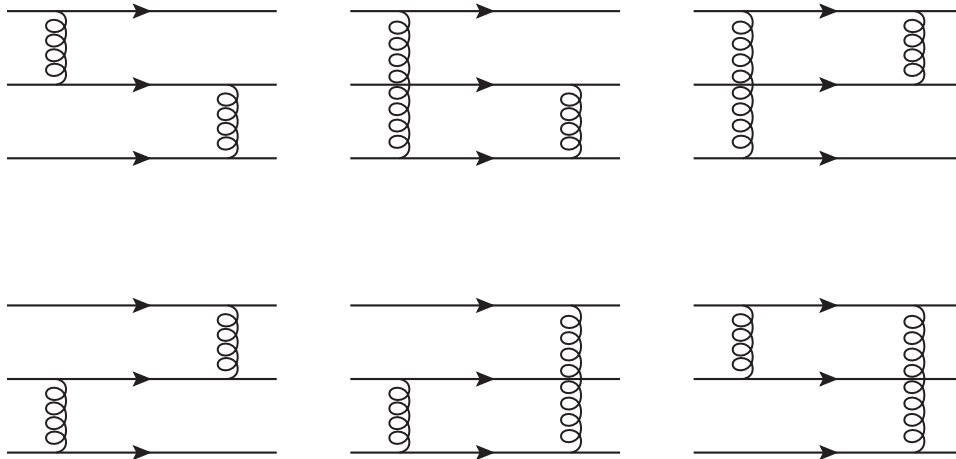


Figure 3.4.: Six basic diagrams

Since we deal with QCD three gluon vertices can in principle also occur, but do not contribute to this order in perturbation theory because the color factor for these diagrams is zero. Note that there would actually be six diagrams with three gluon vertices generated by the FA routine, which we neglect because of the color factor. The next step is to count

the possible insertions for the electromagnetic current into the fermion lines. For example we will take the first diagram from Fig. 3.4. There are seven possibilities to place the current which are shown in Fig. 3.5.

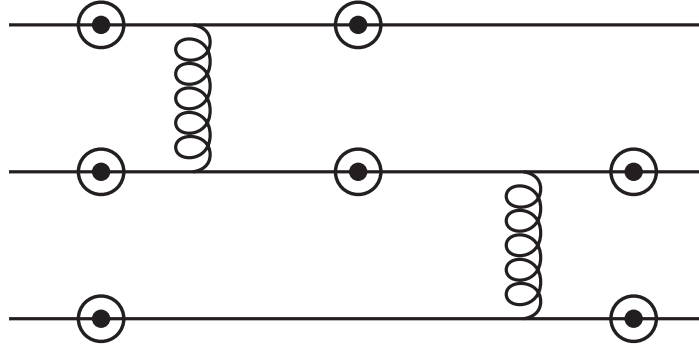


Figure 3.5.: Possible insertion locations for the electromagnetic current $\bar{q}\gamma^\mu q$

If we follow the routine described in Section 2.4 the program we will generate the diagrams for the leading order case. For this we use the following command in the FeynArts environment. First generate the possible topologies:

```
t4n3leadingorder=CreateTopologies[0, 4 -> 3, Adjacencies -> {3, 4}]
```

This comand line generates all topologies for a connected amplitude where 4 initial particles propagate and interact and in the final state only 3 remain. The 0 denotes the fact we are not allowing loops. We are permitting all gluon interactions, due to the adjacencies option. Note that there are actually no 4 gluon vertices to this order of perturbation theory. The next step involves the specification of the participating fields.

```
InsertFields[
  t4n3leadingorder, {V[1], F[3, {1}], F[4, {1}],
    F[4, {2}]} -> {F[3, {1}], F[4, {1}], F[4, {2}]}, Model -> "SMQCD",
  ExcludeParticles -> {S, U[5], V[1], V[2], V[3], Generic},
  Restrictions -> {NoQuarkMixing},
  InsertionLevel -> {Classes}];
```

The 4 incoming particles are a photon $V[1]$, as well as up-, down- and strange- quarks $F[3,1]$, $F[4,1]$ and $F[4,2]$. We use the standard model QCD Lagrangian and do not

allow flavor changing currents. Although it is not necessary to exclude special particles to this order of perturbation theory it is for the NLO case. And since we want to use the same code for verifying the correctness it is obvious to over-restrict our problem. Now FA can produce graphic output for the corresponding amplitudes which are displayed in Figs. 3.6, 3.7 and 3.8.

$$\gamma \ u \ u \ d \rightarrow u \ u \ d$$

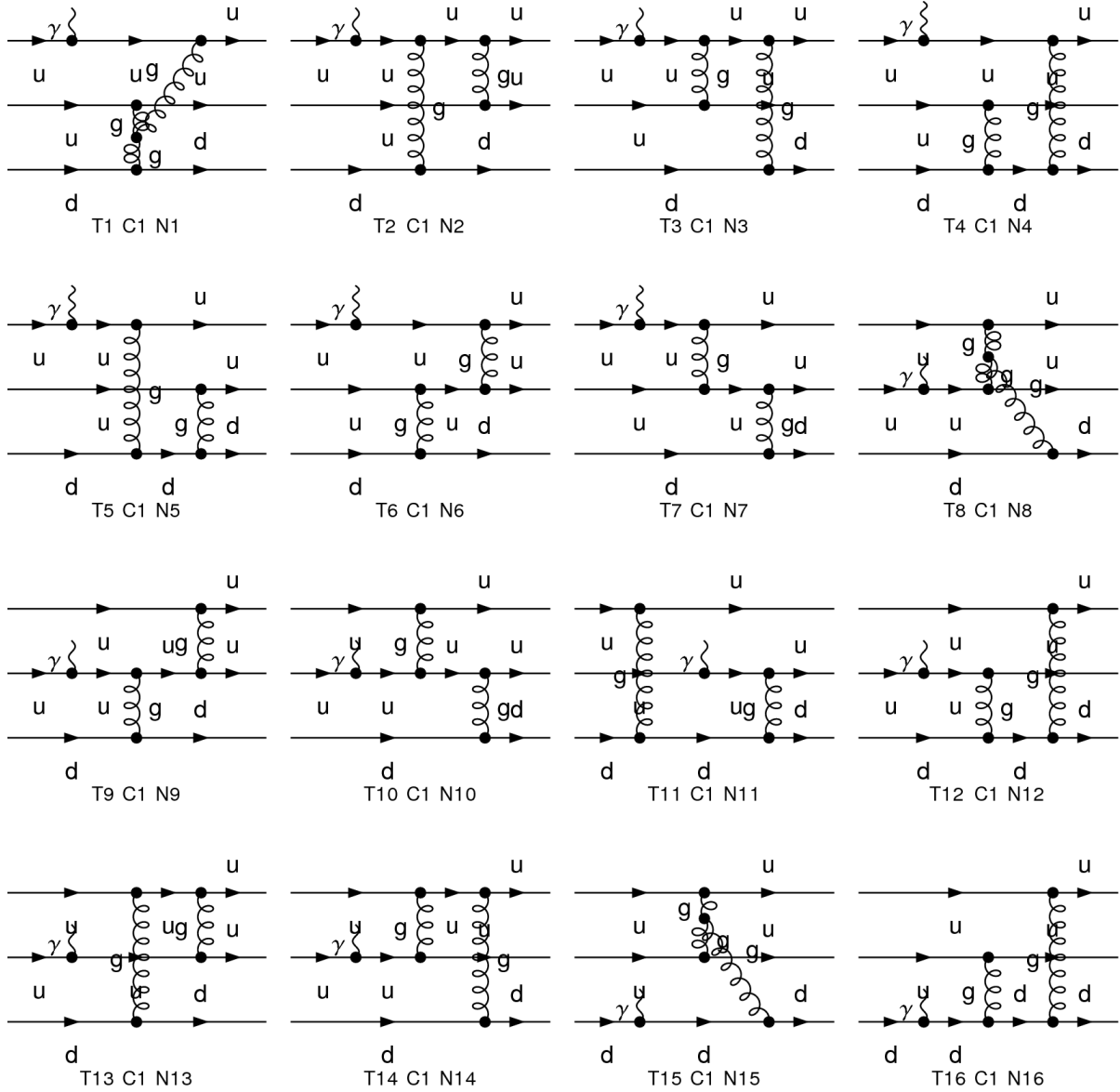


Figure 3.6.: Computer generated LO diagrams 1/3

$$\gamma \ u \ u \ d \rightarrow u \ u \ d$$

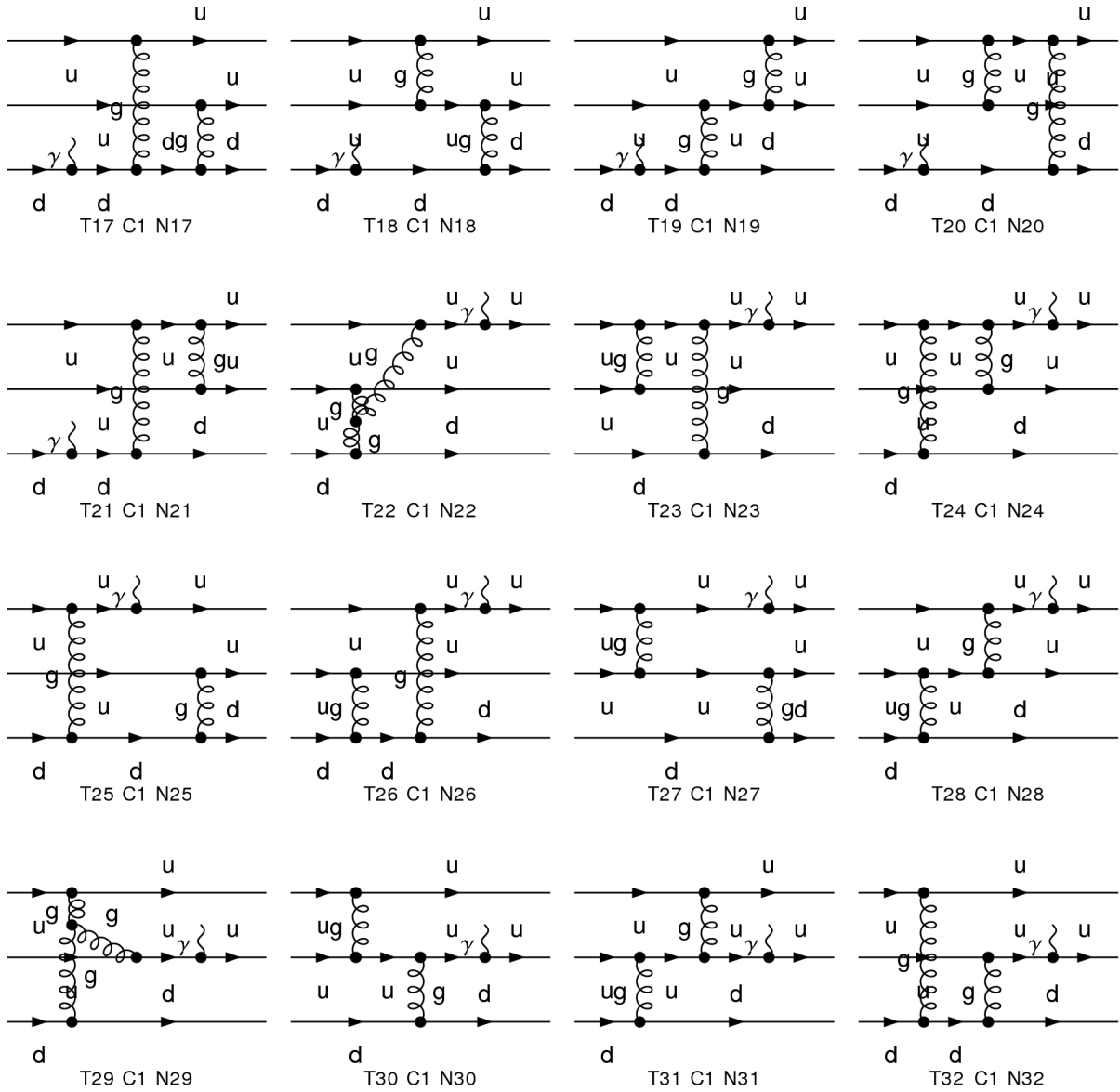


Figure 3.7.: Computer generated LO diagrams 2/3

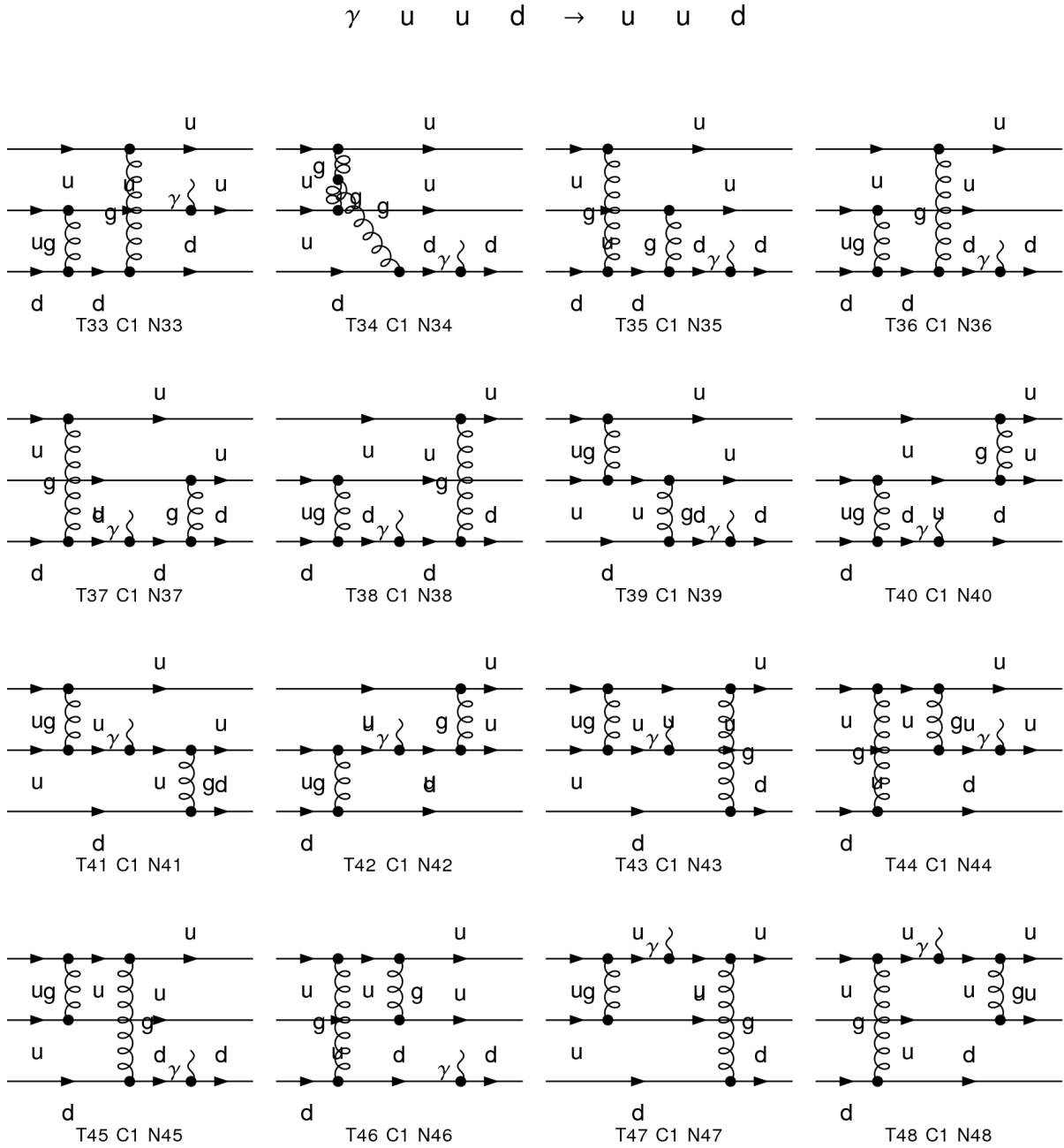


Figure 3.8.: Computer generated LO diagrams 3/3

From FA to FC

The 48 amplitudes generated by FA can now be contracted with the projectors from Section 2.3.2. This can be done within the FeynCalc package. Omitting all structures except

CHAPTER 3. CALCULATIONS

$\bar{N}(P')\gamma^\alpha N(P)$ the final result is given in the Tables 3.3, 3.4 and 3.5.

Table 3.3.: Results for the diagrams in Fig. 3.6.

| N | Result |
|----|---|
| 1 | 0 |
| 2 | $-\frac{2e_u \bar{N}(P') \gamma^\alpha N(P) (A_1 ^2(D-2) + (D-4)^2 T_1 ^2 + (D-2) V_1 ^2)}{a_2 a_3 b_2 b_3 Q^4 (a_2 + a_3) (b_1 + b_2)}$ |
| 3 | $\frac{2e_u \bar{N}(P') \gamma^\alpha N(P) (A_1 ^2(D-4) + ((D-14)D + 32) T_1 ^2 + (D-4) V_1 ^2)}{a_2 a_3 b_2 b_3 Q^4 (a_2 + a_3) (b_1 + b_3)}$ |
| 4 | 0 |
| 5 | $\frac{4e_u \bar{N}(P') \gamma^\alpha N(P) (A_1 ^2 + (3D-8) T_1 ^2 + V_1 ^2)}{a_2 b_2 Q^4 (a_2 + a_3)^2 (b_2 + b_3)^2}$ |
| 6 | 0 |
| 7 | $\frac{4e_u \bar{N}(P') \gamma^\alpha N(P) (A_1 ^2 + (3D-8) T_1 ^2 + V_1 ^2)}{a_3 b_3 Q^4 (a_2 + a_3)^2 (b_2 + b_3)^2}$ |
| 8 | 0 |
| 9 | $-\frac{2e_u \bar{N}(P') \gamma^\alpha N(P) (A_1 ^2(D-2) + (D-4)^2 T_1 ^2 + (D-2) V_1 ^2)}{a_1 a_3 b_1 b_3 Q^4 (a_1 + a_3) (b_1 + b_2)}$ |
| 10 | $\frac{2e_u \bar{N}(P') \gamma^\alpha N(P) (A_1 ^2(D-4) + ((D-14)D + 32) T_1 ^2 + (D-4) V_1 ^2)}{a_1 a_3 b_1 b_3 Q^4 (a_1 + a_3) (b_2 + b_3)}$ |
| 11 | 0 |
| 12 | $\frac{4e_u \bar{N}(P') \gamma^\alpha N(P) (A_1 ^2 + (3D-8) T_1 ^2 + V_1 ^2)}{a_1 b_1 Q^4 (a_1 + a_3)^2 (b_1 + b_3)^2}$ |
| 13 | 0 |
| 14 | $\frac{4e_u \bar{N}(P') \gamma^\alpha N(P) (A_1 ^2 + (3D-8) T_1 ^2 + V_1 ^2)}{a_3 b_3 Q^4 (a_1 + a_3)^2 (b_1 + b_3)^2}$ |
| 15 | 0 |
| 16 | $-\frac{2e_d \bar{N}(P') \gamma^\alpha N(P) (A_1 ^2(D-2) + (D-4)^2 T_1 ^2 + (D-2) V_1 ^2)}{a_1 a_2 b_1 b_2 Q^4 (a_1 + a_2) (b_1 + b_3)}$ |

Table 3.4.: Results for the diagrams in Fig. 3.7.

| N | Result |
|----|--|
| 17 | $-\frac{2e_d \bar{N}(P') \gamma^\alpha N(P) (A_1 ^2(D-2) + (D-4)^2 T_1 ^2 + (D-2) V_1 ^2)}{a_1 a_2 b_1 b_2 Q^4 (a_1 + a_2)(b_2 + b_3)}$ |
| 18 | 0 |
| 19 | $\frac{4e_d \bar{N}(P') \gamma^\alpha N(P) (A_1 ^2(D-2) + (D-4)^2 T_1 ^2 + (D-2) V_1 ^2)}{a_1 b_1 Q^4 (a_1 + a_2)^2 (b_1 + b_2)^2}$ |
| 20 | 0 |
| 21 | $\frac{4e_d \bar{N}(P') \gamma^\alpha N(P) (A_1 ^2(D-2) + (D-4)^2 T_1 ^2 + (D-2) V_1 ^2)}{a_2 b_2 Q^4 (a_1 + a_2)^2 (b_1 + b_2)^2}$ |
| 22 | 0 |
| 23 | $-\frac{2e_u \bar{N}(P') \gamma^\alpha N(P) (A_1 ^2(D-2) + (D-4)^2 T_1 ^2 + (D-2) V_1 ^2)}{a_2 a_3 b_2 b_3 Q^4 (a_1 + a_2)(b_2 + b_3)}$ |
| 24 | $\frac{2e_u \bar{N}(P') \gamma^\alpha N(P) (A_1 ^2(D-4) + ((D-14)D+32) T_1 ^2 + (D-4) V_1 ^2)}{a_2 a_3 b_2 b_3 Q^4 (a_1 + a_3)(b_2 + b_3)}$ |
| 25 | 0 |
| 26 | $\frac{4e_u \bar{N}(P') \gamma^\alpha N(P) (A_1 ^2 + (3D-8) T_1 ^2 + V_1 ^2)}{a_2 b_2 Q^4 (a_2 + a_3)^2 (b_2 + b_3)^2}$ |
| 27 | 0 |
| 28 | $\frac{4e_u \bar{N}(P') \gamma^\alpha N(P) (A_1 ^2 + (3D-8) T_1 ^2 + V_1 ^2)}{a_3 b_3 Q^4 (a_2 + a_3)^2 (b_2 + b_3)^2}$ |
| 29 | 0 |
| 30 | $-\frac{2e_u \bar{N}(P') \gamma^\alpha N(P) (A_1 ^2(D-2) + (D-4)^2 T_1 ^2 + (D-2) V_1 ^2)}{a_1 a_3 b_1 b_3 Q^4 (a_1 + a_2)(b_1 + b_3)}$ |
| 31 | $\frac{2e_u \bar{N}(P') \gamma^\alpha N(P) (A_1 ^2(D-4) + ((D-14)D+32) T_1 ^2 + (D-4) V_1 ^2)}{a_1 a_3 b_1 b_3 Q^4 (a_2 + a_3)(b_1 + b_3)}$ |
| 32 | $\frac{4e_u \bar{N}(P') \gamma^\alpha N(P) (A_1 ^2 + (3D-8) T_1 ^2 + V_1 ^2)}{a_1 b_1 Q^4 (a_1 + a_3)^2 (b_1 + b_3)^2}$ |

Table 3.5.: Results for the diagrams in Fig. 3.8.

| N | Result |
|----|---|
| 33 | 0 |
| 34 | 0 |
| 35 | $-\frac{2e_d\bar{N}(P')\gamma^\alpha N(P)(A_1 ^2(D-2)+(D-4)^2 T_1 ^2+(D-2) V_1 ^2)}{a_1a_2b_1b_2Q^4(a_1+a_3)(b_1+b_2)}$ |
| 36 | $-\frac{2e_d\bar{N}(P')\gamma^\alpha N(P)(A_1 ^2(D-2)+(D-4)^2 T_1 ^2+(D-2) V_1 ^2)}{a_1a_2b_1b_2Q^4(a_2+a_3)(b_1+b_2)}$ |
| 37 | $-\frac{2e_d\bar{N}(P')\gamma^\alpha N(P)(A_1 ^2(D-4)+((D-14)D+32) T_1 ^2+(D-4) V_1 ^2)}{a_1a_2b_1b_2Q^4(a_1+a_3)(b_2+b_3)}$ |
| 38 | $-\frac{2e_d\bar{N}(P')\gamma^\alpha N(P)(A_1 ^2(D-4)+((D-14)D+32) T_1 ^2+(D-4) V_1 ^2)}{a_1a_2b_1b_2Q^4(a_2+a_3)(b_1+b_3)}$ |
| 39 | $\frac{4e_d\bar{N}(P')\gamma^\alpha N(P)(A_1 ^2(D-2)+(D-4)^2 T_1 ^2+(D-2) V_1 ^2)}{a_1b_1Q^4(a_1+a_2)^2(b_1+b_2)^2}$ |
| 40 | 0 |
| 41 | $\frac{2e_u\bar{N}(P')\gamma^\alpha N(P)(A_1 ^2(D-2)+(D-4)^2 T_1 ^2+(D-2) V_1 ^2)}{a_1a_3b_1b_3Q^4(a_1+a_2)(b_2+b_3)}$ |
| 42 | $\frac{2e_u\bar{N}(P')\gamma^\alpha N(P)(A_1 ^2(D-2)+(D-4)^2 T_1 ^2+(D-2) V_1 ^2)}{a_1a_3b_1b_3Q^4(a_2+a_3)(b_1+b_2)}$ |
| 43 | 0 |
| 44 | $\frac{4e_u\bar{N}(P')\gamma^\alpha N(P)(A_1 ^2+(3D-8) T_1 ^2+ V_1 ^2)}{a_3b_3Q^4(a_1+a_3)^2(b_1+b_3)^2}$ |
| 45 | $\frac{4e_d\bar{N}(P')\gamma^\alpha N(P)(A_1 ^2(D-2)+(D-4)^2 T_1 ^2+(D-2) V_1 ^2)}{a_2b_2Q^4(a_1+a_2)^2(b_1+b_2)^2}$ |
| 46 | 0 |
| 47 | $\frac{2e_u\bar{N}(P')\gamma^\alpha N(P)(A_1 ^2(D-2)+(D-4)^2 T_1 ^2+(D-2) V_1 ^2)}{a_2a_3b_2b_3Q^4(a_1+a_2)(b_1+b_3)}$ |
| 48 | $\frac{2e_u\bar{N}(P')\gamma^\alpha N(P)(A_1 ^2(D-2)+(D-4)^2 T_1 ^2+(D-2) V_1 ^2)}{a_2a_3b_2b_3Q^4(a_1+a_3)(b_1+b_2)}$ |

If we now sum over all the 48 diagrams, set the dimension to $D = 4$ and work with the asymptotic wave function we end up with:

$$\begin{aligned}
 \text{FF}(Q^2, a_1, a_2, a_3, b_1, b_2, b_3) &= \frac{120^2 \cdot \bar{N}(P') \gamma^\alpha N(P)}{Q^4} \\
 &\times \left[e_u \left(\frac{40a_1a_2b_1b_2}{(a_1+a_3)^2(b_1+b_3)^2} + \frac{40a_1a_2b_1b_2}{(a_2+a_3)^2(b_2+b_3)^2} + \frac{40a_1a_3b_1b_3}{(a_2+a_3)^2(b_2+b_3)^2} \right. \right. \\
 &+ \frac{40a_2a_3b_2b_3}{(a_1+a_3)^2(b_1+b_3)^2} - \frac{4a_1b_1}{(a_2+a_3)(b_1+b_2)} - \frac{4a_2b_2}{(a_1+a_3)(b_1+b_2)} \\
 &- \frac{16a_1b_1}{(a_2+a_3)(b_1+b_3)} - \frac{16a_2b_2}{(a_1+a_3)(b_2+b_3)} - \frac{4a_1b_1}{(a_1+a_2)(b_2+b_3)} \\
 &- \frac{4a_2b_2}{(a_1+a_2)(b_1+b_3)} + \frac{4a_1b_1}{(a_1+a_2)(b_1+b_3)} + \frac{4a_2b_2}{(a_1+a_2)(b_2+b_3)} \\
 &- \frac{16a_1b_1}{(a_1+a_3)(b_2+b_3)} + \frac{4a_1b_1}{(a_1+a_3)(b_1+b_2)} - \frac{16a_2b_2}{(a_2+a_3)(b_1+b_3)} \\
 &\left. \left. + \frac{4a_2b_2}{(a_2+a_3)(b_1+b_2)} \right) \right. \\
 &+ e_d \cdot \left(\frac{16a_1a_3b_1b_3}{(a_1+a_2)^2(b_1+b_2)^2} + \frac{16a_2a_3b_2b_3}{(a_1+a_2)^2(b_1+b_2)^2} - \frac{4a_3b_3}{(a_1+a_2)(b_1+b_3)} \right. \\
 &- \frac{4a_3b_3}{(a_1+a_2)(b_2+b_3)} - \frac{4a_3b_3}{(a_1+a_3)(b_1+b_2)} + \frac{16a_3b_3}{(a_1+a_3)(b_2+b_3)} \\
 &\left. \left. - \frac{4a_3b_3}{(a_2+a_3)(b_1+b_2)} + \frac{16a_3b_3}{(a_2+a_3)(b_1+b_3)} \right) \right]. \tag{3.39}
 \end{aligned}$$

The last step is to integrate Equation (3.39) over the six momentum fractions

$$\int_0^1 da_1 \int_0^1 da_2 \int_0^1 da_3 \int_0^1 db_1 \int_0^1 db_2 \int_0^1 db_3 \delta(1-\bar{a}) \delta(1-\bar{b}) \text{FF}(Q^2, a_1, a_2, a_3, b_1, b_2, b_3) \tag{3.40}$$

with $\bar{a} = a_1 + a_2 + a_3$ and $\bar{b} = b_1 + b_2 + b_3$ which gives

$$\frac{120^2 \cdot \bar{N}(P') \gamma^\alpha N(P)}{Q^4} (2e_d + e_u). \tag{3.41}$$

Taking the numeric factors from the distribution amplitudes $(1/24)^2$ in Section 2.3.2 and color algebra (3.25), namely $\frac{8}{3}$ the final result for the proton and neutron form factors at leading order with our method reads as:

$$F_1^p = 0 \quad \text{and} \quad F_1^n = \frac{200}{3}. \tag{3.42}$$

This is the same result Chernyak et al. obtain up to a factor of 2. But there are two works by Brooks et al. [49] and Thomson et al. [50] which discuss this topic and conclude that there are simply two different normalization of the wave function which both are equally reasonable and explain the factor two discrepancy. They proposed a rather simple solution for the problem. Take a ratio of two quantities which depend on the normalizations of the wave function. Note that there is an unpublished work of K. Semenov [51] where he recalculated the proton form factor which agrees with the work of Chernyak et al. and our results. Since the result for the asymptotic wave function in the proton case is zero, the factor 2 becomes irrelevant.

3.2. Next-to-leading order

3.2.1. Generating the possible diagrams for the NLO case

In almost the same manner as for the leading case we will now generate all the diagrams contributing to the next order of perturbation theory. First we will construct the corresponding diagrams by hand, which means combinatorial. We will consider 13 types of gluon structures which are depicted in Fig. 3.9. Note that a black dot indicates a four gluon vertex. Now we have to find all possible combinations to connect three fermions, one of them interacts with the external photon, via gluons for the structures given in Fig. 3.9. Let us state some basic remarks. Every gluon attached to a fermion creates the opportunity to place the electromagnetic vertex at one additional position. Furthermore a fermion loop with three gluon insertions increases the number of contributing diagrams by four, because there is the possibility that both a up and a down quark can run through the closed fermion loop and we can have two different fermion line directions in the loop: On the one hand the quark momentum can flow clockwise in the loop and on the other hand counter-clockwise. A fermion loop with only two gluon insertions gives rise to a factor of two due to the possibility of up and down quark running in the loop.

- (a) First we will calculate the number of Feynman diagrams for the structure shown in Fig. 3.9(a). Therefore we will split this structure up into two categories. The first category includes all diagrams in which one of the gluons starts and ends on the same fermion line. This category includes 4 types of graphs shown in Fig. 3.10.

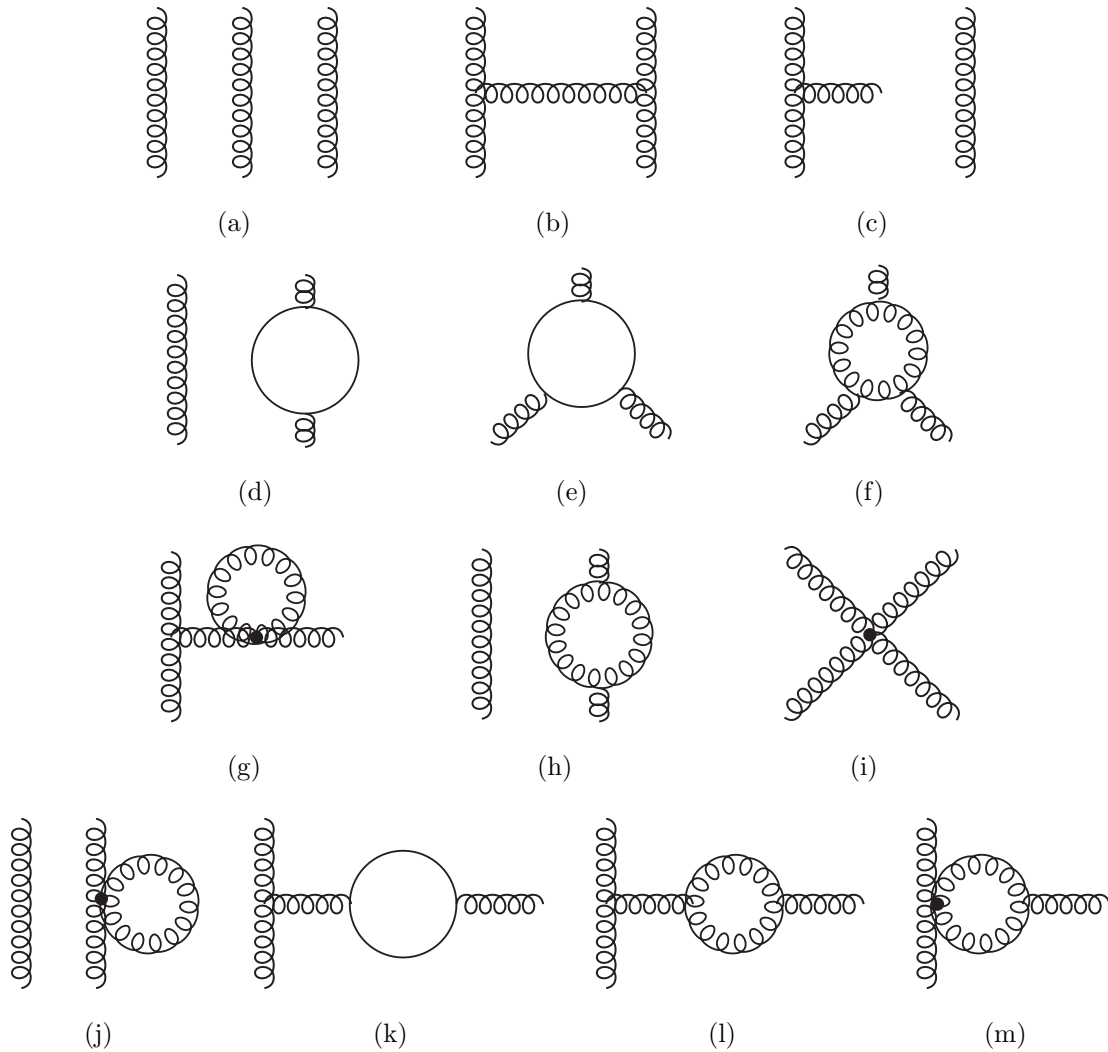


Figure 3.9.: Possible gluon structures for the NLO case

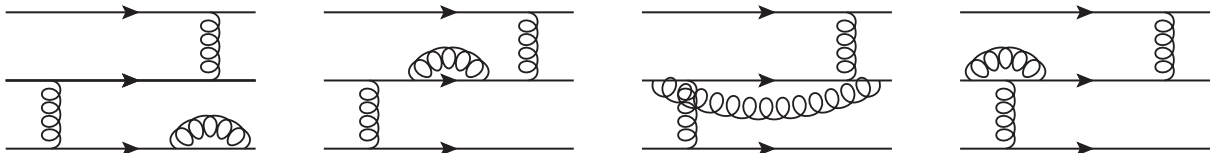


Figure 3.10.: Illustration for counting of structure 3.9(a) I.

The first type the gluon which stays on the same fermion line would be included in the wave function renormalization calculation if there would not be the electromagnetic vertex which can be inserted in two places depicted by the two little circles in Fig.

3.11. Since there are 6 basic diagrams and 6 possibilities to place the third gluon we end up with $6 \cdot 2 \cdot 6 = 72$ diagrams.

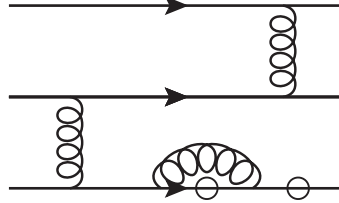


Figure 3.11.: Illustration for counting of structure 3.9(a) II.

The other 3 cases in Fig. 3.10 are pretty straightforward. Each of the second and third set of diagrams produce $6 \cdot 9 = 54$ diagrams since we have 9 possibilities to insert the electromagnetic vertex. For the last case in Fig. 3.10 there are 6 basic diagrams, each of them gives 4 possibilities to place the third gluon and there are also 9 slots to put the vertex and therefore 216 diagrams in total.

The second category deals with the case where all three gluons start and end on different fermion lines. For this case we distinguish 7 types of diagrams, which we write down in the following way:

$$\begin{aligned} & \begin{pmatrix} 1 & 1 & 1 \\ 2 & 2 & 3 \end{pmatrix} \begin{pmatrix} 1 & 1 & 2 \\ 2 & 2 & 3 \end{pmatrix} \begin{pmatrix} 1 & 1 & 1 \\ 2 & 3 & 3 \end{pmatrix} \begin{pmatrix} 1 & 1 & 2 \\ 2 & 3 & 3 \end{pmatrix} \\ & \begin{pmatrix} 1 & 2 & 2 \\ 2 & 3 & 3 \end{pmatrix} \begin{pmatrix} 1 & 1 & 2 \\ 3 & 3 & 3 \end{pmatrix} \begin{pmatrix} 1 & 2 & 2 \\ 3 & 3 & 3 \end{pmatrix} \end{aligned} \quad (3.43)$$

These tuples represent all possibilities to connect the quarklines. So the first tuples means we have two gluons which connect fermion line one and two and one gluon which couples to the first and third quark. All of these tuples give 6 possibilities except for

$$\begin{pmatrix} 1 & 1 & 2 \\ 2 & 3 & 3 \end{pmatrix}$$

which gives 8. So in the end we count $(6 \cdot 6 + 8) \cdot 9 = 396$. The final number of contributing diagrams for the structure 3.9(a) is 792.

- (b) The diagrams governed by structure 3.9(b) is a combination of the 6 basic diagrams depicted in Fig. 3.4 via an additional gluon plus 3 additional diagrams which are given in Fig. 3.12. Since there are 7 possible insertions this structure contributes $7 \cdot (6 + 3) = 63$ diagrams to the final result.

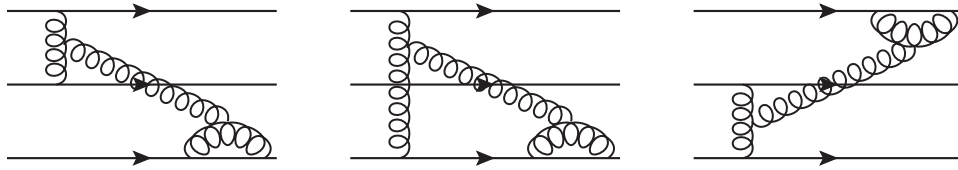


Figure 3.12.: Illustration for counting of structure 3.9(b)

(c) The next structure which we have to take into account, 3.9(c), is also the hardest one to count. On the one hand there are $6 \cdot 4 \cdot 8 = 192$ (6 basic diagrams, 4 possibilities which can be associated with the diagrams shown in Fig. 3.13 and 8 insertions) diagrams.

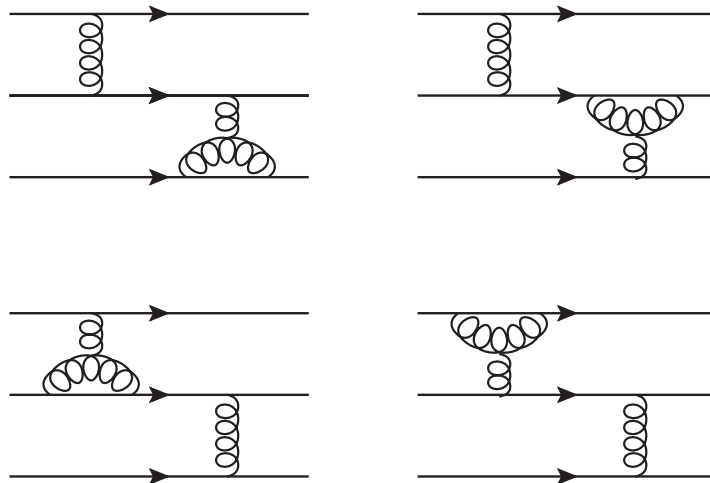


Figure 3.13.: Illustration for counting of structure 3.9(c) I.

On the other hand we can find diagrams in which the last gluon stays on one fermion line, too. But keep in mind that all quark lines have to be connected and so the three legs of the three gluon vertex all have to attach to different fermion lines. For the first diagram in Fig. 3.14 we have 6 possibilities to place the gluon and 2 insertion positions and therefore 12 contributions. For the second type of diagram in Fig. 3.14 there are $8 \cdot 3 = 24$ combinations.

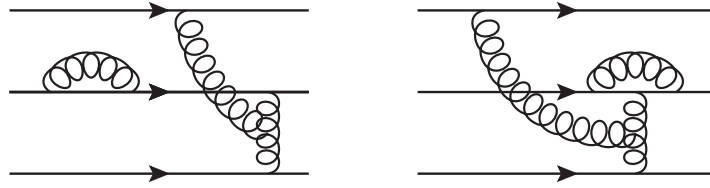


Figure 3.14.: Illustration for counting of structure 3.9(c) II.

There is also the possibility that the gluon which is not part of the three gluon vertex connects two quarks. This gives us additional $8 \cdot 6 = 48$ contributions. The final part of our puzzle deals with diagrams of the type shown in Fig. 3.15.

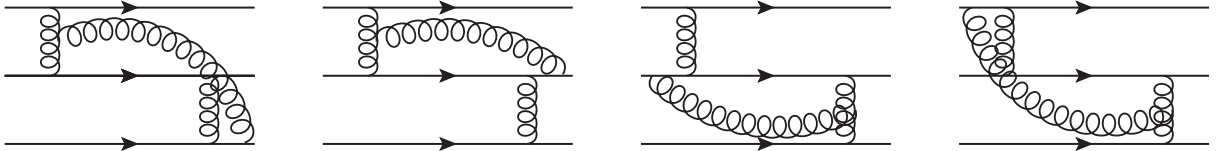


Figure 3.15.: Illustration for counting of structure 3.9(c) III.

From this case we obtain additional $8 \cdot (4 \cdot 6)/2 = 96$ terms to our final result. Note that the factor $1/2$ is included to circumvent double counting.

- (d) For structure 3.9(d) we can use the same considerations as elaborated for the leading order case. In principle we have 6 basic diagrams like in 3.4. The only difference is that one of our gluons is distinguished. Therefore we get an extra factor of two for each structure. Since we have 7 positions of insertion for the electromagnetic vertex on the fermion line and a factor 2 for up and down quark we get $6 \cdot 2 \cdot 7 \cdot 2 = 168$ combination. The occurring fermion loop gives $12 \cdot 2 \cdot 2$ additional possibilities for insertions of the electromagnetic vertex plus a factor of 2 due to the possibility of u type and d type quarks running in the closed loop. The final number of contributing diagrams for the structure in 3.9(d) is $168 + 48 = 216$ diagrams.
- (e) The graphs in 3.9(e) contribute 36 diagrams, because we have $6+3$ possibilities to insert the electromagnetic vertex. A factor of 2 due the possibility of u type and d type quarks running in the closed loop like in the previous case and a second factor 2 due to the different fermion line directions. So we end up with $2 \cdot 2 \cdot 9 = 36$ contributions.
- (f) Structure 3.9(f) is trivial since we have no freedom. We have to connect all three quarks with each other and therefore all three free legs have to attach to one of the

- fermions. But only one gluon insertion on each quark line leaves us with 6 positions for the electromagnetic vertex. And therefore 6 diagrams contribute to the final result.
- (g) Also pretty trivial is the structure in 3.9(g). There are only 3 ways to connect all the quarks via the gluons in the present case. In conclusion we have only one quark gluon vertex on each fermion line and therefore there are only 6 positions for the electromagnetic vertex (2 on each line). We obtain 18 additional diagrams for our final calculation.
 - (h) For 3.9(h) the same as for 3.9(d) holds except for the absence of the factor of 4 due to the additional fermion loop. 84 more diagrams for our final result.
 - (i) The structure shown in 3.9(i) gives only rise to 3 different possibilities to connect all 3 fermion lines. Since three of the four legs of the four gluon vertex are already fixed by the need for connection of all quarks lines there are only 3 options left. For the electromagnetic vertex we have now seven different places for insertion. So we end up with 21 diagrams which connect all quarks with the structure 3.9(i).
 - (j) The same statement as for 3.9(h) holds. Consequently the structure in 3.9(j) contributes 84 additional diagrams.
 - (k) For structure 3.9(k) we can add 48 diagrams. Three possible connections of all quark lines, 8 electromagnetic insertions and a factor of two due to the occurrence of a fermion loop with two gluon insertions.
 - (l) The same statement as for 3.9(g) holds and therefore 18 contributions.
 - (m) The same statement as for 3.9(g) holds and therefore 18 contributions.

In order to ensure only physical polarizations add to the final result we have to include ghost fields. For every closed gluon loop we need also a ghost loop. Therefore we get $2 \cdot 6$ for structure 3.9(f), 84 for 3.9(h) and 18 for 3.9(l). So in total 114 additional diagrams. Note the factor two for the contributions from 3.9(f) is due to the fact, that the direction of the gluons for a closed gluon loop is fixed due to the 3 three gluon vertices, but not for the ghost-gluon vertex. The final number of diagrams contributing to this order of perturbation theory is summarized in Table 3.6.

Table 3.6.: Summary of contributing terms

| Structure ID | Number of contributing diagrams |
|--------------|---------------------------------|
| 3.9(a) | 792 |
| 3.9(b) | 63 |
| 3.9(c) | 372 |
| 3.9(d) | 216 |
| 3.9(e) | 36 |
| 3.9(f) | 6 |
| 3.9(g) | 18 |
| 3.9(h) | 84 |
| 3.9(i) | 21 |
| 3.9(j) | 84 |
| 3.9(k) | 48 |
| 3.9(l) | 18 |
| 3.9(m) | 18 |
| ghosts | 114 |
| Σ | 1890 |

Now we are ready to use FeynArts [21, 22], introduced in section Section 2.4, to generate the diagrams needed for this order of perturbation theory. In principle we follow the steps of the leading order cases but allow loop contributions.

3.2.2. Color

The starting point for the calculation of the next-to-leading order color structure is the same as for the leading order case, i.e. see equation (3.22). The only difference is the appearance of graphs with three and four gluon vertices which do not vanish. In the following section we will derive the different color structures and give expressions generated by FeynCalc in a completely automated way. All results obtained by this routine have been recalculated by hand, using the identities and relations in Appendix A, and reproduce the same numeric values for the corresponding structure.

Table 3.7.: Color structure for the diagrams in 3.16 obtained via FeynCalc

| ID | Mathematica | $N = 3$ |
|-----------|---|-----------------|
| CS1 | $-\frac{1}{8}(1 - C_A)(2 - C_A)(C_A + 1)^2(1 - 2C_F)(C_A - 2C_F)$ | $\frac{20}{9}$ |
| CS2 | $-\frac{1}{8}(1 - C_A)(2 - C_A)(C_A + 1)^3/C_A^2$ | $-\frac{16}{9}$ |
| CS3 | $-\frac{1}{8}(1 - C_A)(2 - C_A)(C_A + 1)^2/C_A^2$ | $-\frac{4}{9}$ |
| CS4 | $\frac{1}{4}(2 - C_A)(C_A^2 + C_A + 1)C_F(C_A - 2C_F)$ | $-\frac{13}{9}$ |
| CS5 | $\frac{1}{4}(2 - C_A)(2C_A + 1)C_F(C_A - 2C_F)$ | $-\frac{7}{9}$ |
| CS6 | $\frac{1}{4}(2 - C_A)(-C_A^3 + C_A^2 + 2C_A + 1)C_F(C_A - 2C_F)$ | $\frac{11}{9}$ |
| CSSE | $-\frac{1}{8}(1 - C_A)^2(2 - C_A)(C_A + 1)^3/C_A^2$ | $\frac{32}{9}$ |
| CS2F1 | $-\frac{1}{4}i(2 - C_A)C_A^2C_F(C_A - 2C_F)$ | $\frac{5}{3}$ |
| CS2F2 | $\frac{1}{8}(1 - C_A)(2 - C_A)(C_A + 1)^2(C_A - 2C_F)$ | $\frac{4}{3}$ |
| CS1G1 | $\frac{1}{8}i(1 - C_A)(2 - C_A)(C_A + 1)^2$ | $4i$ |
| CS1G2 | $-\frac{1}{4}i(2 - C_A)C_AC_F$ | i |
| CS1G3 | $-\frac{1}{4}i(2 - C_A)C_A^2C_F$ | $3i$ |
| CS1G4 | $-\frac{1}{8}i(1 - C_A)(2 - C_A)(C_A + 1)^2$ | $-4i$ |
| CS1G5 | $\frac{1}{4}i(2 - C_A)C_AC_F$ | $-i$ |
| CS1G6 | $\frac{1}{4}i(2 - C_A)C_A^2C_F$ | $-3i$ |
| CS2G | $\frac{1}{4}(2 - C_A)C_A^2C_F$ | -3 |
| CSGO/CSGG | $\frac{1}{2}(2 - C_A)C_A(C_A + 1)C_F$ | -8 |
| CS4G | $C_A^2(C_A^2 - 4C_F - 1)$ | 24 |

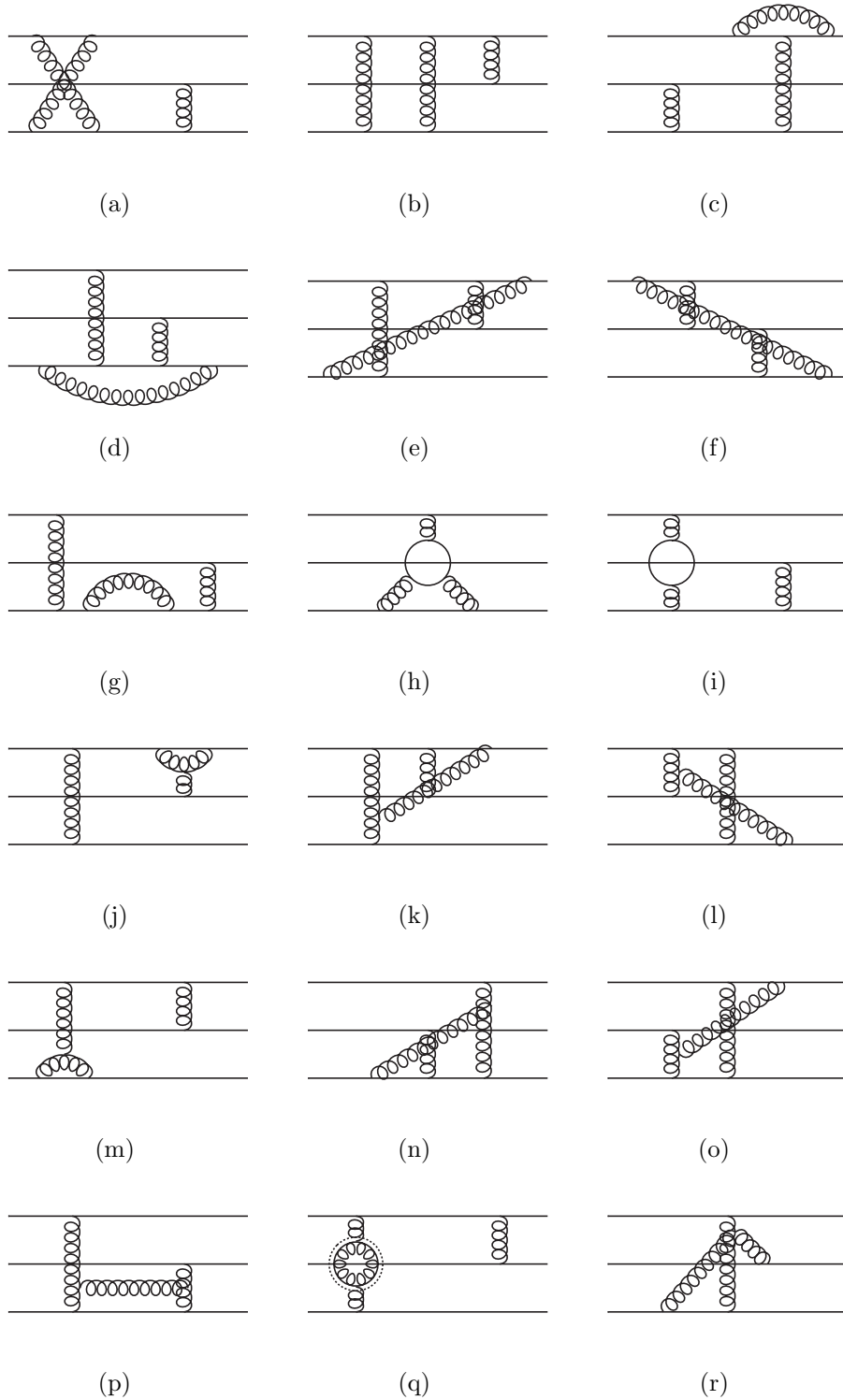


Figure 3.16.: Possible color structures for next-to-leading order diagrams
 (a)=CS1, (b)=CS2, (c)=CS3, (d)=CS4, (e)=CS5, (f)=CS6, (g)=CSSE, (h)=CS2F1,
 (i)=CS2F2, (j)=CS1G1, (k)=CS1G2, (l)=CS1G3, (m)=CS1G4, (n)=CS1G5,
 (o)=CS1G6, (p)=CS2G, (q)=CSGG/CSGO, (r)=CS4G

Let us state some remarks concerning these color factors:

- All structures containing a three gluon vertex inherit some ambiguities. So for example the structure CS2G gives a factor of -3 if one strictly follows the Feynman rules from [26] with total antisymmetric tensors always running counter clockwise. But in the routine we wrote Mathematica always tries to order it alphabetically and produces always $+3$. The additional sign is absorbed into the rest of the amplitude.
- The same statement holds for the structures CS1G1 to CS1G6. There should be a symmetric count of each color structure. But in reality the signs are quasi random due to the fact that FeynArts tries to arrange it in a alphabetic way.
- The color factors for the gluon and ghost loop diagrams should be identical. But we observed that FA rearranges the indices in that way we get $+8$ for CSGG and -8 for CSGO. The correct value for the Feynman rules from [26] is -8 .

Actually there are more possible diagrams which are depicted in Fig. 3.17:

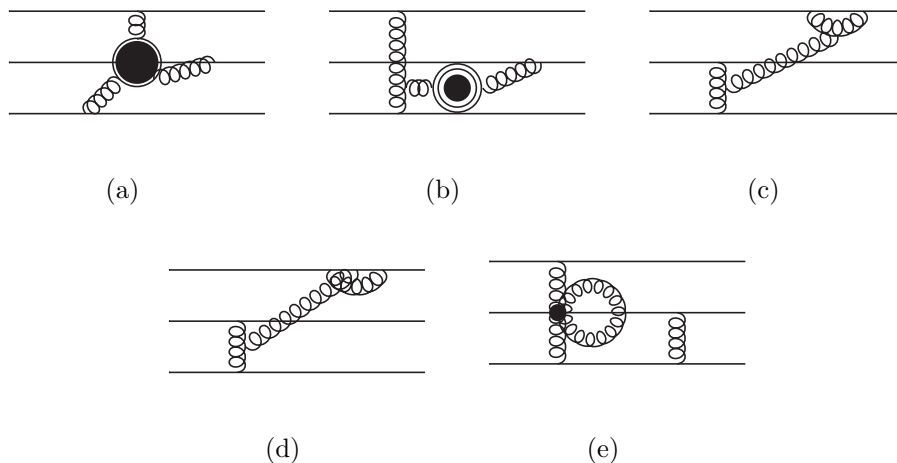


Figure 3.17.: Additional color structures which can be neglected due to the fact that they are zero because of color algebra or generating scaleless integrals. The black circle in 3.17(a) denotes gluon and ghost loops and the black circles in 3.17(b) denotes gluon, ghost and fermion loops.

(a)=CS0nr1, (b)=CS0nr2, (c)=CS0nr3, (d)=CS0nr4, (e)=CS0nr5

The color structures in Fig. 3.17(a) and 3.17(b) are zero for the same reason. Taking Eq. (3.22) into account and applying it to either of the cases we obtain:

$$(\text{Tr}(T^a T^c T^b) + \text{Tr}(T^a T^b T^c)) \mathcal{F}^{abc} = \frac{1}{2} d^{abc} \mathcal{F}^{abc} \quad (3.44)$$

Here d^{abc} is the totally symmetric structure constant and \mathcal{F}^{abc} is a function containing traces and anti-symmetric tensors. One can show that for all insertions for the circle in Fig. 3.17(b) the function \mathcal{F}^{abc} is totally antisymmetric and therefore is zero. For the case of Fig. 3.17(a) the same holds except the insertion is a fermion loop, e.g. CS2F1 3.16(h). The color structure in Fig. 3.17(c) reads with Eq. (3.22) and the identity in Appendix A as:

$$\begin{aligned}
 \text{CS0nr3} &= f^{bac} f^{cde} (\text{Tr}(T^b T^a T^e T^d) + \text{Tr}(T^b T^a T^d T^e)) \\
 &= f^{bac} f^{cde} (\text{Tr}(T^b T^a T^e T^d) - \frac{\delta^{ba} \delta^{de}}{2}) \\
 &= -d^{def} f^{abc} (d^{abf} - i f^{abf}) f^{cde} = 0 .
 \end{aligned} \tag{3.45}$$

This is true for all possible fermion line attachments. The same holds for the color structure in 3.17(d). The last possible configuration refers to the closed gluon loop due to a four-gluon vertex 3.17(e). This sort of diagram is not zero because of the corresponding color factor but produces scaleless integrals

$$\int d^D q \frac{1}{(q^2 + i\epsilon)^n} = 0 . \tag{3.46}$$

These kind of integrals give zero when evaluated in dimensional regularization [26].

3.2.3. Tracing

Up to now we have only generated all possible diagrams and solved the color algebra for our NLO calculation. As mentioned at the beginning of this chapter, we can use the code of the LO calculation. Therefore we apply the formulas in Equations (3.12), (3.14), (3.15) and (3.17) to our 1890 diagrams. The mayor problem of this step is the huge amount of gamma matrices. There are two extreme cases which can occur and pose the biggest problems concerning the computation time:

1. All vertices, quark gluon and the electromagnetic except for one quark gluon vertex are positioned on the first two fermion lines. This leads to expressions with 12 Dirac matrices in the trace:

$$\text{Tr}(\gamma^\alpha \not{p}_{f1} \gamma^\beta \not{p}_{f2} \gamma^\gamma \not{p}_{f3} \gamma^\delta \not{P} \gamma^\gamma \not{p}_{f4} \gamma^\beta \not{P}') . \tag{3.47}$$

2. Only one quark gluon vertex on each of the first two lines leads to:

$$\bar{N}(P') \gamma^\beta \not{p}_{f1} \gamma^\gamma \not{p}_{f2} \gamma^\alpha \not{p}_{f3} \gamma^\delta \not{p}_{f4} \gamma^\beta N(P) . \tag{3.48}$$

Here \not{p}_{fi} denote internal quark propagators with momentum p_{fi} .

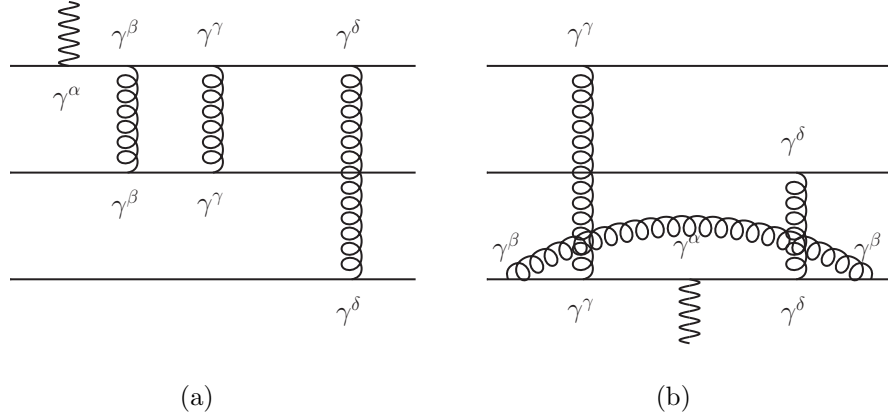


Figure 3.18.: Maximal number of Dirac matrices in a trace and between the two nucleon spinors

One crucial point to mention: The following operations and simplifications could not be executed to all diagrams in the same order. For example it was often necessary to simplify expressions before contracting the open Lorentz indices. These simplifications have been applied to the amplitudes:

- make use of the Dirac equation: $\not{P}N(P) = 0$ and $\bar{N}(P')\not{P}' = 0$.
- dealing with massless nucleons and quarks: $P^2 = 0$ and $(P')^2 = 0$.
- the latter also leads to $0 = (P + Q)^2 \rightarrow P \cdot Q = -\frac{Q^2}{2}$.

Here P is the momentum of the initial nucleon and $P' = P + Q$ is the momentum of the outgoing nucleon. Note that Q^2 is not the $Q^2 = -q^2$ from the definition of the form factor, but the momentum transfer q^2 . So here small q denotes the loop momenta and Q is the momentum transfer. After using the simplifications we end up with expressions of the form:

$$\int d^D q f_{\mu\nu\beta\rho}(Q, P, g) \prod_{i=1}^7 \frac{q^\mu q^\nu q^\beta q^\rho \bar{N}(P') \gamma^\alpha N(P)}{(q + x_i P + y_i Q)^2} G(Q^2). \quad (3.49)$$

Here f is an arbitrary Lorentz structure, for example $g^{\mu\nu} P^\beta Q^\rho$, G is a function purely depending on Q^2 and b_i are coefficients containing arbitrary sums of the momentum fractions.

3.2.4. Integration

The reduction algorithm of Duplanić and Nižić [23] implemented in Mathematica by Nils Offen is not able to calculate an integral with maximal number of Lorentz indices and legs. I.e. 4 open indices and 7 external legs like the one in Eq.(3.49) and illustrated in Fig. 3.19. This is not because of limited applicability of the algorithm, but lack of sufficiently large machine power.

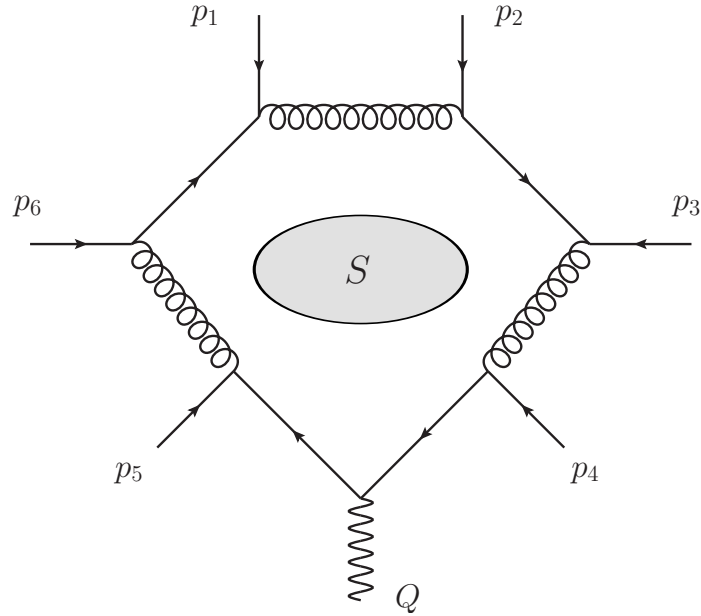


Figure 3.19.: Most complex diagram contributing to this order of perturbation theory. Schematic 7 point integral. For example $p_1 = x_1 P$ denotes the momentum of the incoming up quark.

Due to this we had to invent a procedure to cancel scalar products in the numerator containing the loop momentum q with some of the propagators in the denominator. This was done by extracting all the information of the propagator denominators, namely the x_i and y_i , from Eq. (3.49) and solve a simple linear equation system. After getting rid of one scalar product containing at least one loop momentum we can repeat this procedure up to the point when there is no solution for the linear equations. Now we will give the essential steps of this procedure: First re-express the scalar product in the numerator as a sum over

all propagators:

$$X \cdot q = \sum_{i=1}^N c_i (q + x_i P + y_i Q)^2 . \quad (3.50)$$

Here X can be P , Q or q which will lead to different conditions for solving the linear equation (3.50) and $N \in \mathbb{N}$ and $N \in [2, 7]$ for our problem. If one expands Eq. (3.50) one ends up with:

$$X \cdot q = \sum_{i=1}^N (c_i q^2 + c_i x_i^2 P^2 + (y_i^2 c_i - x_i y_i c_i) Q^2 + 2x_i c_i P \cdot q + 2y_i c_i Q \cdot q) . \quad (3.51)$$

Here we have used the identity $P \cdot Q = -\frac{Q^2}{2}$. Since $P^2 = 0$ we can omit this term in our further discussion. The term proportional to Q^2 does not pose any threat to the complexity of our calculation since it does obviously not depend on the loop momenta. Now we will perform the computation, i.e. we will give the different condition for the three cases $P \cdot q$, $Q \cdot q$ and $q \cdot q$.

- For $P \cdot q$ we solve $\sum_{i=1}^N c_i = 0$, $\sum_{i=1}^N y_i c_i = 0$ and $\sum_{i=1}^N x_i c_i = 1/2$.
- For $Q \cdot q$ we solve $\sum_{i=1}^N c_i = 0$, $\sum_{i=1}^N y_i c_i = 0$ and $\sum_{i=1}^N x_i c_i = 1/2$.
- For $q \cdot q$ we solve $\sum_{i=1}^N c_i = 1$, $\sum_{i=1}^N y_i c_i = 0$ and $\sum_{i=1}^N x_i c_i = 0$.

Let us recapitulate shortly. The x_i and y_i are input parameters from our generated diagrams. With a simple ‘‘Solve’’ command we can now get the coefficients c_i . Depending on how many coefficients c_i are unequal zero (n), we transform a N -point tensor integral of rank M into n ($N - 1$)-point tensor integral of rank $(M - 1)$ or $(M - 2)$ for X being q . This procedure can be applied recursively until no more solutions can be found.

With this method we can reduce our problem from having up to 7-point integrals of rank 4 to only scalar 7-, 6- and 5-point integrals and lower point tensor integrals. After integration we set $D = 4 + 2\epsilon$ and make a series expansion in ϵ . We separate terms which are finite, proportional to $1/\epsilon$ and proportional to $1/\epsilon^2$. The sum over all diagrams cancels out all double poles. The terms proportional to the single pole, denoted by $FF_{\epsilon-1}(a_1, a_2, b_1, b_2, Q^2)$, have been integrated over

$$\int_1^0 da_1 \int_{1-a_1}^0 da_2 \int_{b_1}^0 db_1 \int_{1-b_1}^0 db_2 FF_{\epsilon-1}(a_1, a_2, b_1, b_2, Q^2) \quad (3.52)$$

analytically and numerical with the Cuba library [52].

4. Results and checks

We have performed three non trivial checks in order to prove the consistency of our result with the leading order result of Chernyak et al.[20], the cancellation of all $1/\epsilon^2$ poles and the consensus of our next-to-leading order results which generate $1/\epsilon$ poles. The leading order is denoted by $T_H^{\alpha_S^2}$ and the next-to-leading order by $T_H^{\alpha_S^3}$.

$$\begin{aligned} T_H^{\alpha_S^2} &= \frac{3200}{3} \pi^2 \alpha_S^2 (2e_d + e_u) . \\ T_H^{\alpha_S^3} &= \frac{1600}{9} \frac{1}{\epsilon} \pi \alpha_S^3 (2n_f - 35) (2e_d + e_u) + \text{finite} . \end{aligned} \quad (4.1)$$

The non trivial checks are:

1. The code we used to calculate the NLO result is exactly the same with which we reproduced the leading order result by Chernyak [20] up to the aforementioned factor 2.
2. Due to the special kinematics in some of the diagrams $1/\epsilon^2$ poles appear. These poles appear when there is an overlap of collinear and soft divergences. But they cancel in the sum of all graphs.
3. Since we deal with a physical quantity the final result should, after renormalization, be finite. Therefore the $1/\epsilon$ divergences from Eq. (4.1) must cancel.

$$\left(T_H^{\alpha_S^3} + T_H^{\alpha_S^2} \left((\sqrt{Z_q})^6 + Z_{\alpha_S}^2 + Z_{f_N}^2 \right) \right) = 0 . \quad (4.2)$$

After setting $C_F = 4/3$, $C_A = 3$ and the gauge parameter $a = 1$ we end up with the

corresponding Z -factors:

$$Z_q = 1 + \frac{\alpha_S}{3\pi} \frac{1}{\epsilon} \quad \text{quark field renormalization} \quad (4.3)$$

$$Z_{\alpha_S} = 1 + \frac{\alpha_S}{4\pi} \frac{1}{\epsilon} \left(11 - \frac{2}{3} n_f \right) \quad \text{gauge field renormalization} \quad (4.4)$$

$$Z_{f_N} = 1 - \frac{\alpha_S}{3\pi} \frac{1}{\epsilon} \quad \text{renormalization of the distribution amplitude} \quad (4.5)$$

Note that the difference in signs from the renormalization constants from Eq. (2.51),..., (2.55) is due to the shift from $D = 4 - 2\epsilon$ to $D = 4 + 2\epsilon$. The renormalization constant for the leading twist distribution amplitude Z_{f_N} was taken from [53]. So adding up the next-to-leading and leading order times the appropriate renormalization constants we obtain for the term proportional to $\frac{1}{\epsilon}$:

$$\frac{1600}{9} \frac{1}{\epsilon} \pi \alpha_S^3 (2n_f - 35) (2e_d + e_u) + \left(\frac{\alpha_S}{\pi\epsilon} + \frac{\alpha_S}{2\pi\epsilon} \left(11 - \frac{2}{3} n_f \right) - \frac{2\alpha_S}{3\epsilon\pi} \right) \frac{3200}{3} \pi^2 \alpha_S^2 (2e_d + e_u) \quad (4.6)$$

It is easy to check that this is zero. Up to now everything was calculated completely analytically. For the finite part in Eq. (4.1) this does not hold anymore. More than this: We were not able to even compute some parts of the finite results numerically. The occurring denominators have overlapping poles (between a_i and b_i) all over the integration path. We could calculate all terms which do not have such mixing between the incoming and outgoing momentum fractions. Since the final result is only given for the asymptotic wave function there was no need to calculate the mixed cases vector-axial amplitude. But we have calculated all leading twist combination in an completely general form up to the point that one has to insert a certain model for the wave function and integrate over the corresponding momentum fractions:

$$\begin{aligned} & V_1^*(x_1, x_2, x_3) T_H^{\alpha_S^3}(x_1, x_2, x_3, y_1, y_2, y_3, Q^2, \mu^2) V_1(y_1, y_2, y_3) \\ & A_1^*(x_1, x_2, x_3) T_H^{\alpha_S^3}(x_1, x_2, x_3, y_1, y_2, y_3, Q^2, \mu^2) A_1(y_1, y_2, y_3) \\ & V_1^*(x_1, x_2, x_3) T_H^{\alpha_S^3}(x_1, x_2, x_3, y_1, y_2, y_3, Q^2, \mu^2) A_1(y_1, y_2, y_3) \\ & A_1^*(x_1, x_2, x_3) T_H^{\alpha_S^3}(x_1, x_2, x_3, y_1, y_2, y_3, Q^2, \mu^2) V_1(y_1, y_2, y_3) \\ & T_1^*(x_1, x_2, x_3) T_H^{\alpha_S^3}(x_1, x_2, x_3, y_1, y_2, y_3, Q^2, \mu^2) T_1(y_1, y_2, y_3) . \end{aligned} \quad (4.7)$$

One remarkable thing to mention is the fact that all information for each diagram is preserved till the end of the calculation. So there is the possibility to trace back every gauge invariant substructure, the color factors and all double and single poles to a certain diagram or integral.

5. Conclusion and outlook

We have started the first complete next-to-leading order calculation for the hard scattering kernel of the collinear factorized electromagnetic nucleon form factor. To achieve this task we developed a routine completely written in Mathematica to avoid unpleasant ambiguities due to export/import procedures to other programs or programming languages.

In the second chapter we gave a short introduction into QCD and the history of form factors. Among other things we also presented a detailed description how to translate the scattering picture into a theoretically accessible form which could be further processed with the Mathematica package FeynArts invented by Hagen Eck [21], Sepp Küblbeck et al. [22] and Thomas Hahn [2]. The amplitudes generated by this program can be calculated by the reduction algorithm introduced at the end of this chapter.

In chapter 3 we gave a step by step guide to calculate on the one hand the leading order contribution via the approach by Chernyak [20] and on the other hand with the routine we developed. After ensuring the consistency of both results, we applied the same routine, up to the point of integration, to the next-to-leading order problem. The result obtained in this way had to be integrated in D -dimensions over the loop momentum for which we implemented the reduction algorithm formulated by Duplancić and Nižić [23] into a Mathematica routine. The expressions obtained by this algorithm had to be preprocessed before we were able to integrate this results over the corresponding momentum fractions. After this task has been achieved we present three nontrivial checks in Chapter 4. All checks have been done analytically and have been verified numerically with the Cuba Mathematica package [52]. The finite result has been calculated for the most part in the same way. Only the four dimensional integrals containing denominators which mix the initial and final momentum fractions could not be solved up to now.

Our code could be used, by only slightly modifying two steps of our routine, for the two-photon exchange form factors. These are prime candidates for solving the discrepancy between Rosenbluth separation and polarization transfer measurements.

A. Color

The following identities and relations can be found in every textbook about QCD. We will mainly follow the work of Muta [26]. QCD is a quantum field theory based on the gauge group $SU(N)$ with $N = 3$. The generators T^A , with $a = 1 \dots (N^2 - 1)$ of the $SU(N)$ are traceless, Hermitian matrices which generate the closed algebra

$$[T^A, T^B] = if^{ABC}T^C , \quad (\text{A.1})$$

with f^{abc} being the totally antisymmetric structure constant. Quarks and gluons transform under different representations of the $SU(3)$. Quarks transform according to the 3-dimensional fundamental representation, which fulfills an additional anti-commutation relation:

$$\{T^A, T^B\} = \frac{1}{N}\delta_{AB} + d^{ABC}T^C . \quad (\text{A.2})$$

The totally symmetric tensor d^{ABC} can be written as:

$$d^{ABC} = 2\text{Tr}[\{T^A, T^B\}T^C] . \quad (\text{A.3})$$

On the other hand the gluons transform under the adjoint representation in which the generator T^A is a $(N^2 - 1) \times (N^2 - 1)$ dimensional matrix and its elements $(T^A)_{ij}$ are given by:

$$(T^A)_{ij} = -if^{Aij} . \quad (\text{A.4})$$

Since our final states are protons or neutrons we have to anti-symmetrize the hard scattering part with regard to color. Therefore we introduce the totally anti-symmetric tensor ϵ^{ijk} . Two tensors can be replaced by:

$$\epsilon^{ijk}\epsilon^{lmn} = \det \begin{pmatrix} \delta^{il} & \delta^{im} & \delta^{in} \\ \delta^{jl} & \delta^{jm} & \delta^{jn} \\ \delta^{kl} & \delta^{km} & \delta^{kn} \end{pmatrix} . \quad (\text{A.5})$$

APPENDIX A. COLOR

For our purpose the following relations and definitions come in handy: For the Levi Civita symbol we use the following identities:

$$\epsilon^{ijk}\epsilon^{ijk} = 6 \tag{A.6}$$

$$\epsilon^{ijk}\epsilon^{ijm} = 2\delta^{km} \tag{A.7}$$

$$\epsilon^{ijk}\epsilon^{imn} = \delta^{jm}\delta^{kn} - \delta^{jn}\delta^{km} . \tag{A.8}$$

For the generators we can utilize:

$$\text{Tr}(T^A) = 0 \tag{A.9}$$

$$\text{Tr}(T^A T^B) = \frac{1}{2}\delta^{AB} \tag{A.10}$$

$$T^A T^A = C_F \mathbb{1} \tag{A.11}$$

$$\text{Tr}(T^A T^A) = C_A C_F . \tag{A.12}$$

Here $C_A = N$ and $C_F = \frac{(N-1)^2}{N}$. Besides relying on Mathematica we also calculate the color factors by hand. For this we follow the work of Borodulin et al. [54]

B. Feynman Rules

The Feynman rules are taken from [26]. The QCD Lagrangian reads:

$$\mathcal{L}_{QCD} = \bar{\psi}(i\not{D} - m)\psi - \frac{1}{4}F_{\mu\nu}^A F^{\mu\nu,A} - \frac{1}{2a}(\partial^\mu A_\mu^A)^2. \quad (\text{B.1})$$

With a being the gauge parameter and

$$F_{\mu\nu} = T^A F_{\mu\nu}^A = T^A (\partial_\mu A_\nu^A - \partial_\nu A_\mu^A + gf^{ABC} A_\mu^B A_\nu^C) \quad (\text{B.2})$$

the gluon field strength tensor. The corresponding Feynman rules are stated in Tab B.1 and B.2 in which the following abbreviations are used:

$$V_{\mu_1\mu_2\mu_3}(k_1, k_2, k_3) = (k_1 - k_2)_{\mu_3} g_{\mu_1\mu_2} + (k_2 - k_3)_{\mu_1} g_{\mu_2\mu_3} + (k_3 - k_1)_{\mu_2} g_{\mu_3\mu_1}$$

$$d_{\mu\nu}(k) = g_{\mu\nu} - \frac{(1-a)k_\mu k_\nu}{k^2} \quad (\text{B.3})$$

$$A^{abcd,\mu\nu\rho\sigma} = f^{abe} f^{cde} (g^{\mu\rho} g^{\nu\sigma} - g^{\mu\sigma} g^{\nu\rho})$$

$$+ f^{ace} f^{bde} (g^{\mu\nu} g^{\rho\sigma} - g^{\mu\sigma} g^{\nu\rho})$$

$$+ f^{ade} f^{bce} (g^{\mu\nu} g^{\rho\sigma} - g^{\mu\rho} g^{\nu\sigma}). \quad (\text{B.4})$$

Noteworthy is the convention that every unknown loop momentum is integrated over

$$\int \frac{d^4q}{(2\pi)^4} \quad (\text{B.5})$$

and fermion loops give rise to a factor of -1 .

Table B.1.: Feynman rules I.

Propagators:

Quark propagator $i \xrightarrow{p} j$ $\delta_{ij} \frac{1}{m - \not{p}}$

Gluon propagator $A \mu \text{---} B \nu$ $\delta_{AB} \frac{d_{\mu\nu}(k)}{k^2}$

Ghost propagator $A \text{---} B$ $\delta_{AB} \frac{-1}{k^2}$

Vertices:

Quark-gluon vertex $i \text{---} j$ $g \gamma_\mu T_{ij}^A$

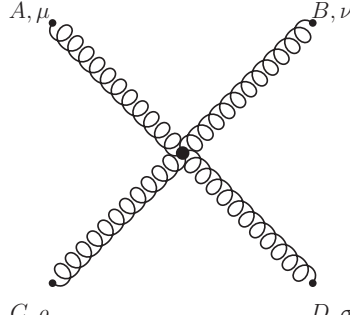
Ghost-gluon vertex $B \text{---} C$ $-ig f^{ABC} k_\mu$

3-gluon vertex $a_1 \mu_1, a_2 \mu_2, a_3 \mu_3$ $-if^{a_1 a_2 a_3} V_{\mu_1 \mu_2 \mu_3}(k_1, k_2, k_3)$

Table B.2.: Feynman rules II.

Vertices:

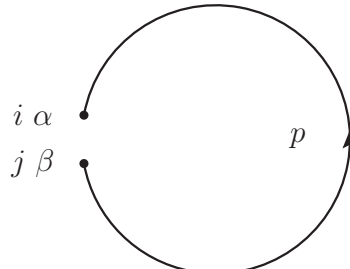
4-gluon vertex



$$-g^2 A_{\mu\nu\rho\sigma}^{ABCD}$$

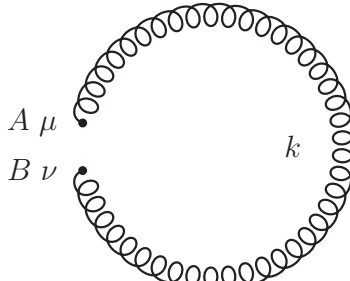
Loops:

Fermion loop



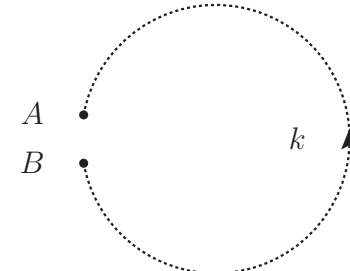
$$\int \frac{d^4 p}{(2\pi)^4} i\delta_{ij}\delta_{\alpha\beta}$$

Gluon loop



$$-\int \frac{d^4 k}{(2\pi)^4} i\delta_{AB}g^{\mu\nu}$$

Ghost loop



$$\int \frac{d^4 k}{(2\pi)^4} i\delta_{AB}$$

C. Dimensional regularization

In order to keep gauge invariance, one can use the dimensional regularization scheme introduced by t'Hooft in 1972 [55], in which we shift our dimension from

$$4 \rightarrow D = 4 - 2\epsilon, \tag{C.1}$$

and simultaneously redefine our coupling

$$g \rightarrow g\mu^\epsilon \tag{C.2}$$

where μ is an arbitrary (energy-) scale. The ultraviolet divergences now appear as ϵ -poles in the amplitude. The major advantages of dimensional regularization are:

- dimensional regularization preserves Lorentz invariance, i.e. after performing the calculation in d -dimensions one can simply take the limit $\epsilon \rightarrow 0$ and one ends up with a 4-dimensional Lorentz invariant result.
- the regularized theory stays gauge invariant.
- dimensional regularization covers infrared and ultraviolet divergences.

A major disadvantage is that all amplitudes or quantities containing a γ^5 matrix can not be extended to D dimension, because there is no generalization of the γ^5 matrix to dimension $4 \pm 2\epsilon$.

D. Mandelstam variables

In order to describe the kinematics of a scattering process it is convenient to introduce a minimal set of relativistic invariants. For our case, the elastic electron-nucleon scattering, the same number of particles in the initial and final state are needed as in the work of S. Mandelstam [56], who investigated the pion-nucleon scattering. For $2 \rightarrow 2$ scattering, one can describe the process through two Lorentz invariant quantities. In the original work these invariants had the the abbreviation s , t , u and s_c . The c stands for crossing symmetry. The modern terminology for these Lorentz invariant Mandelstam variables are s , t and u . They are defined as:

$$\begin{aligned} s &= (p_1 + p_2)^2 = (p_3 + p_4)^2 \\ t &= (p_1 - p_3)^2 = (p_2 - p_4)^2 \\ u &= (p_1 - p_4)^2 = (p_2 - p_3)^2 . \end{aligned} \tag{D.1}$$

The first is the center of mass enrgie and second one is the momentum transfer. In Fig. D.1 the different scattering channels are illustrated.

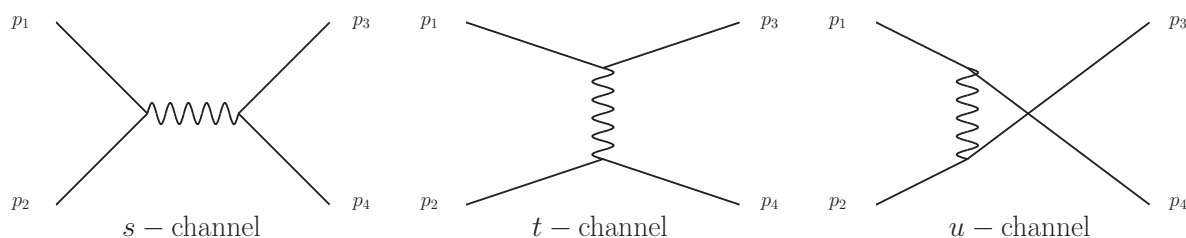


Figure D.1.: Feynman diagrams for the different scattering channels

The three Mandelstam variables for the considered process are not independent from each other. One can show that

$$s + t + u = \sum_{i=1}^4 m_i^2 \tag{D.2}$$

APPENDIX D. MANDELSTAM VARIABLES

where $p_i^2 = m_i^2$. Therefore there are only two independent relativistic quantities which describe the $2 \rightarrow 2$ scattering process.

E. Experimental results for G_E and G_M

Here we present the experimental results for the electric G_E and magnetic G_M form factor due to Rosenbluth separation method and polarization experiments. All plots are taken from the review of Perdrisat et al. [7]. The data points have been taken from works of more or less all electron collider facilities: I.e. Stanford Linear Accelerator Center (SLAC), the Continuous Electron Beam Accelerator Facility (CEBAF) at the Thomas Jefferson National Accelerator Facility (JLab), the Cambridge Electron Accelerator (CEA) at the MIT, Elektronen-Stretcher-Anlage (ELSA) in Bonn, the Mainz Microtron (MAMI) in Mainz and the Hadron-Electron Ring Accelerator (HERA) at DESY Hamburg. Further experiments have been done in Orsay, Amsterdam and at Cornell University. A summary of world data for the nucleon form factors is given in the work of Gao [4]. The experiments include scattering of low and high energy electrons (polarized, unpolarized) onto polarized and unpolarized proton, neutron, hydrogen, deuterium and helium targets.

E.1. Rosenbluth separation method

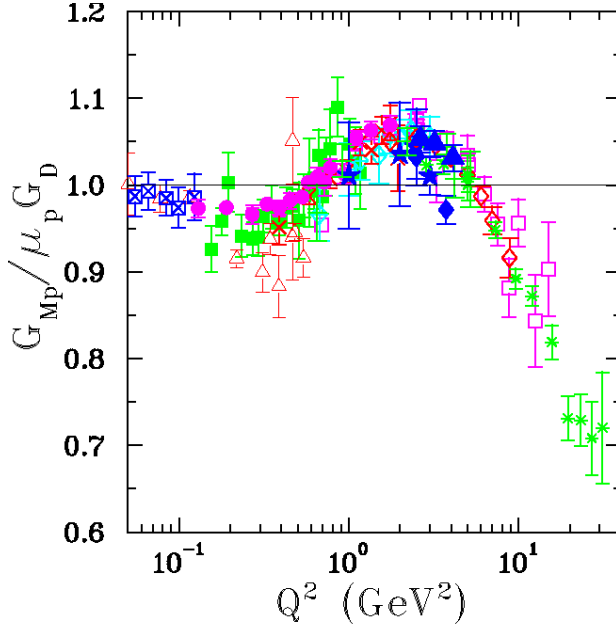
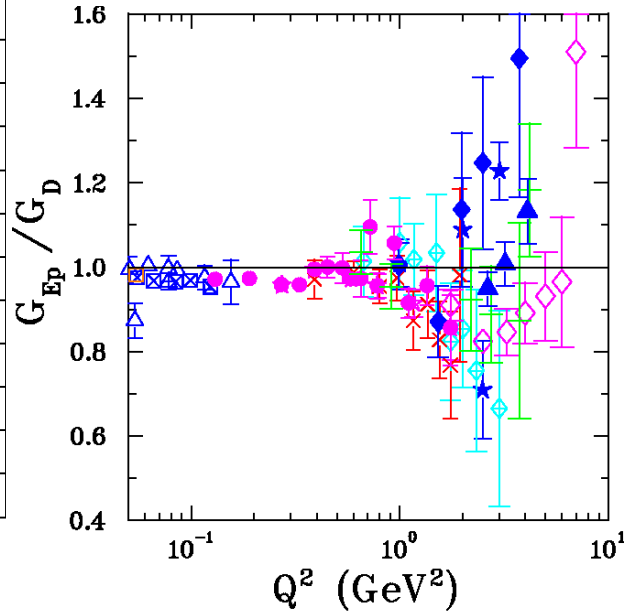

 Figure E.1.: G_{Mp}

 Figure E.2.: G_{Ep}

Figure E.3.: E.1: G_{Mp} obtained by Rosenbluth separation method. The data points are from works of: Han63 [57], Jan66 [58], Cow68 [59], Lit70 [60], Pri71 [9], Ber71 [11], Han73 [10], Bar73 [12], Bor75 [61], Sil93 [62], And94 [14], Wal94 [63], Chr04[64], Qat [65]

E.2: G_{Ep} obtained by Rosenbluth separation method. The data points are from works of: Han63[57], Litt70[60], Pri71[9], Ber71[11], Bar73[12], Han73[10], Bor75[61], Sim80[66], And94[14], Wal94[63], Chr04[64], Qat05[65]

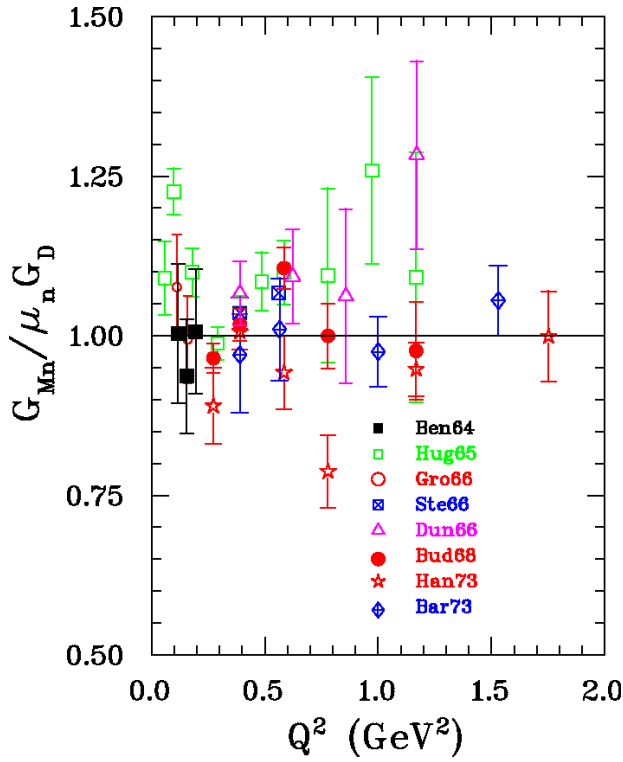
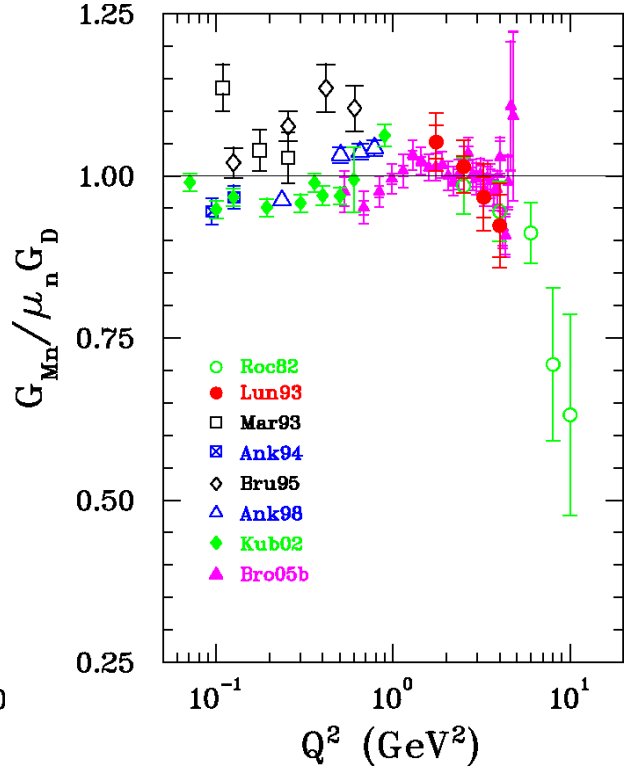

 Figure E.4.: G_{Mn}

 Figure E.5.: G_{Mn}

Figure E.6.: E.4: G_{Mn} obtained by Rosenbluth separation method older experiments: Ben64 [67], Hig65 [68], Gro66 [69], Ste66 [70], Dun66 [71], Bud68 [72], Han73 [10], Bar73 [12]

E.5: G_{Mn} obtained by Rosenbluth separation method, newer experiments: Roc82 [73], Lun93 [13], Mar93 [74], Ank94 [75], Bru95 [76], Ank98 [77], Kub02 [78], Bro05b [79]

E.2. Polarization transfer

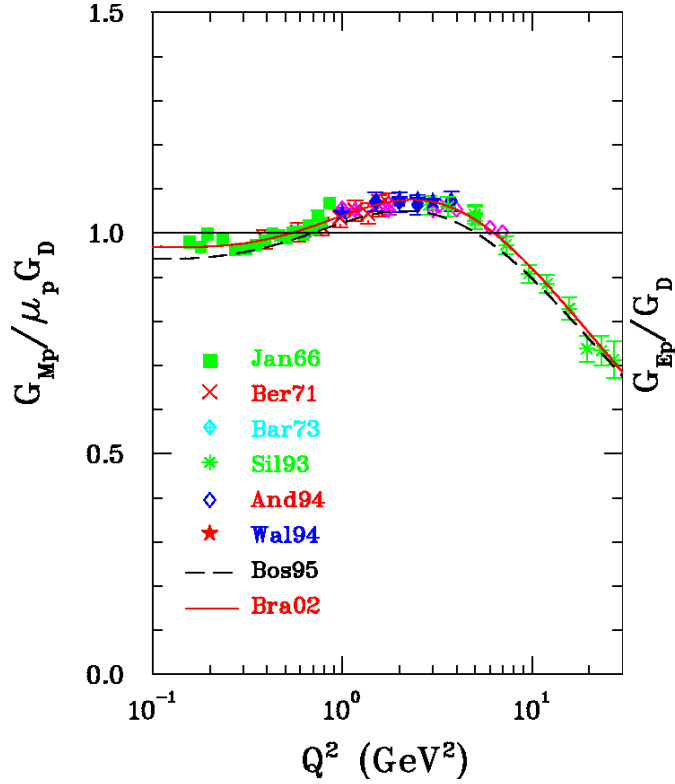


Figure E.7.: G_{Mp}

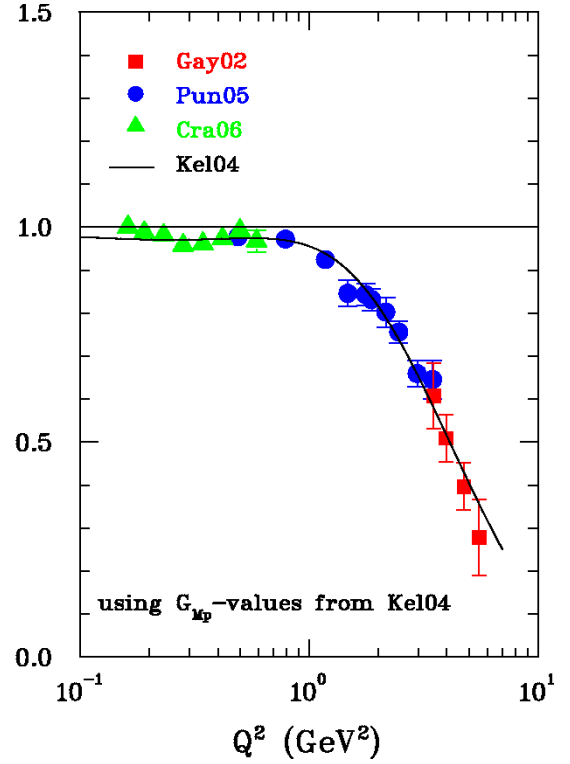


Figure E.8.: G_{Ep}

Figure E.9.: E.7: G_{Mp} obtained older values of Rosenbluth separation values up to 1 GeV Bra02 [80] and by polarization experiments Pun05[81], Gay02[82]
 E.8: G_{Ep} obtained by polarization experiments: Gay02 [82], Pun05 [81], Cra06[83], Kel04 [84]

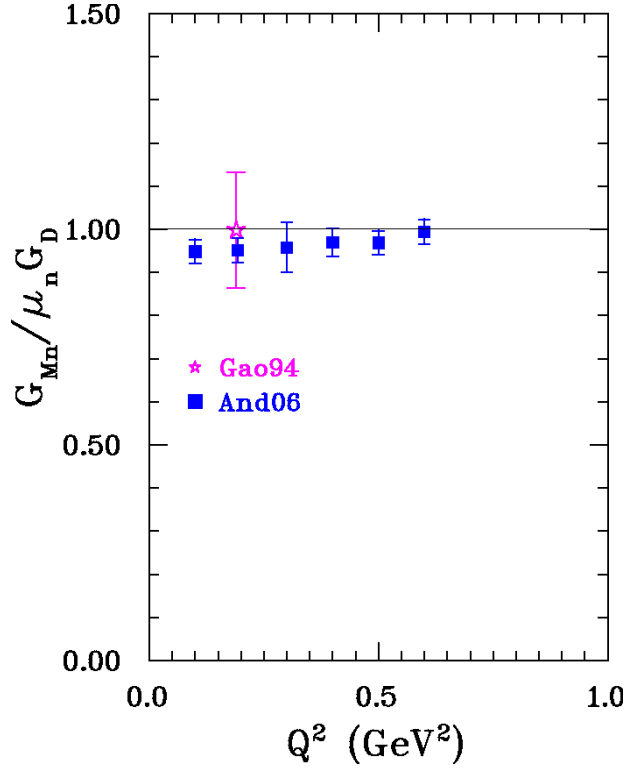
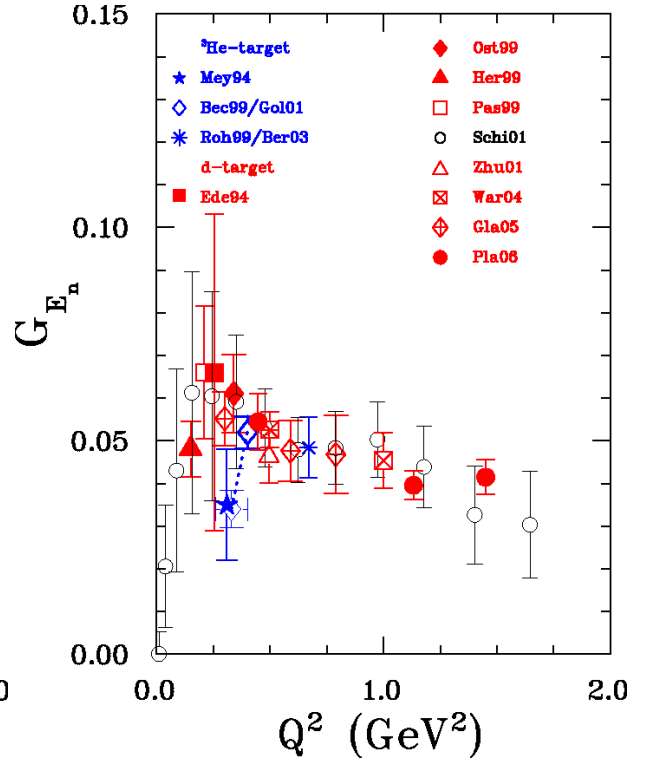

 Figure E.10.: G_{Mn}

 Figure E.11.: G_{En}

Figure E.12.: E.10: G_{Mn} obtained by polarization experiments: Gao94 [85], And06 [86]

E.11: G_E^n obtained by polarization experiments: ^3He : Mey94 [87], Bec99 [88], Gol01 [89], Roh99 [90], Ber03 [91]

^2H : Ede94 [92], Pas99 [93], Ost99 [94], Abo99 [95], Shi01 [96], Zhu01 [97], War04 [98], Gla05 [99], Pla05 [100]

F. Light-cone kinematics

We can define two independent vectors on the light-cone which characterize the latter:

$$n_+^\mu = (1, 0, 0, -1) \quad \text{and} \quad n_-^\mu = (1, 0, 0, 1) . \quad (\text{F.1})$$

Multiplying those two vectors leads to:

$$n_+^2 = n_-^2 = 0, \quad n_+ \cdot n_- = 2 . \quad (\text{F.2})$$

Every four-vector can be decomposed into these two light-like vectors plus a perpendicular component:

$$a^\mu = a_+ \frac{n_-^\mu}{2} + a_- \frac{n_+^\mu}{2} + a_\perp^\mu \quad (\text{F.3})$$

where $a_\pm \equiv a \cdot n_\pm$. A scalar product between two four vectors gives:

$$a^\mu b_\mu = \frac{a_+ b_- + a_- b_+}{2} - \vec{a}_\perp \cdot \vec{b}_\perp . \quad (\text{F.4})$$

G. Decomposition of the three quark matrix element

The operator product expansion for the three quark matrix element without definite twist taken from the work of Braun et al. [43]

$$\begin{aligned}
4 \langle 0 | \epsilon^{ijk} u_\alpha^i(a_1 z) u_\beta^j(a_2 z) d_\gamma^k(a_3 z) | P \rangle = & \\
& \mathcal{S}_1 M C_{\alpha\beta} (\gamma_5 N)_\gamma + \mathcal{S}_2 M^2 C_{\alpha\beta} (\not{z} \gamma_5 N)_\gamma + \mathcal{P}_1 M (\gamma_5 C)_{\alpha\beta} N_\gamma + \mathcal{P}_2 M^2 (\gamma_5 C)_{\alpha\beta} (\not{z} N)_\gamma \\
& + \mathcal{V}_1 (\not{P} C)_{\alpha\beta} (\gamma_5 N)_\gamma + \mathcal{V}_2 M (\not{P} C)_{\alpha\beta} (\not{z} \gamma_5 N)_\gamma + \mathcal{V}_3 M (\gamma_\mu C)_{\alpha\beta} (\gamma^\mu \gamma_5 N)_\gamma \\
& + \mathcal{V}_4 M^2 (\not{z} C)_{\alpha\beta} (\gamma_5 N)_\gamma + \mathcal{V}_5 M^2 (\gamma_\mu C)_{\alpha\beta} (i \sigma^{\mu\nu} z_\nu \gamma_5 N)_\gamma + \mathcal{V}_6 M^3 (\not{z} C)_{\alpha\beta} (\not{z} \gamma_5 N)_\gamma \\
& + \mathcal{A}_1 (\not{P} \gamma_5 C)_{\alpha\beta} N_\gamma + \mathcal{A}_2 M (\not{P} \gamma_5 C)_{\alpha\beta} (\not{z} N)_\gamma + \mathcal{A}_3 M (\gamma_\mu \gamma_5 C)_{\alpha\beta} (\gamma^\mu N)_\gamma \\
& + \mathcal{A}_4 M^2 (\not{z} \gamma_5 C)_{\alpha\beta} N_\gamma + \mathcal{A}_5 M^2 (\gamma_\mu \gamma_5 C)_{\alpha\beta} (i \sigma^{\mu\nu} z_\nu N)_\gamma + \mathcal{A}_6 M^3 (\not{z} \gamma_5 C)_{\alpha\beta} (\not{z} N)_\gamma \\
& + \mathcal{T}_1 (P^\nu i \sigma_{\mu\nu} C)_{\alpha\beta} (\gamma^\mu \gamma_5 N)_\gamma + \mathcal{T}_2 M (z^\mu P^\nu i \sigma_{\mu\nu} C)_{\alpha\beta} (\gamma_5 N)_\gamma \\
& + \mathcal{T}_3 M (\sigma_{\mu\nu} C)_{\alpha\beta} (\sigma^{\mu\nu} \gamma_5 N)_\gamma + \mathcal{T}_4 M (P^\nu \sigma_{\mu\nu} C)_{\alpha\beta} (\sigma^{\mu\rho} z_\rho \gamma_5 N)_\gamma \\
& + \mathcal{T}_5 M^2 (z^\nu i \sigma_{\mu\nu} C)_{\alpha\beta} (\gamma^\mu \gamma_5 N)_\gamma + \mathcal{T}_6 M^2 (z^\mu P^\nu i \sigma_{\mu\nu} C)_{\alpha\beta} (\not{z} \gamma_5 N)_\gamma \\
& + \mathcal{T}_7 M^2 (\sigma_{\mu\nu} C)_{\alpha\beta} (\sigma^{\mu\nu} \not{z} \gamma_5 N)_\gamma + \mathcal{T}_8 M^3 (z^\nu \sigma_{\mu\nu} C)_{\alpha\beta} (\sigma^{\mu\rho} z_\rho \gamma_5 N)_\gamma . \tag{G.1}
\end{aligned}$$

All those functions depend on $P \cdot z$ and do not have definite twist. The geometric twist t is defined as

$$t = l^{\text{can}} - s . \tag{G.2}$$

Here l^{can} is the canonical scaling dimension and s its Lorentz spin. The collinear- or light-cone- twist is defined in the same way but the spin is replaced by the spin projection on the light-cone.

$$t_{\text{col}} = l^{\text{can}} - s_{\text{col}} . \tag{G.3}$$

To achieve twist ordered invariant functions we go to the infinite momentum frame. In addition we define a second light like vector $p_\mu = P_\mu - \frac{1}{2} z_\mu \frac{M^2}{P \cdot z}$. Assuming the nucleon is

APPENDIX G. DECOMPOSITION OF THE THREE QUARK MATRIX ELEMENT

moving in the + direction of e_z only two components survive: $p_+ \sim Q$ and z_- . The infinite momentum limit gives $p_+ \sim Q \rightarrow \infty$ with fixed $P \cdot z = p \cdot z \sim 1$. Here Q is the large scale of the process. Expanding the matrix element in p_+ is the same as power counting in Q .

$$N(P, \lambda) = \frac{1}{2p \cdot z} (\not{p} \not{z} + \not{z} \not{p}) N(P, \lambda) = N^+(P, \lambda) + N_\gamma^-(P, \lambda). \quad (\text{G.4})$$

With (G.4) we can identify two projectors

$$\Lambda^+ = \frac{\not{p} \not{z}}{2p \cdot z} \quad \text{and} \quad \Lambda^- = \frac{\not{z} \not{p}}{2p \cdot z}, \quad (\text{G.5})$$

which project onto the different components (\pm) of the nucleon spinors. With the use of the Dirac equation $\not{P}N(P) = MN(P)$ we can show that:

$$\not{p}N(P) = MN^+(P) \quad \text{and} \quad \not{z}N(P) = \frac{2p \cdot z}{M} N^-(P). \quad (\text{G.6})$$

With the Equations (G.4) to (G.6) it is understood:

$$\Lambda^+ N = N^+ \sim \sqrt{p^+} \quad \text{and} \quad \Lambda^- N = N^- \sim 1/\sqrt{p^+}. \quad (\text{G.7})$$

After re-writing the decomposition (G.1) in terms of plus and minus components the distribution amplitudes S_i, P_i, \dots have definite twist:

$$\begin{aligned} 4 \langle 0 | \epsilon^{ijk} u_\alpha^i(a_1 z) u_\beta^j(a_2 z) d_\gamma^k(a_3 z) | P \rangle = & \\ & S_1 M C_{\alpha\beta} (\gamma_5 N^+)_\gamma + S_2 M C_{\alpha\beta} (\gamma_5 N^-)_\gamma + P_1 M (\gamma_5 C)_{\alpha\beta} N_\gamma^+ + P_2 M (\gamma_5 C)_{\alpha\beta} N_\gamma^- \\ & + V_1 (\not{p} C)_{\alpha\beta} (\gamma_5 N^+)_\gamma + V_2 (\not{p} C)_{\alpha\beta} (\gamma_5 N^-)_\gamma + \frac{V_3}{2} M (\gamma_\perp C)_{\alpha\beta} (\gamma^\perp \gamma_5 N^+)_\gamma \\ & + \frac{V_4}{2} M (\gamma_\perp C)_{\alpha\beta} (\gamma^\perp \gamma_5 N^-)_\gamma + V_5 \frac{M^2}{2pz} (\not{z} C)_{\alpha\beta} (\gamma_5 N^+)_\gamma + \frac{M^2}{2pz} V_6 (\not{z} C)_{\alpha\beta} (\gamma_5 N^-)_\gamma \\ & + A_1 (\not{p} \gamma_5 C)_{\alpha\beta} N_\gamma^+ + A_2 (\not{p} \gamma_5 C)_{\alpha\beta} N_\gamma^- + \frac{A_3}{2} M (\gamma_\perp \gamma_5 C)_{\alpha\beta} (\gamma^\perp N^+)_\gamma \\ & + \frac{A_4}{2} M (\gamma_\perp \gamma_5 C)_{\alpha\beta} (\gamma^\perp N^-)_\gamma + A_5 \frac{M^2}{2pz} (\not{z} \gamma_5 C)_{\alpha\beta} N_\gamma^+ + \frac{M^2}{2pz} A_6 (\not{z} \gamma_5 C)_{\alpha\beta} N_\gamma^- \\ & + T_1 (i\sigma_{\perp p} C)_{\alpha\beta} (\gamma^\perp \gamma_5 N^+)_\gamma + T_2 (i\sigma_{\perp p} C)_{\alpha\beta} (\gamma^\perp \gamma_5 N^-)_\gamma \\ & + T_3 \frac{M}{pz} (i\sigma_{pz} C)_{\alpha\beta} (\gamma_5 N^+)_\gamma + T_4 \frac{M}{pz} (i\sigma_{zp} C)_{\alpha\beta} (\gamma_5 N^-)_\gamma \\ & + T_5 \frac{M^2}{2pz} (i\sigma_{\perp z} C)_{\alpha\beta} (\gamma^\perp \gamma_5 N^+)_\gamma + \frac{M^2}{2pz} T_6 (i\sigma_{\perp z} C)_{\alpha\beta} (\gamma^\perp \gamma_5 N^-)_\gamma \\ & + M \frac{T_7}{2} (\sigma_{\perp \perp'} C)_{\alpha\beta} (\sigma^{\perp \perp'} \gamma_5 N^+)_\gamma + M \frac{T_8}{2} (\sigma_{\perp \perp'} C)_{\alpha\beta} (\sigma^{\perp \perp'} \gamma_5 N^-)_\gamma. \end{aligned} \quad (\text{G.8})$$

Here it is understood that $\sigma_{pz} = \sigma^{\mu\nu} p_\mu z_\nu$, $\gamma_\perp \gamma^\perp = \gamma^\mu g_{\mu\nu}^\perp \gamma^\nu$ with $g_{\mu\nu}^\perp = g_{\mu\nu} - (p_\mu z_\nu + z_\mu p_\nu)/pz$. A three quark operator has minimal twist of three. The invariant functions can be connected to the distribution amplitudes in the following way: For scalar and pseudo-scalar DA we obtain:

$$\begin{aligned} \mathcal{S}_1 &= S_1, & 2p \cdot z \mathcal{S}_2 &= S_1 - S_2, \\ \mathcal{P}_1 &= P_1, & 2p \cdot z \mathcal{P}_2 &= P_2 - P_1, \end{aligned} \tag{G.9}$$

for vector distributions:

$$\begin{aligned} \mathcal{V}_1 &= V_1, & 2p \cdot z \mathcal{V}_2 &= V_1 - V_2 - V_3, \\ 2\mathcal{V}_3 &= V_3, & 4p \cdot z \mathcal{V}_4 &= -2V_1 + V_3 + V_4 + 2V_5, \\ 4p \cdot z \mathcal{V}_5 &= V_4 - V_3, & (2p \cdot z)^2 \mathcal{V}_6 &= -V_1 + V_2 + V_3 + V_4 + V_5 - V_6, \end{aligned} \tag{G.10}$$

for axial vector distributions:

$$\begin{aligned} \mathcal{A}_1 &= A_1, & 2p \cdot z \mathcal{A}_2 &= -A_1 + A_2 - A_3, \\ 2\mathcal{A}_3 &= A_3, & 4p \cdot z \mathcal{A}_4 &= -2A_1 - A_3 - A_4 + 2A_5, \\ 4p \cdot z \mathcal{A}_5 &= A_3 - A_4, & (2p \cdot z)^2 \mathcal{A}_6 &= A_1 - A_2 + A_3 + A_4 - A_5 + A_6, \end{aligned} \tag{G.11}$$

and, finally, for tensor distributions:

$$\begin{aligned} \mathcal{T}_1 &= T_1, & 2p \cdot z \mathcal{T}_2 &= T_1 + T_2 - 2T_3, \\ 2\mathcal{T}_3 &= T_7, & 2p \cdot z \mathcal{T}_4 &= T_1 - T_2 - 2T_7, \\ 2p \cdot z \mathcal{T}_5 &= -T_1 + T_5 + 2T_8, & (2p \cdot z)^2 \mathcal{T}_6 &= 2T_2 - 2T_3 - 2T_4 + 2T_5 + 2T_7 + 2T_8, \\ 4p \cdot z \mathcal{T}_7 &= T_7 - T_8, & (2p \cdot z)^2 \mathcal{T}_8 &= -T_1 + T_2 + T_5 - T_6 + 2T_7 + 2T_8. \end{aligned} \tag{G.12}$$

Since we deal with massless nucleons only the leading twist distribution amplitudes V_1, A_1 and T_1 , which correspond directly to the invariant functions $\mathcal{V}_1, \mathcal{A}_1$ and \mathcal{T}_1 , contribute to our calculations.

APPENDIX G. DECOMPOSITION OF THE THREE QUARK MATRIX ELEMENT

H. Dirac algebra

The following definitions and conventions are used [27]: The metric tensor $g_{\mu\nu}$, which defines the metric of our Minkowski space and specifies the anti-commutation relation of the Dirac matrices

$$\{\gamma_\mu, \gamma_\nu\} = \gamma_\mu\gamma_\nu + \gamma_\nu\gamma_\mu = 2g_{\mu\nu}\mathbb{1}_4 \quad (\text{H.1})$$

reads

$$g_{\mu\nu} = g^{\mu\nu} = \begin{pmatrix} 1 & 0 & 0 & 0 \\ 0 & -1 & 0 & 0 \\ 0 & 0 & -1 & 0 \\ 0 & 0 & 0 & -1 \end{pmatrix}. \quad (\text{H.2})$$

Four vectors and scalar products are denoted in the following way:

$$\begin{aligned} v^\mu &= (v^0, \vec{v}), & v_\mu &= g_{\mu\nu}v^\nu = (v^0, -\vec{v}) \\ v \cdot w &= g_{\mu\nu}v^\mu w^\nu = v^0 w^0 - \vec{v} \cdot \vec{w}. \end{aligned} \quad (\text{H.3})$$

For a matrix the following notations are used:

- the inverse of a matrix A is denoted by A^{-1} .
- the complex conjugate of a matrix A is denoted by A^* .
- the transposed of a matrix A is denoted by A^T .
- the complex transposed or adjoint of a matrix A is denoted by $A^\dagger = (A^T)^*$.

The Dirac representation for the γ -matrices reads:

$$\begin{aligned} \gamma^0 = +\gamma_0 &= \begin{pmatrix} 1 & 0 & 0 & 0 \\ 0 & 1 & 0 & 0 \\ 0 & 0 & -1 & 0 \\ 0 & 0 & 0 & -1 \end{pmatrix} & \gamma^1 = -\gamma_1 &= \begin{pmatrix} 0 & 0 & 0 & 1 \\ 0 & 0 & 1 & 0 \\ 0 & -1 & 0 & 0 \\ -1 & 0 & 0 & 0 \end{pmatrix} \\ \gamma^2 = -\gamma_2 &= \begin{pmatrix} 0 & 0 & 0 & -i \\ 0 & 0 & i & 0 \\ 0 & i & 0 & 0 \\ -i & 0 & 0 & 0 \end{pmatrix} & \gamma^3 = -\gamma_3 &= \begin{pmatrix} 0 & 0 & 1 & 0 \\ 0 & 0 & 0 & -1 \\ -1 & 0 & 0 & 0 \\ 0 & 1 & 0 & 0 \end{pmatrix}. \end{aligned} \quad (\text{H.4})$$

An alternative form of the Dirac matrices in the Dirac representation is to express them via the Pauli matrices $\vec{\sigma}^\mu = (\sigma^0, \sigma^1, \sigma^2, \sigma^3)$:

$$\sigma^0 = \begin{pmatrix} 1 & 0 \\ 0 & 1 \end{pmatrix} \sigma^1 = \begin{pmatrix} 0 & 1 \\ 1 & 0 \end{pmatrix} \sigma^2 = \begin{pmatrix} 0 & -i \\ i & 0 \end{pmatrix} \sigma^3 = \begin{pmatrix} 1 & 0 \\ 0 & -1 \end{pmatrix} \quad (\text{H.5})$$

$$\gamma^0 = \begin{pmatrix} \sigma^0 & 0 \\ 0 & -\sigma^0 \end{pmatrix} \gamma^i = \begin{pmatrix} 0 & \sigma^i \\ -\sigma^i & 0 \end{pmatrix}. \quad (\text{H.6})$$

The following statements hold:

$$(\gamma^0)^T = (\gamma^0)^\dagger = \gamma^0.$$

$$(\gamma^i)^\dagger = -(\gamma^i) \quad \text{with } i = 1, 2, 3.$$

$$(\gamma^i)^T = -(\gamma^i) \quad \text{with } i = 1, 3.$$

$$(\gamma^i)^T = (\gamma^i) \quad \text{with } i = 2.$$

The definition of γ^5 and some properties are:

$$\begin{aligned} \gamma^5 &= \gamma_5 \equiv i\gamma^0\gamma^1\gamma^2\gamma^3 \\ (\gamma^5)^\dagger &= (\gamma^5)^T = \gamma^5 \\ (\gamma^5)^2 &= 1 \\ \{\gamma^\mu, \gamma^5\} &= 0. \end{aligned}$$

We define the charge conjugation matrix C as:

$$C \equiv \gamma^0\gamma^2.$$

It is easy to show that for C the following identities hold:

$$\begin{aligned}C^2 &= 1 \\C^\dagger &= C^{-1} = C \\C^* &= C^T = -C \\C\gamma^\mu C &= -(\gamma^\mu)^T \text{ and } C(\gamma^\mu)^T C = -\gamma^\mu.\end{aligned}\tag{H.7}$$

Finally we will present some useful identities which may come handy:

$$\begin{aligned}\gamma_0 C \gamma_0 &= -C \\ \gamma_0 \gamma^5 \gamma_0 &= -\gamma^5.\end{aligned}\tag{H.8}$$

The properties for traces of Dirac matrices read as:

$$\text{Tr}(\gamma^\mu) = 0\tag{H.9}$$

$$\text{Tr}(\gamma^\mu \gamma^\nu) = 4g^{\mu\nu}.\tag{H.10}$$

Bibliography

- [1] Wolfram-Research, *Mathematica Version 8.0*. Wolfram Research, Inc., 2010.
- [2] T. Hahn, *FeynArts 3.7 Users Guide*. <http://www.feynarts.de/>, March, 2012.
- [3] R. Hofstadter, H. Fechter, and J. McIntyre, *Scattering of high energy electrons and the method of nuclear recoil*, *Phys.Rev.* **91** (1953) 422.
- [4] H.-y. Gao, *Nucleon electromagnetic form factors*, *Int.J.Mod.Phys.* **E12** (2003) 1, [arXiv:nuc1-ex/0301002](https://arxiv.org/abs/nuc1-ex/0301002).
- [5] C. E. Hyde and K. de Jager, *Electromagnetic form factors of the nucleon and compton scattering*, *Ann.Rev.Nucl.Part.Sci.* **54** (2004) 217, [arXiv:nuc1-ex/0507001](https://arxiv.org/abs/nuc1-ex/0507001).
- [6] J. Arrington, C. Roberts, and J. Zanotti, *Nucleon electromagnetic form factors*, *J.Phys.* **G34** (2007) 23, [arXiv:nuc1-th/0611050](https://arxiv.org/abs/nuc1-th/0611050).
- [7] C. Perdrisat, V. Punjabi, and M. Vanderhaeghen, *Nucleon electromagnetic form factors*, *Prog.Part.Nucl.Phys.* **59** (2007) 694, [arXiv:hep-ph/0612014](https://arxiv.org/abs/hep-ph/0612014).
- [8] J. Arrington, K. de Jager, and C. F. Perdrisat, *Nucleon form factors: A Jefferson Lab perspective*, *J.Phys.Conf.Ser.* **299** (2011) 012002, [arXiv:1102.2463](https://arxiv.org/abs/1102.2463) [nuc1-ex].
- [9] L. Price, J. Dunning, M. Goitein, K. Hanson, T. Kirk, et al., *Backward-angle electron-proton elastic scattering and proton electromagnetic form factors*, *Phys.Rev.* **D4** (1971) 45.
- [10] K. Hanson, J. Dunning, M. Goitein, T. Kirk, L. Price, et al., *Large angle quasielastic electron-deuteron scattering*, *Phys.Rev.* **D8** (1973) 753.
- [11] C. Berger, V. Burkert, G. Knop, B. Langenbeck, and K. Rith, *Electromagnetic form factors of the proton at squared four momentum transfers between 10fm^{-2} and 50fm^{-2}* , *Phys.Lett.* **B35** (1971) 87.
- [12] W. Bartel, F. Busser, W. Dix, R. Felst, D. Harms, et al., *Measurement of proton and neutron electromagnetic form factors at squared four momentum transfers up*

- to $3(\text{GeV}/c)^2$, *Nucl.Phys.* **B58** (1973) 429.
- [13] P. E. Bosted, L. Clogher, A. Lung, L. Stuart, J. Alster, et al., *Measurements of the electric and magnetic form factors of the proton from $Q^2 = 1.75(\text{GeV}/c)^2$ to $8.83(\text{GeV}/c)^2$* , *Phys.Rev.Lett.* **68** (1992) 3841.
- [14] L. Andivahis, P. E. Bosted, A. Lung, L. Stuart, J. Alster, et al., *Measurements of the electric and magnetic form factors of the proton from $Q^2 = 1.75(\text{GeV}/c)^2$ to $8.83(\text{GeV}/c)^2$* , *Phys.Rev.* **D50** (1994) 5491.
- [15] **Jefferson Lab Hall A** Collaboration, M. Jones et al., *$G(E(p))/G(M(p))$ ratio by polarization transfer in $\vec{e}p \rightarrow e\vec{p}$* , *Phys.Rev.Lett.* **84** (2000) 1398, [arXiv:nuc1-ex/9910005](https://arxiv.org/abs/nuc1-ex/9910005).
- [16] **Resonance Spin Structure** Collaboration, M. Jones et al., *Proton $G(E)/G(M)$ from beam-target asymmetry*, *Phys.Rev.* **C74** (2006) 035201, [arXiv:nuc1-ex/0606015](https://arxiv.org/abs/nuc1-ex/0606015).
- [17] A. Efremov and A. Radyushkin, *Factorization and asymptotical behavior of pion form factor in QCD*, *Phys.Lett.* **B94** (1980) 245.
- [18] V. Chernyak, A. Zhitnitsky, and V. Serbo, *Asymptotic hadronic form factors in quantum chromodynamics*, *JETP Lett.* **26** (1977) 594.
- [19] G. P. Lepage and S. J. Brodsky, *Exclusive processes in quantum chromodynamics: The form factors of yaryons at large momentum transfer*, *Phys.Rev.Lett.* **43** (1979) 545.
- [20] V. Chernyak and I. Zhitnitsky, *Nucleon wave function and nucleon form factors in QCD*, *Nucl.Phys.* **B246** (1984) 52.
- [21] H. Eck, *FeynArts 2.0- Developing of a generic Feynman diagramm generator*. PhD thesis, <http://www.feynarts.de/>, 1995.
- [22] J. Küblbeck, M. Böhm, and A. Denner, *Feyn arts – computer-algebraic generation of Feynman graphs and amplitudes*, *Comput.Phys.Commun.* **60** (1990) 165.
- [23] G. Duplancić and B. Nizić, *Reduction method for dimensionally regulated one loop N point Feynman integrals*, *Eur.Phys.J.* **C35** (2004) 105, [arXiv:hep-ph/0303184](https://arxiv.org/abs/hep-ph/0303184).
- [24] A. I. Davydychev, *A Simple formula for reducing Feynman diagrams to scalar integrals*, *Phys.Lett.* **B263** (1991) 107.
- [25] A. Grozin, *Lectures on QED and QCD: Practical calculation and renormalization of one- and multi-loop Feynman diagrams*.
- [26] T. Muta, *Foundations of quantum chromodynamics. Second edition*, World

-
- Sci.Lect.Notes Phys.* (1998) .
- [27] M. E. Peskin and D. V. Schroeder, *An introduction to quantum field theory*. Westview Press, 1995.
- [28] M. Rosenbluth, *High energy elastic scattering of electrons on protons*, *Phys.Rev.* **79** (1950) 615.
- [29] R. Hofstadter and R. McAllister, *Electron scattering from the proton*, *Phys.Rev.* **98** (1955) 217.
- [30] R. Hofstadter, *Electron scattering and nuclear structure*, *Rev. Mod. Phys.* **28** (1956) 214.
- [31] R. Mcallister and R. Hofstadter, *Elastic scattering of 188 MeV electrons from the proton and the Alpha particle*, *Phys.Rev.* **102** (1956) 851.
- [32] B. Povh, K. Rith, C. Scholz, and F. Zetdche, *Teilchen und Kerne*. 2009.
- [33] O. Nachtmann, *Elementarteilchenphysik- Phänomene und Konzepte*. Roman U. Sexl, 1986.
- [34] **Particle Data Group** Collaboration, K. Olive et al., *Review of Particle Physics*, *Chin.Phys.* **C38** (2014) 090001.
- [35] N. Dombey, *Scattering of polarized leptons at high energy*, *Rev.Mod.Phys.* **41** (1969) 236.
- [36] M. L. Swartz, *Physics with polarized electron beams*, *Conf.Proc.* **C8708101** (1987) 83.
- [37] R. Arnold, C. E. Carlson, and F. Gross, *Polarization transfer in elastic electron scattering from nucleons and deuterons*, *Phys.Rev.* **C23** (1981) 363.
- [38] A. Akhiezer and M. Rekalov, *Polarization effects in the scattering of leptons by hadrons*, *Sov.J.Part.Nucl.* **4** (1974) 277.
- [39] V. Braun, A. Lenz, and M. Wittmann, *Nucleon form factors in QCD*, *Phys.Rev.* **D73** (2006) 094019, [arXiv:hep-ph/0604050](https://arxiv.org/abs/hep-ph/0604050).
- [40] G. P. Lepage and S. J. Brodsky, *Exclusive processes in perturbative quantum chromodynamics*, *Phys.Rev.* **D22** (1980) 2157.
- [41] E. Salpeter and H. Bethe, *A relativistic equation for bound state problems*, *Phys.Rev.* **84** (1951) 1232.
- [42] G. Wick, *Properties of Bethe-Salpeter wave functions*, *Phys.Rev.* **96** (1954) 1124.
- [43] V. Braun, R. Fries, N. Mahnke, and E. Stein, *Higher twist distribution amplitudes*

- of the nucleon in QCD, Nucl.Phys.* **B589** (2000) 381, [arXiv:hep-ph/0007279](#).
- [44] K. G. Wilson, *Confinement of quarks, Phys. Rev.* **D10** (1974) 2445.
- [45] M. Gruber, *The nucleon wave function at the origin, Phys.Lett.* **B699** (2011) 169, [arXiv:1011.0758 \[hep-ph\]](#).
- [46] G. Duplančić and B. Nizić, *NLO calculations of the exclusive processes in PQCD, arXiv:hep-ph/0304255*.
- [47] G. Korenblit, V. A. Naumov, and V. Chernyak, *Asymptotics of hadron exclusive electroproduction amplitudes. (in Russian) , Sov.J.Nucl.Phys.* **29** (1979) 77.
- [48] S. J. Brodsky and G. R. Farrar, *Scaling laws at large transverse momentum, Phys.Rev.Lett.* **31** (1973) 1153.
- [49] T. C. Brooks and L. J. Dixon, *Recalculation of proton compton scattering in perturbative QCD, Phys.Rev.* **D62** (2000) 114021, [arXiv:hep-ph/0004143](#).
- [50] R. Thomson, A. Pang, and C.-R. Ji, *Real and virtual nucleon compton scattering in the perturbative limit, Phys.Rev.* **D73** (2006) 054023, [arXiv:hep-ph/0602164](#).
- [51] K. Semenov, *A simple formula for the nucleon form factor*.
- [52] T. Hahn, *CUBA: A Library for multidimensional numerical integration, Comput.Phys.Commun.* **168** (2005) 78, [arXiv:hep-ph/0404043](#).
- [53] A. Manashov, *Private communication*.
- [54] V. Borodulin, R. Rogalev, and S. Slabospitsky, *CORE: COmpendium of RELations: Version 2.1, arXiv:hep-ph/9507456*.
- [55] G. 't Hooft and M. Veltman, *Regularization and renormalization of gauge fields, Nucl.Phys.* **B44** (1972) 189.
- [56] S. Mandelstam, *Determination of the pion – nucleon scattering amplitude from dispersion relations and unitarity. General theory, Phys.Rev.* **112** (1958) 1344.
- [57] L. Hand, *Electric and magnetic form factor of the nucleon, Rev.Mod.Phys.* **35** (1963) 335.
- [58] T. Janssens, R. Hofstadter, E. Hughes, and M. Yearian, *Proton form factors from elastic electron-proton scattering, Phys.Rev.* **142** (1966) 922.
- [59] D. Coward, H. DeStaebler, R. A. Early, J. Litt, A. Minten, et al., *Electron-proton scattering at high momentum transfers, Phys.Rev.Lett.* **20** (1968) 292.
- [60] J. Litt, G. Buschhorn, D. Coward, H. DeStaebler, L. W. Mo, et al., *Measurement of the ratio of the proton form factors, G_E/G_M , at high momentum transfers and the*

- question of scaling, *Phys.Lett.* **B31** (1970) 40.
- [61] F. Borkowski, P. Peuser, G. Simon, V. Walther, and R. Wendling, *Electromagnetic form factors of the proton at low four-momentum transfer*, *Nucl.Phys.* **B93** (1975) 461.
- [62] A. Sill, R. Arnold, P. E. Bosted, C. Chang, J. Gomez, et al., *Measurements of elastic electron-proton scattering at large momentum transfer*, *Phys.Rev.* **D48** (1993) 29.
- [63] R. Walker, B. Filippone, J. Jourdan, R. Milner, R. McKeown, et al., *Measurements of the proton elastic form factors for $1(\text{GeV}/c)^2 \leq Q^2 \leq 3(\text{GeV}/c)^2$ at SLAC*, *Phys.Rev.* **D49** (1994) 5671.
- [64] **E94110** Collaboration, M. Christy et al., *Measurements of electron proton elastic cross-sections for $0.4(\text{GeV}/c)^2 < Q^2 < 5.5(\text{GeV}/c)^2$* , *Phys.Rev.* **C70** (2004) 015206, [arXiv:nucl-ex/0401030](#).
- [65] I. Qattan, J. Arrington, R. Segel, X. Zheng, K. Aniol, et al., *Precision Rosenbluth measurement of the proton elastic form factors*, *Phys.Rev.Lett.* **94** (2005) 142301, [arXiv:nucl-ex/0410010](#).
- [66] G. Simon, C. Schmitt, F. Borkowski, and V. Walther, *Absolute electron-proton cross-Sections at low momentum transfer measured with a high pressure gas target system*, *Nucl.Phys.* **A333** (1980) 381.
- [67] D. Benaksas, D. Drickey, and D. Frerejacque, *Electromagnetic form factors of the deuteron*, *Phys.Rev.Lett.* **13** (1964) 353.
- [68] E. Hughes, T. Griffy, M. Yearian, and R. Hofstadter, *Neutron form factors from inelastic electron-deuteron Scattering*, *Phys.Rev.* **139** (1965) B458.
- [69] B. Grossetête, S. Jullian, and P. Lehmann, *Electrodisintegration of the deuteron around $q^2 = 3.5F^{-2}$* , *Phys.Rev.* **141** (1966) 1435.
- [70] P. Stein, M. Binkley, R. McAllister, A. Suri, and W. Woodward, *Measurements of neutron form factors*, *Phys.Rev.Lett.* **16** (1966) 592.
- [71] L. Chan, K. Chen, J. Dunning, N. Ramsey, J. Walker, et al., *Nucleon form factors and their Interpretation*, *Phys.Rev.* **141** (1966) 1298.
- [72] R. Budnitz, J. Appel, L. Carroll, J. Chen, J. Dunning, et al., *Neutron form factors from quasielastic electron deuteron scattering*, *Phys.Rev.* **173** (1968) 1357.
- [73] S. Rock, R. Arnold, P. E. Bosted, B. Chertok, B. Mecking, et al., *Measurement of elastic electron-neutron scattering and inelastic electron-deuteron scattering*

- cross-sections at high momentum transfer, *Phys.Rev.* **D46** (1992) 24.
- [74] P. Markowitz, J. Finn, B. Anderson, H. Arenhovel, A. Baldwin, et al., *Measurement of the magnetic form factor of the neutron*, *Phys.Rev.* **C48** (1993) 5.
- [75] H. Anklin, D. Fritschi, J. Jourdan, M. Loppacher, G. Masson, et al., *Precision measurement of the neutron magnetic form factor*, *Phys.Lett.* **B336** (1994) 313.
- [76] E. Bruins, T. Bauer, H. den Bok, C. Duif, W. van Hoek, et al., *Measurement of the neutron magnetic form-factor*, *Phys.Rev.Lett.* **75** (1995) 21.
- [77] H. Anklin, L. deBever, K. Blomqvist, W. Boeglin, R. Bohm, et al., *Precise measurements of the neutron magnetic form factor*, *Phys.Lett.* **B428** (1998) 248.
- [78] G. Kubon, H. Anklin, P. Bartsch, D. Baumann, W. Boeglin, et al., *Precise neutron magnetic form factors*, *Phys.Lett.* **B524** (2002) 26, [arXiv:nucl-ex/0107016](#).
- [79] **CLAS** Collaboration, W. Brooks and J. Lachniet, *Precise determination of the neutron magnetic form factor to higher Q^2* , *Nucl.Phys.* **A755** (2005) 261–264, [arXiv:nucl-ex/0504028](#) [[nucl-ex](#)].
- [80] E. Brash, A. Kozlov, S. Li, and G. Huber, *New empirical fits to the proton electromagnetic form factors*, *Phys.Rev.* **C65** (2002) 051001, [arXiv:hep-ex/0111038](#).
- [81] V. Punjabi, C. Perdrisat, K. Aniol, F. Baker, J. Berthot, et al., *Proton elastic form factor ratios to $Q^2 = 3.5\text{GeV}^2$ by polarization transfer*, *Phys.Rev.* **C71** (2005) 055202, [arXiv:nucl-ex/0501018](#).
- [82] **Jefferson Lab Hall A** Collaboration, O. Gayou et al., *Measurement of $G(Ep)/G(Mp)$ in $\vec{e}p \rightarrow e\vec{p}$ to $Q^2 = 5.6\text{GeV}^2$* , *Phys.Rev.Lett.* **88** (2002) 092301, [arXiv:nucl-ex/0111010](#).
- [83] C. B. Crawford, A. Sindile, T. Akdogan, R. Alarcon, W. Bertozzi, et al., *Measurement of the proton electric to magnetic form factor ratio from $^1\vec{H}(\vec{e}, e'p)$* , *Phys.Rev.Lett.* **98** (2007) 052301, [arXiv:nucl-ex/0609007](#).
- [84] J. Kelly, *Simple parametrization of nucleon form factors*, *Phys.Rev.* **C70** (2004) 068202.
- [85] H. Gao, J. Arrington, E. Beise, B. Bray, R. Carr, et al., *Measurement of the neutron magnetic form factor from inclusive quasielastic scattering of polarized electrons from polarized ^3He* , *Phys.Rev.* **C50** (1994) 546.
- [86] **Jefferson Lab E95-001** Collaboration, B. Anderson et al., *Extraction of the neutron magnetic form factor from quasi-elastic $^3\vec{H}e(\vec{e}, e')$ at*

- $Q^2 = 0.1(\text{GeV}/c)^2 - 0.6(\text{GeV}/c)^2$, *Phys.Rev.* **C75** (2007) 034003, [arXiv:nucl-ex/0605006](#).
- [87] M. Meyerhoff, D. Eyl, A. Frey, H. Andresen, J. Annand, et al., *First measurement of the electric form factor of the neutron in the exclusive quasielastic scattering of polarized electrons from polarized ^3He* , *Phys.Lett.* **B327** (1994) 201.
- [88] J. Becker, H. Andresen, J. Annand, K. Aulenbacher, K. Beuchel, et al., *Determination of the neutron electric form factor from the reaction $^3\text{He}(e, e'n)$ at medium momentum transfer*, *Eur.Phys.J.* **A6** (1999) 329.
- [89] J. Golak, G. Ziemer, H. Kamada, H. Witala, and W. Gloeckle, *Extraction of electromagnetic neutron form factors through inclusive and exclusive polarized electron scattering on polarized ^3He target*, *Phys.Rev.* **C63** (2001) 034006, [arXiv:nucl-th/0008008](#).
- [90] D. Rohe, P. Bartsch, D. Baumann, J. Becker, J. Bermuth, et al., *Measurement of the neutron electric form factor G_{En} at $0.67(\text{GeV}/c)^2$ via $^3\vec{H}e(\vec{e}, e'\vec{n})$* , *Phys.Rev.Lett.* **83** (1999) 4257.
- [91] J. Bermuth, P. Merle, C. Carasco, D. Baumann, D. Bohm, et al., *The neutron charge form factor and target analyzing powers from $^3\vec{H}e(\vec{e}, e'\vec{n})$ -scattering*, *Phys.Lett.* **B564** (2003) 199, [arXiv:nucl-ex/0303015](#).
- [92] T. Eden, R. Madey, W. Zhang, B. Anderson, H. Arenhovel, et al., *Electric form factor of the neutron from $^2\text{H}(\vec{e}, e'\vec{n})^1\text{H}$ reaction at $Q^2 = 0.255(\text{GeV}/c)^2$* , *Phys.Rev.* **C50** (1994) 1749.
- [93] I. Passchier, R. Alarcon, T. Bauer, D. Boersma, J. van den Brand, et al., *The charge form factor of the neutron from the reaction $^2\vec{H}(\vec{e}, e'\vec{n})p$* , *Phys.Rev.Lett.* **82** (1999) 4988, [arXiv:nucl-ex/9907012](#).
- [94] M. Ostrick, C. Herberg, H. Andresen, J. Annand, K. Aulenbacher, et al., *Measurement of the neutron electric form factor $G_{E,n}$ in the quasifree $^2\text{H}(\vec{e}, e'\vec{n})p$ reaction*, *Phys.Rev.Lett.* **83** (1999) 276.
- [95] **Jefferson Lab t(20) Collaboration**, D. Abbott et al., *A Precise measurement of the deuteron elastic structure function $A(Q^2)$* , *Phys.Rev.Lett.* **82** (1999) 1379, [arXiv:nucl-ex/9810017](#).
- [96] R. Schiavilla and I. Sick, *Neutron charge form factor at large q^2* , *Phys.Rev.* **C64** (2001) 041002, [arXiv:nucl-ex/0107004](#).
- [97] **E93026 Collaboration**, H. Zhu et al., *A measurement of the electric form factor of*

- the neutron through $\vec{d}(\vec{e}, e'n)p$ at $Q^2 = 0.5(\text{GeV}/c)^2$,
Phys.Rev.Lett. **87** (2001) 081801, [arXiv:nucl-ex/0105001](#).
- [98] **Jefferson Lab E93-026** Collaboration, G. Warren et al., *Measurement of the electric form factor of the neutron at $Q^2 = 0.5(\text{GeV}/c)^2$ and $1.0(\text{GeV}/c)^2$* ,
Phys.Rev.Lett. **92** (2004) 042301, [arXiv:nucl-ex/0308021](#).
- [99] D. Glazier, M. Seimetz, J. Annand, H. Arenhovel, M. Ases Antelo, et al.,
Measurement of the electric form factor of the neutron at $Q^2 = 0.3(\text{GeV}/c)^2 - 0.8(\text{GeV}/c)^2$, *Eur.Phys.J.* **A24** (2005) 101,
[arXiv:nucl-ex/0410026](#).
- [100] **Jefferson Laboratory E93-038** Collaboration, B. Plaster et al., *Measurements of the neutron electric to magnetic form factor ratio G_{En}/G_{Mn} via the ${}^2\text{H}(\vec{e}, e'\vec{n}){}^1\text{H}$ reaction to $Q^2 = 1.45(\text{GeV}/c)^2$* , *Phys.Rev.* **C73** (2006) 025205,
[arXiv:nucl-ex/0511025](#).

Acknowledgements

Here comes the most pleasant part of this thesis: To thank all the people who made it happen.

- Of course my advisor Prof. Dr. Vladimir Braun for giving me the chance to do a doctor's degree in the first place. But more than this he always found time for discussions and created a pleasant and familiar atmosphere in his group. In addition he gave me a lot of extra time to pursue our goal of solving the problem completely.
- I also want to thank Prof. Dr. Andreas Schäfer for ensuring the financial support for our project.
- Special thanks goes to my roommate and collaborator Nils Offen. Not only providing the computer program for solving the nasty integrals and helping to solve various issues concerning this project, but also for proof reading the thesis and stoically answering questions on diverse aspects of particle physics.
- In addition I want to thank Alexander Manashov and Philip Wein for fruitful discussions.
- The last one to thank in the domain of physics is Michael Gruber. With his expertise in LaTeX he helped me out many times. He also provided useful input to my Mathematica code. Especially grateful I am for his precise proof reading of this thesis.
- Heidi Decock and Monika Maschek took care of all administrative issues.
- All SysAdmins for helping to keep the machine running.

Now to the things outside of physics:

- First of all I want to thank my parents for supporting me all my life. Without their financial and mental support this thesis would never have been possible.
- My little brother for supporting me in so many ways that I can not numerate all of them.
- My girlfriend Neele, who provided emotional support, which was necessary a lot of

Bibliography

times.

- My friends and cousin, Coco, Max, Osti, Hausi, Andi and Gregor for gaining distance to the world of physics when needed.